PhD degree in Molecular Medicine (curriculum in Molecular Oncology)

European School of Molecular Medicine (SEMM),

University of Milan and University of Naples "Federico II"

Settore disciplinare: Bio/11

Novel functions of the SNARE protein Snap29 in membrane trafficking and cell division

Elena Morelli

IFOM, Milan

Matricola n. R09394

Supervisor: Dr. Thomas Vaccari

IFOM, Milan

Anno accademico 2013-2014

Parts of this thesis have been published in:

Morelli E, Ginefra P, Mastrodonato V, Beznoussenko G, Rusten TE, Bilder D, Stenmark H, Mironov AA, Vaccari T (2014). Multiple functions of the SNARE protein Snap29 in autophagy, endocytic and exocytic trafficking during epithelia formation in *Drosophila*. Autophagy. DOI: 10.4161/15548627.2014.981913

Figure 20H-I'' and Figure 26A-N were performed by Valeria Mastrodonato.

TABLE OF CONTENTS

LIST OF ABBREVIATIONS

ATG, Autophagy related protein

CEDNIK, CErebral Dysgenesis, Neuropathy, Ichthyosis, and palmoplantar Keratoderma

CGN, Cis-Golgi-Network

COPI, COated Protein complex I

COPII, COated Protein complex II

CPC, Chromosomal Passenger Complex

CUS, Comparment of Unconventional Secretion

EE, Early Endosomes

EM, Electron Microscopy

ER, Endoplasmic Reticulum

ESCRT, Endosomal Sorting Complex Required for Transport

FE, Follicular Epithelium

HPIV3, Human ParaInfluenza Virus type 3

ILV, Intra Luminal Vesicle

INM, Inner Nuclear Membrane

KT, Kinetochore

MN, MiNinuclei

MT, MicroTubules

MVB, Multi Vesicular Body

NE, Nuclear Envelope

NEBD, Nuclear Envelope BreakDown

NPC, Nuclear Pore Complex

NSF, N-ethylmaleimide Sensitive Factor

NuMa, Nuclear Mitotic Apparatus protein

NUP, Nucleoporin

OGT, O-GlyNAc Transferase

PAS, Phagophore Assembling Site

PCM, Pericentriolar Material

PIP3, Phosphatidyl Inositol Triphosphate

PLK1, Polo like-kinase 1

PM, Plasma Membrane

ONM, Outer Nuclear Membrane

RE, Recycling Endosomes

TGN, Trans Golgi Network

TC, Tethering Complex

t-SNARE, target-SNARE

SAC, Spindle Assembly Checkpoint

SM, Sec1/Munc18-1

SNAP, SyNaptosomal Associated Protein

SNARE, Soluble NSF Attachment Protein Receptors

Syb, Synaptobrevin

Syt1, Synaptotagmin1

Syx, Syntaxin

VAMP, Vesicle Associated Membrane Proteins

v-SNARE, vesicular-SNARE

FIGURES INDEX

1. ABSTRACT

Vesicular trafficking within cells is an important process for tissue development and homeostasis. A key step of vesicular trafficking is the fusion between two membranes, a process in which SNARE (Soluble NSF Attachment Protein Receptors) proteins play a fundamental role. SNAP29 (SyNaptosomal Associated Proteins 29) is a ubiquitous SNARE, regulating membrane fusion in different trafficking compartments and in different contexts in non dividing cells. We isolated a loss of function mutant in *usnp*, the gene encoding the *Drosophila* homolog of the human protein SNAP29 (Snap29 hereafter), that, when made homozygous in developing epithelial organs, disrupts epithelial architecture. *In vivo*, we find that Snap29 interacts with multiple SNARE proteins, localizes to a number of trafficking organelles, and is required for proper Golgi Apparatus morphology. In addition, we show that Snap29 is required for fusion of autophagosomes with lysosomes together with Syx17 and Vamp7, and that lack of Snap29 results in excess secretion, suggesting that Snap29 might act negatively in regulation of vesicle fusion at the plasma membrane.

Interestingly, at the onset of mitosis, when trafficking compartments re-shape to allow the formation of the mitotic spindle, Snap29 is found at the outer KT in *Drosophila* S2 cells and localizes at spindle microtubules and centrosomes in mammalian cells. Depletion of Snap29 in *Drosophila* and mammalian cells leads to spindle assembly defects, associated to pro-metaphase delay in mammalian cells, and to the formation of daughter cells containing mininuclei. Mechanistically, lack of SNAP29 correlates with absence at KT of ZWINT-1 and ZWILCH, a component of RZZ complex, and with weak KTs-MTs attachments. In addition, we find that SPINDLY, the adaptor for recruitment to KTs of dynein/dynactin and MAD1, a component of the Spindle Assembly Checkpoint machinery, fail to be removed from KTs at the end of metaphase in SNAP29 depleted mammalian cells forced to

reassemble the spindle after treatment with microtubules depolymerization drug.

Finally, we show that cell division is impaired in *Snap29* mutant tissues *in vivo*, that autophagy defects are not the cause of the altered epithelial tissues architecture in Snap29 mutants and that the trafficking and cell division function of Snap29 are molecularly distinct.

All together our findings support a role of Snap29 at key steps of membrane trafficking and in cell division. Our study contribute to shed light on the pathogenesis of CEDNIK, a human congenital syndrome caused by SNAP29 inactivation. In addition to this, we propose that the function of SNAP29 in cell division might be evolutionarly related to that of complexes tethering MTs to vesicular organelles in interphase. We surmise that such function could be potentially relevant to development of aneuploidy in tumor-like masses.

2. INTRODUCTION

2.1 SNARE proteins control vesicle and organelle dynamics

2.1.1 Membrane fusion and regulation of SNARE complex formation

In eukaryotic cells, membrane trafficking is a highly regulated process that drives transport of cargo-containing vesicles from a donor compartment to a specific target compartment. The cycle of a transported vesicle can be divided into several steps. The first one corresponds to the budding of a coated vesicle from a donor compartment, followed by the scission of the vesicle. Subsequently, the vesicle is stripped of its coating and transported by motor proteins toward a recipient compartment, where resident tethering factors mediate vesicle docking. This latter step is essential for membrane fusion between the vesicle and the recipient compartment (Bonifacino 2014) (Figure 1).

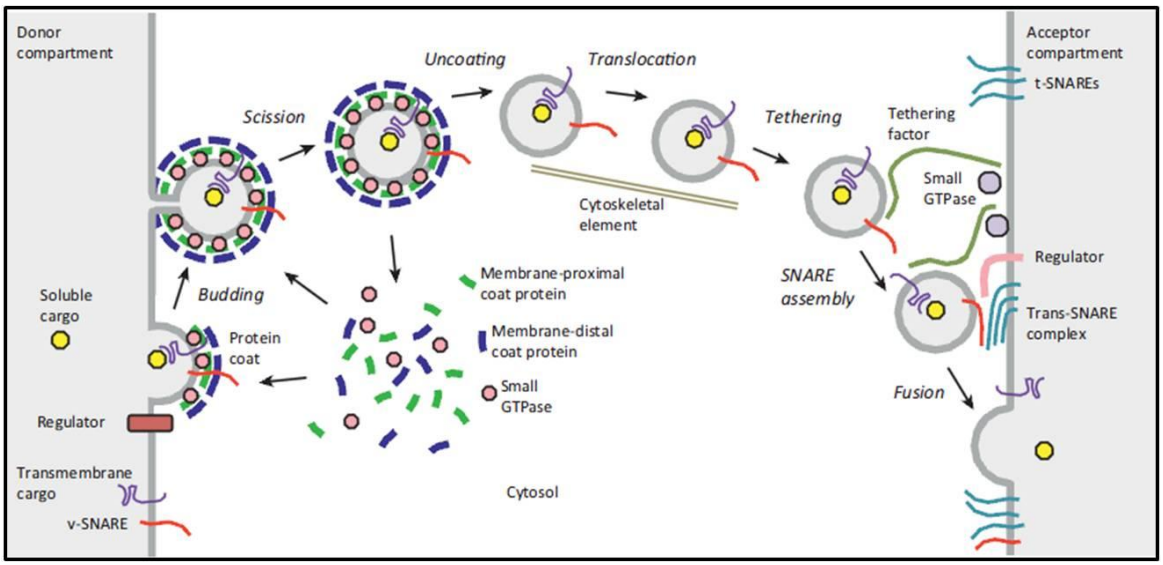

Figure 1. Life cycle of a transported vesicle. Figure adapted from Bonifacino 2014.

The main regulators of membrane fusion are SNARE proteins, which constitute a conserved, large protein family widely expressed in bacteria and eukariotyc cells (for review Bonifacino & Glick 2004, Malsam et al. 2008, Jahn & Scheller 2006). The majority of these proteins possess a single trans-membrane domain and a cytoplasmic portion. Some SNAREs lack the trans-membrane domain, but contain a post-translational acyl-modification, such as a palmitoylation, farnesylation or miristylation for membrane anchoring (Jahn & Scheller 2006). The functional domain of SNAREs is the SNARE motif. The SNARE motif is fundamental for membrane fusion and is composed of 60-70 amino acids organized in an alpha helix. SNARE proteins are divided into vesicular-SNAREs (v-SNAREs), such as Vesicle Associated Membrane Proteins (VAMPs) and Synaptobrevins (Syb), which are carried by vesicles, and target-SNAREs (t-SNARE), such as Syntaxins (Syx) and SyNaptosomal Associated Proteins (SNAPs), which reside on target membranes (Jahn & Scheller 2006, Hong 2005). To induce membrane fusion, SNAREs interact through their SNARE motif to form a four-helix bundle, the so-called trans-SNARE complex. This complex brings lipid bilayers into close proximity so that they fuse together. After fusion, all the SNARE proteins of the complex are on the same membrane and form a parallel four-helix bundle named cis-SNARE complex (Figure 2) (for review Rizo & Südhof 2002, Littleton et al. 2001).

SNARE proteins can also be classified according to structural features. Indeed, the four-helix bundle mainly consists of hydrophobic interactions, except for one hydrophilic interaction, called ‘0’ layer, which is composed of three glutamine residues and an arginine residue. In particular, R-SNAREs contribute to the interaction with arginine, while three kind of Q-SNAREs, Qa-, Qb- and Qc- contribute with glutamine residues (Sutton et al. 1998). In general, Q-SNAREs correspond to t-SNAREs, while R-SNAREs correspond to v-SNAREs.

After fusion, disassembly of the SNARE complex is achieved by an ATP-dependent dissociation of the SNARE complex mediated by α-SNAP and NSF (N-ethylmaleimide

Sensitive Factor). α-SNAP is an adaptor that binds the SNARE complex and helps the recruitment of the ATPase NSF. SNARE complex disassembly ensures that SNARE proteins are reused for repeated vesicle fusion processes (Figure 2) (Bonifacino & Glick 2004).

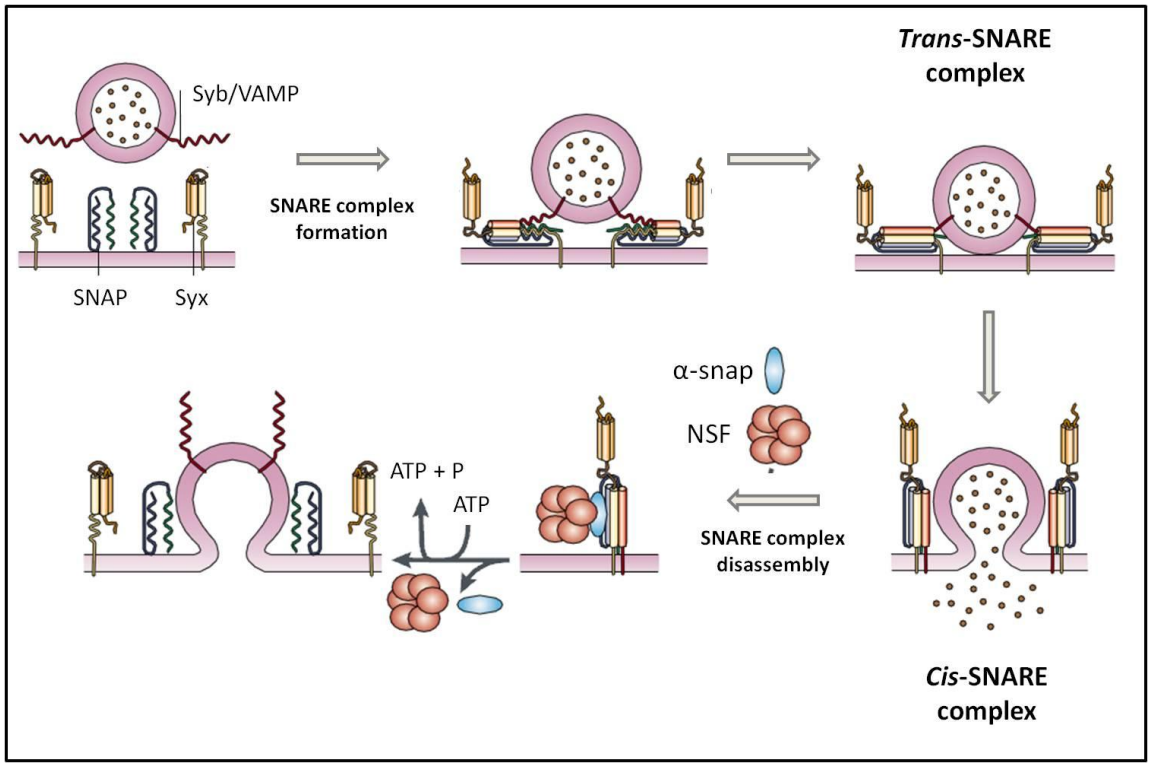

Figure 2. Fusion between a vesicle and a target membrane. SNARE complex formation is essential for fusion. The complex is disassembled by NSF and α-Snap and SNARE are recycled for subsequent fusion events. Figure adapted from Rizo & Südhof 2002.

It is well established that specific sets of SNAREs promote different fusion events. The specificity for each fusion event is determined by the type of SNARE proteins involved as well as by tethering complexes (TC) and regulatory proteins belonging to RAB and Sec1/Munc18-1 (SM) protein families and others. The RAB and SM regulatory proteins contribute to selectively promote binding of specific SNAREs and actively participate in membrane fusion (for review Malsam et al. 2008, Rothman 2009). For example, lack of

Munc18-1 in neurons results in increased of undocked synaptic vesicles (Voets et al. 2001).

The small Ras-like GTPases, RABs, switch between a cytoplasmatic GDP-bound inactive conformation and a membrane associated active GTP-bound form (Hutagalung & Novick 2011, Mizuno-Yamasaki et al. 2012). In the active conformation, GTPases recruit a variety of effectors to mediate different functions. For instance, RABs are important for cargo selection, vesicle budding, coating and vesicle transport, vesicle docking and tethering at target membranes and eventually membrane fusion. To promote membrane fusion, RABs can either bind directly SNARE proteins or indirectly, through interaction with proteins that regulate SNARE function, such as SMs. RABs are required for fusion events in the majority of trafficking compartments; non functional GTP-bound RAB forms, depletion of RABs or inhibition of RAB function with specific antibodies prevent membrane fusion to the target compartment (Grosshans et al. 2006, Fukuda 2003).

The interaction between certain SM proteins and Syntaxins has been well characterized. SM proteins interact with Syntaxins through two mechanisms. SMs can bring the N-terminal domain of Syntaxins into close proximity with their C-terminal regions, blocking them in a closed conformation. This process has been described primarily for Munc18-1 in the regulation of Syntaxin1 (Syx1) at the plasma membrane (PM) (Dulubova et al. 1999, Misura et al. 2000). In particular, NMR analysis showed that in isolation, Syx1 adopts a "closed conformation" which correlates with inhibition of exocytosis. A mutation in Syx1 abolishing Munc18-1 binding disrupts the closed structure and results in lack of inhibition of exocytosis. Therefore, Munc18-1 negatively regulates vesicles exocytosis by blocking the activity of Syx1, possibly to prevent premature fusion events (Dulubova et al. 1999). Syx1 is then reactivated by regulatory components which are present on the membrane of the incoming vesicle. Alternatively, SMs can interact with the N-terminus and with part of the SNARE motif leaving the protein in an open conformation (Hu et al. 2010, Latham et al. 2007, D'Andrea-Merrins et al. 2007, Khvotchev et al. 2007, Carpp et al. 2006,

Dulubova et al. 2007). It is reported that SM proteins bind to Syntaxins also independently of fusion, to prevent Syntaxins degradation or formation of premature SNARE complexes (Toonen & Verhage 2007, Braun & Jentsch 2007).

Tethering complexes, including those containing SM proteins, are heterogeneous and fall into two categories: the long coiled-coil ones and the multisubunit complex proteins. Both dock the membrane of a vesicle and drive its binding to a specific target membrane. The specific intracellular location in the endo-membrane system of diverse classes of TCs is now well defined (for review Chia & Gleeson 2014). For example the exocyst complex is responsible for targeting post-Golgi secretory vesicles to the PM (Togneri et al. 2006); the COG (conserved oligomeric Golgi), the TRAPP (transport protein particle) and the GARP/VFT (Golgi associated retrograde protein) complexes regulate transport of Golgi vesicles between different Golgi Apparatus compartments (Ungar et al. 2006, Oka & Krieger 2005); the HOPS/class C Vps (homotypic fusion and vacuole protein sorting) complex and the partially overlapping CORVET complex helps vesicles to fuse with endosomes and lysosomes (Seals et al. 2000, Peplowska et al. 2007); p115, Golgins and early endosomal antigen 1 (EEA1) tether vesicles at the Golgi Apparatus and at endosomes (Sönnichsen et al. 1998, Christoforidis & Mcbride 1999). With the exception of the exocyst and the CORVET, the interaction of all complexes with SNARES has been documented.

Although SNARE complex formation is tightly controlled and a high degree of specificity is required for selective membrane fusion, it has been shown that in conditions in which SNAREs are not functional, compensation occurs. In some cases, SNAREs of the same subfamily provide a functional redundancy, while in others the RAB and SM proteins increase their activity to force membrane fusion even in absence of a SNARE in the trans-SNARE complex (Bethani et al. 2009).

2.1.2 SNARE proteins in Golgi Apparatus and Endoplasmic Reticulum network dynamics

Within cells, new membranes for organelle or vesicle formation originate in the Endoplasmic Reticulum (ER) and Golgi Apparatus. These compartments are constituted of membranes that are interconnected with tubules, and are in continuity with the Nuclear Envelope (NE) in the case of the ER, or form a ribbon of interconnected membrane stacks called cisternae, in the case of the Golgi Apparatus. The cisternae physically separate the Cis-Golgi-Network (CGN), which faces the ER, and the Trans-Golgi Network (TGN), which is polarized toward the PM (Glick 2000). At the ER, newly-synthesized proteins are packaged into Coated protein complex II (COPII) vesicles containing Syx18 and Syx17 which are then transported toward the Cis-Golgi in a process called anterograde transport (Miller & Schekman 2013, Steegmaier et al. 2000, Nogueira et al. 2014). Once at the Golgi Apparatus, cargoes transported in COPII vesicles are modified and sorted for transport to a specific intracellular compartment or to the PM. Proteins from the Golgi Apparatus can also be transported back to the ER via Coated protein complex I (COPI) vesicles (Figure 3) (Barlowe 1998). However, COPI-coated vesicles also function in the anterograde transport from the ER to Golgi Apparatus or from the Golgi Apparatus to the TGN (Bannykh et al. 1996, Rowe et al. 1996). The SNARE protein Syx5 is important to dock COPI vesicles to trans-Golgi membranes (Hay et al. 1997). SNAREs that mediate COPI vesicles trafficking have been identified in *S. cerevisiae* and include Sec22, which is involved in anterograde transport and the SNAREs Ufe1p, Use1p, and Sec20p that interact with a tethering complex called Dsl1 in yeast, which mediates retrograde transport from the Golgi apparatus to the ER (Flanagan & Barlowe 2006, Andag & Schmitt 2003, Kraynack et al. 2005, Ren et al. 2010, Tripathi et al. 2009). In mammals, the mammalian homolog of Ufe1p, Syx18, together with the SNARE p31, associates to the NRZ complex, which is structurally and functionally related to the yeast Dsl1 complex. Indeed the NRZ complex

also regulates retrograde transport of COPI vesicle toward the ER (Figure 9) (for review (Andag & Schmitt 2003).

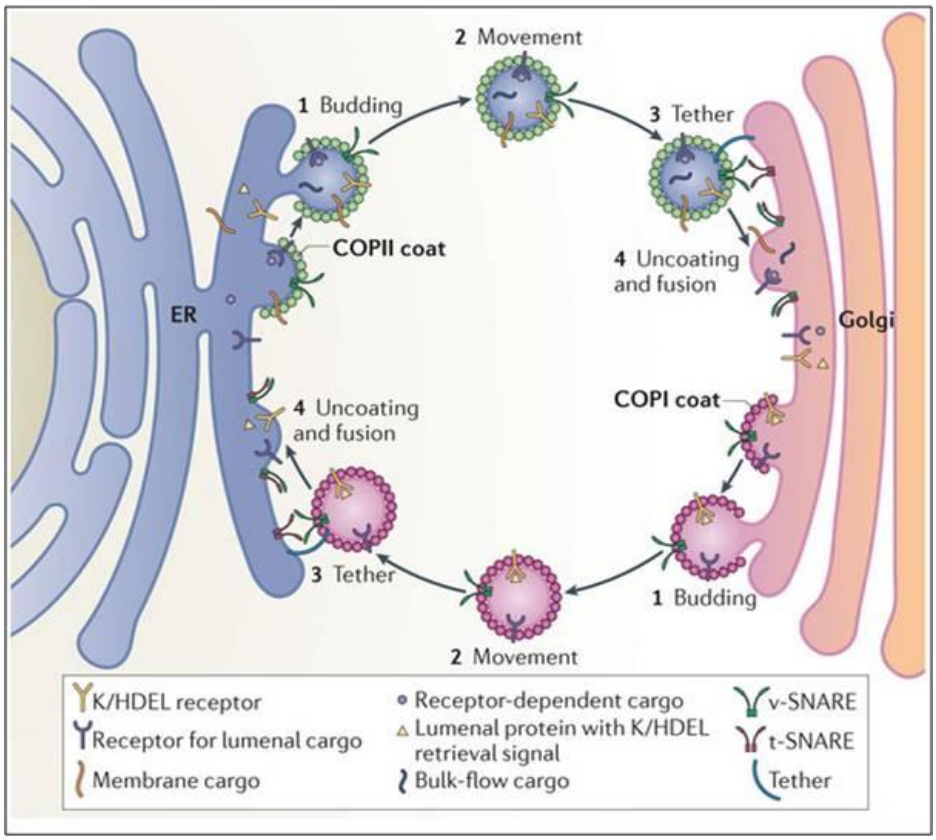

Figure 3. Vesicle transport at ER-Golgi apparatus**.** COPII coated vesicles originate from the ER and transport newly synthesized proteins toward the Golgi Apparatus (anterograde transport). COPI coated vesicles form at the CGN and are transported toward the ER (retrograde transport). Adapted from Brandizzi & Barlowe 2013.

As mentioned above, several SM and RAB proteins coordinate vesicles transport and fusion within the Golgi vesicles (for Review Sztul & Lupashin 2006). Among RAB effectors, GRASP55, GRASP65 and GOLGIN84 have a role in the stacking of Golgi cisternae to one another and in tethering of vesicles destined to fuse with the Golgi Apparatus (Short et al. 2001, Diao et al. 2003, Satoh et al. 2012, Puthenveedu et al. 2006, Shorter et al. 1999). However, different studies have showed that in mammals, *Drosophila* and *C. elegans*, depletion of the two isoforms of GRASPs does not cause alteration in cisternae organization or in vesicles secretion from the Golgi Apparatus (Lee et al. 2014,

Behnia et al. 2007, Puthenveedu et al. 2006, Short et al. 2001, Shorter & Warren 2002, Shorter et al. 1999). Consistent with this, plants have lost GRASP genes but the Golgi cistarnae are normally stacked (Hawes et al. 2010). However, GRASP proteins have been shown to be required for Golgi Apparatus fragmentation during mitosis in yeast and in mammalian cells (Colanzi et al. 2003, Short et al. 2001, Lin et al. 2001). Recently, GRASPs have also been proposed to regulate a Golgi Apparatus independent unconventional secretion which is discussed in detail below (Kinseth et al. 2007).

2.1.3 SNARE function in autophagy

Macroautophagy (autophagy hereafter) is a degradative pathway that is conserved among eukaryotes and is required for turnover of organelles and long-lived proteins (for review, Mizushima & Komatsu 2011, Xie & Klionsky 2007). Autophagy is regulated by three main serine/threonine kinases: AMP-K (AMP-activated protein kinase), mTOR (mammalian Target of Rapamycin) and Ulk1/2 (unc-51-like kinase 1/2), the two mammalian homologs of yeast Atg1 (Autophagy related protein 1) kinase (Egan et al. 2014). Autophagy negatively correlates with mTOR activation. Indeed, when mTOR is active, it phosphorylates and inhibits Atg1, which is essential for initiation of autophagy. However, in conditions of low energy, AMP-K inactivates mTOR, thus suppressing Atg1 phosphorylation. Atg1 is now free to phosphorylate Beclin1 which subsequently associates to Vps34, a Phosphatidyl Inositol 3 Kinase (PI3K), to activates autophagy. Vps34 is required for the production of Phosphatidyl Inositol triphosphate (PIP3) from Phosphate Inositide (PI) which provides phospholipids for *de novo* formation of autophagosome membranes (Funderburk et al. 2010, Zhong et al. 2009, Matsunaga et al. 2010). In yeast, the initiation of autophagy takes place at the so-called Phagophore Assembling Site (PAS), while in eukaryotes it occurs by the assembly of an isolated double membrane called phagophore which sequesters portions of cytoplasm. First, Atg13 and Atg17 associate with the phagophore. Then, Atg5 conjugates Atg12 to membranes and subsequently together

they interact with Atg16L1. After this event, Atg16L1 positive structures undergo a series of homotypic fusion events that expand the phagophore membrane (Moreau et al. 2011). When a double-membrane organelle, called autophagosome, is formed, LC3, the mammalian ortholog of yeast Atg8, is cleaved by Atg4 to generate LC3-I. LC3-I is then covalently conjugated to phosphatidylethanolamine (PE), thus generating a membrane associated form, known as LC3-II. This event triggers Atg12-Atg5-Atg16L1 complex disassembly. LC3-II positive autophagosomes are now ready to fuse the outer membrane with that of a lysosome and to release the content of the autophagosome into the lysosomal lumen, where it will be degraded (Figure 4).

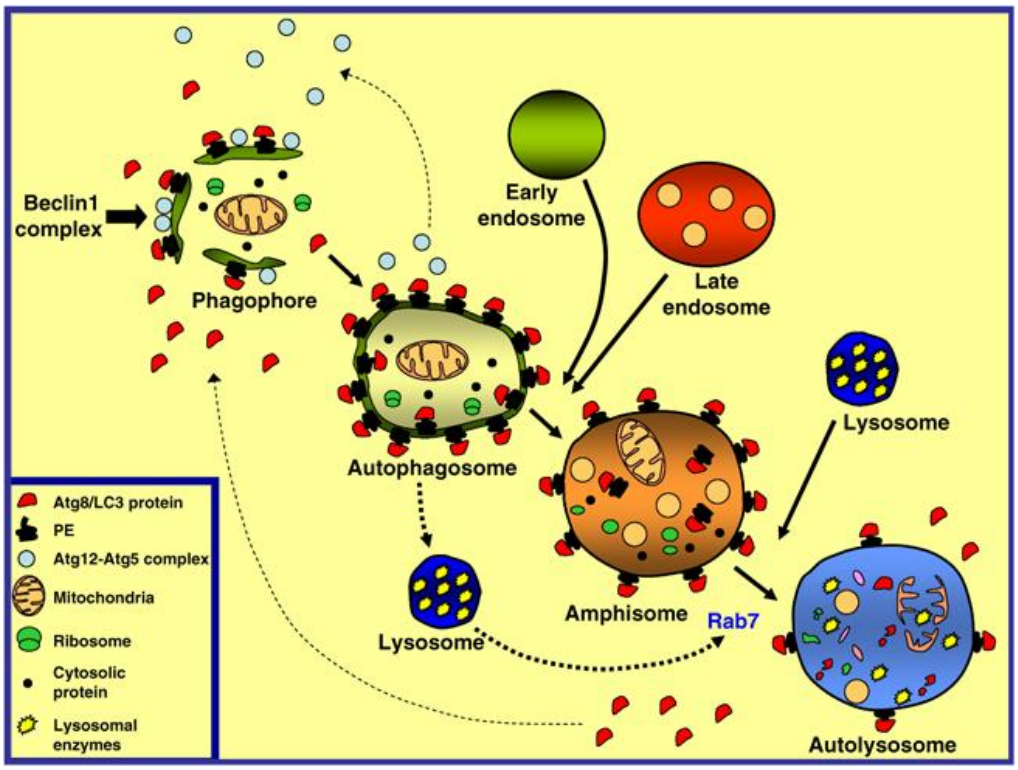

Figure 4. The autophagic cascade. Autophagic and endocytic pathways converge to lysosome for degradation. Figure adapted from Fader & Colombo 2009.

An aspect of the autophagy pathway that has come into focus very recently regards the origin of the membrane that generates the phagophore. Interestingly, amino acid starvation in mammalian cells induces the formation of a PI3P-containing ER-associated

compartment called Omegasome (Simonsen & Stenmark 2008, Matsunaga et al. 2010), which is proposed to provide membranes for autophagosome formation. In addition, under conditions of restricted calories, Atg proteins of the phagophore have been observed co-localize with markers of different intracellular trafficking compartments. In particular, in mammalian cells, Atg14 and Atg5 are found at ER-mitochondria contact sites (Hamasaki et al. 2013, Hailey et al. 2011, Hayashi-Nishino et al. 2009).

In addition, the Rubinsztein group described an association of Atg16L1 with Clathrin-positive endosomes, suggesting a further connection with plasma- or endosomal-membranes (Ravikumar, Moreau & Rubinsztein 2010). Finally, in yeast, it has been shown that the Golgi Apparatus is important to mediate phagophore expansion and indeed many proteins involved in trafficking of Golgi vesicles and in endocytosis are also required for autophagy initiation (Van der Vaart & Reggiori 2014). *Null* mutants of yeast SNAREs Sec22, Sec2, Sec4, Sso1, Sec9 and Tlg2, which are required for Golgi trafficking and endocytosis, show impairment of autophagosome formation and a failure to recruit Atg9-containing vesicles to the PAS (Holthuis et al. 1998, Geng & Klionsky 2010, Nair et al. 2011, Mari & Reggiori 2010, Reggiori et al. 2004). Importantly, over-expression of the R/vSNARE Ykt6, which is involved in Golgi secretion and in a number of vacuole fusion routes, rescues autophagosome formation defects in *Sec22* mutants, indicating that also Ykt6 is important for autophagy initiation (Nair et al. 2011). In mammals, Syx17 has been recently shown to control the early steps of autophagy and appears essential to recruit Atg14 and Atg5 at the ER-Mitochondria contact sites (Hamasaki et al. 2013). In addition, VAMP7, SYX7, SYX8 and Vtib have been proposed to participate to homotypic fusion at the phagophore and co-localize with Atg16L1 (Bonifacino & Glick 2004, Hong 2005, Moreau K 2011). When VAMP7-, SYX7-, SYX8- depleted cells are treated with Bafilomycin A1 to block lysosome activity, a decreased number of LC3II-positive vesicles is observed, suggesting that these SNAREs are all involved in autophagosome formation. Importantly, the R/v-SNARE Ykt6 in yeast, and the t-SNARE Syx17 in mammals have

been shown to regulate both autophagy initiation and fusion of autophagosomes with lysosomes. For the latter, in yeast Ykt6 forms a SNARE complex with Vam3 and Vam7, while Syx17 associates with VAMP8 and SNAP29 in mammals and with Snap29 and Vamp7 in *Drosophila* (Ungermann et al. 1999, Itakura et al. 2012, Takáts et al. 2013).

Autophagosomes can also fuse with the Multi Vesicular Body (MVB), a late endocytic compartment containing intracellular luminal vesicles (ILVs), to generate an organelle called amphisome (Figure 4). *In vitro*, it has been documented that autophagosomes require the SNARE Vtib to form an amphisome (Morvan et al. 2014), while in mammalian cells it has been shown that RAB11 on the membrane of the recycling/late endosomes collaborates with VAMP3 for the membrane fusion events that generate the amphisomes. In particular, it has been shown in mammalian cells that starvation or rapamycin treatment promotes fusion of autophagosomes with MVBs (Fader & Colombo 2009). Eventual fusion of amphisomes with lysosomes appears regulated by the v-SNARE VAMP7 and the GTPase RAB7 (Jäger et al. 2004).

2.1.4 Routes of conventional and unconventional secretion involving SNAREs

Exocytosis, also referred to as secretion, involves the transport of vesicles containing recycled or newly synthesized molecules from an intracellular compartment to the PM. Conventional secretion consists of the exocytosis of vesicles originating from the TGN or from Early Endosome (EE). In the former, vesicles contain newly synthesized molecules, while in the latter, the content is recycled, and the particular type of EE is called the Recycling Endosome (RE). RAB11 has been described as a master regulator of REs (Welz et al. 2014).

The best characterized SNARE complex functioning at the PM in conventional secretion is composed of the t-SNAREs Syx1 and Snap25, and of the v-SNARE Synaptobrevin (Syb1). This complex controls neurotransmitter release in neurons. In this

context, the fusion event is triggered at the PM by an increase of intracellular Ca^{2+} concentration controlled by the Ca^{2+} sensor Synaptotagmin1 (Rickman et al. 2004). In non-neuronal tissue, vesicle secretion is in contrast mainly regulated by the t-SNARE Snap23 and by Syntaxin 4 (Syx4) in addition to Syx1 (Ravichandran et al. 1996). Importantly, after fusion the v-SNAREs are retrieved back to the TGN and EEs by endocytosis.

Over the past years, examples of unconventional secretion have also been reported. Molecules transported by unconventional routes usually lack the signaling sequence for translocation into ER (Nickel & Rabouille 2009). This is the case of the Acb1 and AcbA proteins, which in *Dictyostelium discoideum* are secreted via a Golgi Apparatus independent process with the involvement of GRASP proteins (Kinseth et al. 2007). Importantly, it has been shown that Acb1 and AcbA co-localize at the ER with Sec13, in a region that has been named Compartment for Unconventional Secretion (CUS). A recent study in yeast identified Grh1, one of the autophagy initiating factors, as a regulator of unconventional secretion. Indeed, under conditions that promote Acb1 secretion, Grh1 co-localizes with Sec13. Although other proteins required for autophagosome formation at the PAS in yeast, such as Atg9 and Atg8, are present at the CUS, it has been shown that CUS and PAS biogenesis are independent, and that neither Atg9 or Atg8 participate in the assembly of CUS. In addition, in contrast to PAS biogenesis, the formation of a CUS is not promoted by rapamycin treatment (Bruns et al. 2011). Nevertheless, starvation induces localization of Atg5, Atg7, Atg8 and Atg12 at the CUS and correlates with secretion of Acb1 containing vesicles (Duran et al. 2010). Finally, CUS areas are enriched in PI3P and are positive for the ESCRT-I component Vps23 but not for components of Golgi membranes (Bruns et al. 2011). The t-SNARE Sso1/Syx1 is required to mediate fusion of Acb1 containing vesicles with the PM (Duran et al. 2010). In addition, Elecron Microscopy analysis reveals that CUS are formed by membrane structures resembling Omegasomes. Thus, it has been proposed that CUS is a site at which autophagosomes are indeed formed to be selectively delivered to the PM rather than to lysosomes. In agreement with this,

proteins that in yeast control fusion of autophagosomes with lysosomes appear dispensable for the transport or fusion of Acb1 containing vesicles (Bruns et al. 2011).

MVBs are implicated in an additional secretion route in which they fuse with the PM and release the ILVs (called exosomes) into the extracellular milieu (Kowal et al. 2014, Baixauli et al. 2014). Many different cell types secrete exosomes containing different cargos. For example, it has been reported secretion of MVBs containing miRNA or viruses (Mittelbrunn & Sánchez-Madrid 2012, Tamai et al. 2012, Mori et al. 2008). In mammals, it has been proposed that in conditions of induced autophagy, amphisomes could also fuse with the PM to secrete exosomes outside the cells (Fader & Colombo 2009). However, to date it is unclear which SNAREs mediate fusion of MVBs and amphisomes with the PM.

2.1.5 The SNARE protein SNAP29

The SNAP family is composed of Qb/Qc t-SNAREs and consists of four members in mammals, which are SNAP25, SNAP23, SNAP47 and SNAP29 (Figure 5). The best characterized member of the family is SNAP25, which mediates synaptic transmission in neurons. SNAP23 is the non-neuronal counterpart of SNAP25 and is mainly expressed in non-neural tissues to regulate exocytosis (Ravichandran et al. 1996, Polgár et al. 2003). SNAP47 and SNAP29 both lack the conserved cysteine residues present in SNAP25 and SNAP23 for palmitolylation, and both localize to a wide array of membrane compartments (Holt et al. 2006). SNAP47 and SNAP29 are also present in neurons. SNAP47 is enriched in synaptic vesicle fractions, where it has been proposed to act similarly to SNAP25. However, even though SNAP47 can be part of a SNARE complex with Syx1A and Syb2 *in vitro*, it is less efficient then SNAP25 in driving vesicle fusion (Holt et al. 2006). SNAP29 also interacts with Syx1A in rat neurons, but in contrast to SNAP47, it appears to act antagonistically to SNAP25. In fact, at synapses SNAP29 has been found to compete with α-SNAP during the disassembly of SNARE complex and consequently to down modulate

synaptic transmission (Su et al. 2001b). Consistent with this model, it has been demonstrated that over-expression of SNAP29 in murine pre-synaptic hippocampal neurons inhibits synaptic transmission, causing a defect in synaptic vesicles turnover. In agreement with these data, knockdown of SNAP29 in neurons increases the efficiency of synaptic transmission. This evidence suggests that SNAP29 acts as a negative modulator for neurotransmitter release possibly by negatively regulating recycling of the SNARE fusion machinery (Pan et al. 2005). In addition, SNAP29 contributes to myelin formation in oligodendrocytes by interaction with the GTPase, such as Rab34 and Rab25 (Schardt et al. 2009, Rotem-Yehudar et al. 2001). A negative role for SNAP29 has not been yet reported in non-neuronal tissue.

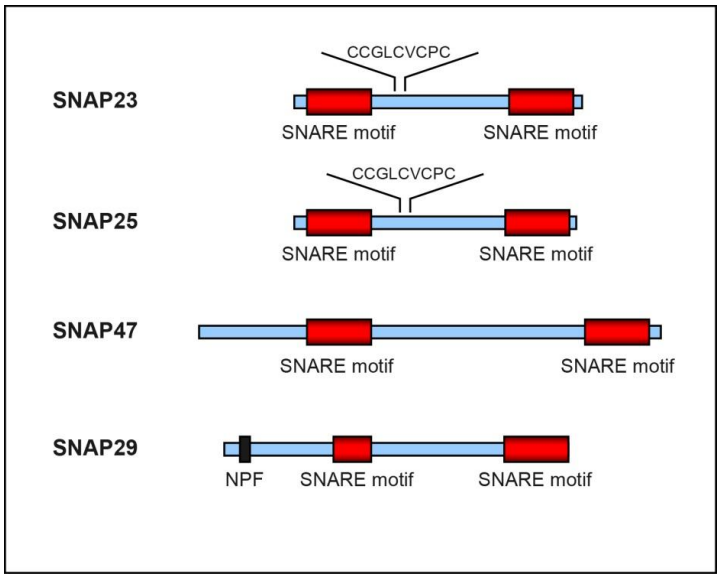

Figure 5. The SNAP protein family. All four members contain two SNARE motifs. SNAP29 and SNAP47 lack palmitoylation sites for membrane anchoring. In addition SNAP29 contains a NPF domain, which interacts with endocytic adaptors such as EHD1. Figure adapted from Rapaport et al. 2010.

In vitro, SNAP29 interacts with a large number of Syntaxins, localizes to multiple intracellular organelles, such as the PM, the EE and RE, and its lack causes alteration of these compartments (Steegmaier 1998, Rapaport et al. 2010). SNAP29 also localizes to the Golgi Apparatus. In particular, it has been shown that SNAP29 associates to the COG

subunits COG4, 6, and 8, and functions in the tethering of Golgi vesicles implicated in retrograde transport (Willett et al. 2013). Finally, SNAP29 has been reported to regulate endocytosis of the Insulin-like Growth Factor Receptor (IGF-1R). Unique among the members of the SNAP family, SNAP29 contains at its N-terminal, an asparigine-proline-phenylalanine (NPF) motif that binds the endocytic adaptor EHD1, and both proteins are present in complex with IGF-1R (Rotem-Yehudar et al. 2001).

Very recently, a requirement for SNAP29 in regulation of membrane fusion during autophagy has been reported in mammalian cells and *Drosophila* tissues (Itakura & Mizushima 2013, Itakura et al. 2012, Ding et al. 2014, Guo et al. 2014, Mizushima 2014, Takáts et al. 2013, Morelli et al 2014). It has been demonstrated that SNAP29 interacts with SYX17 and VAMP8 in HeLa cells and with Syx17 and Vamp7 (the homolog of VAMP8) in *Drosophila*. Itakura et al proposed that SNAP29, which is not anchored to any organelle, together with SYX17, localizes to autophagosome membranes while VAMP8 is on the lysosome membrane. When such SNARE complex forms, fusion between the two organelles occurs. SNAP29-depleted HeLa cells show an increase of LC3-I organelles, suggesting that mature autophagosomes accumulate in absence of SNAP29. Importantly, it has very recently been shown that SYX17/VAMP8/SNAP29 complex formation is enhanced when the activity of the O-GlcNAc transferase (OGT) is shut down. OGT is an enzyme that post-translationally modifies several proteins and its role in regulating autophagy is unknown. In both mammalian cells and *C.elegans*, OGT knock-down or OGT inhibition promote autophagosome formation and maturation. Interestingly, SNAP29 has been identified as the only autophagic protein modified by OGT. Importantly, when OGT is depleted or is not functional, SNAP29 is not modified and its ability to bind SYX17 and VAMP8 increases (Guo et al. 2014). In agreement with this evidence, a recent publication showed that SNAP29 binding to Syx17 is blocked by the viral Phoshoprotein (P) expressed by the Human ParaInfluenza Virus type 3 (HPIV3), which replicates within autophagosomes. The P protein specifically binds the SNARE motifs of SNAP29

suppressing its ability to form a SNARE complex. Thus, HPIV3 infected cells display accumulation of autophagosomes (Ding et al. 2014).

Importanly, Snap29 controls endocytic recycling, protein secretion and autophagy also in *C. elegans* (Sato et al. 2011b, Kang et al. 2011).

Loss of function mutations in the human SNAP29 gene cause CEDNIK (CErebral Dysgenesis, Neuropathy, Ichthyosis, and palmoplantar Keratoderma), an inherited autosomal recessive syndrome. The two reported SNAP29 mutations associated with CEDNIK introduce frame-shifts leading to premature truncations of the SNAP29 protein (Sprecher et al. 2005, Fuchs-Telem et al. 2011). It has been shown that fibroblasts derived from CEDNIK patients display impairment of the endocytic pathway and defects in the morphology of EE and Golgi Apparatus. An impairment of β-integrin recycling was also observed (Rapaport et al. 2010). A SNAP29 depleted *Danio rerio* (Zebrafish) line has been also proposed as a model for CEDNIK syndrome. In such animals, keratinocytes do not develop properly and generate an epidermis with altered architecture, characterized by spicule-like protrusions. Intracellularly, keratinocytes accumulate empty vacuoles, suggesting the existence of a defect in vesicle trafficking (Li et al. 2011a). However, the contribution of these altered processes in the pathogenesis of CEDNIK is unclear.

In *Drosophila*, the Snap family consist of three members, Snap25, Snap24 (the Snap23 homolog) and Snap29. As in mammals, Snap25 is mainly found in neurons, while Snap24 and Snap29 are ubiquitously expressed. Loss of function mutations in the *Snap25* gene are associated with severe neurological defects and *Snap25 null* mutants die at the pharate adult stage, due to impairment of synaptic transmission (Vilinsky et al. 2002). In contrast, it has been shown that Snap24 exerts a major role in salivary glands, where it mediates secretion of granules during the massive exocytic events that occur during glue secretion (Niemeyer & Schwarz 2000). Interestingly, a certain degree of redundancy exists between Snap25 and Snap24. Under physiologic conditions, Snap24 is not sufficiently expressed in neurons to support neurotransmission activity in Snap25 *null* mutants. However, upon

ectopic over expression of Snap24, neurotrasmission is restored and adult lethality is rescued (Vilinsky et al. 2002).

2.2 Trafficking and mitosis

2.2.1 The cell cycle and the onset of mitosis

In eukaryotic cells, the cell cycle is divided in four stages: G1, S, G2 (Interphase) and mitosis (M) (Figure 6). During G1, cells grow and synthesize proteins necessary for DNA replication, which occurs in the subsequent S phase. During G2, cells continue to grow and start to express proteins necessary for cell division. At the final stage of G2, the cytoskeleton and intracellular organelles are subjected to global re-shaping to allow the initiation of the M phase. The M phase is composed of two events: mitosis (segregation of sister chromatids) and cytokinesis (cell division) (Blow & Tanaka 2005). The cell cycle is regulated by cyclin-dependent kinases (CDKs). Distinct CDKs are expressed at different phases to promote formation and activation of different cyclin-CDK complexes. In brief, cyclin D-CDK4/6 enables G1 progression; Cyclin E/A-CDK2 initiates DNA replication and centrosome duplication; Cyclin A/B-CDK1 triggers mitotic entry while cyclin B-CDK1 also controls mitotic progression (Garrett et al. 2001; Sullivan & Morgan 2007).

Mitosis consists of four phases: prophase, metaphase, anaphase and telophase (Figure 6). During prophase, the chromatin is packed into well-defined structures called chromosomes, formed by two sister chromatids joined at a contact site known as the centromere. The centromeric region works as an anchoring platform for the kinetochore (KT), a multiprotein structure required for attachment of microtubules (MTs) for subsequent chromosomes segregation (Cheeseman 2014; Cheeseman & Desai 2008). At the onset of prophase, cytoskeleton, nucleus and trafficking compartments re-organize to allow the formation of the mitotic spindle and for subsequently separation into the two daughter cells (for review Jongsma et al. 2014). New MTs originate around centrosomes in

structures called asters to promote Nuclear Envelope Breakdown (NEBD) (Burke & Ellenberg 2002). Then, while centrosomes migrate to opposite poles, MTs emanating from asters start to catch chromosomes by interacting with their KTs. Some MTs contact KTs (k-fibers), while others extend towards the opposite pole (interpolar MTs). When each chromatid is correctly attached to MTs derived from opposite poles (bi-orientation attachment), metaphase occurs and tension exerted by MTs on KTs of sister chromatids is required to maintain chromosomes align at the metaphase plate (Musacchio & Hardwick 2002).

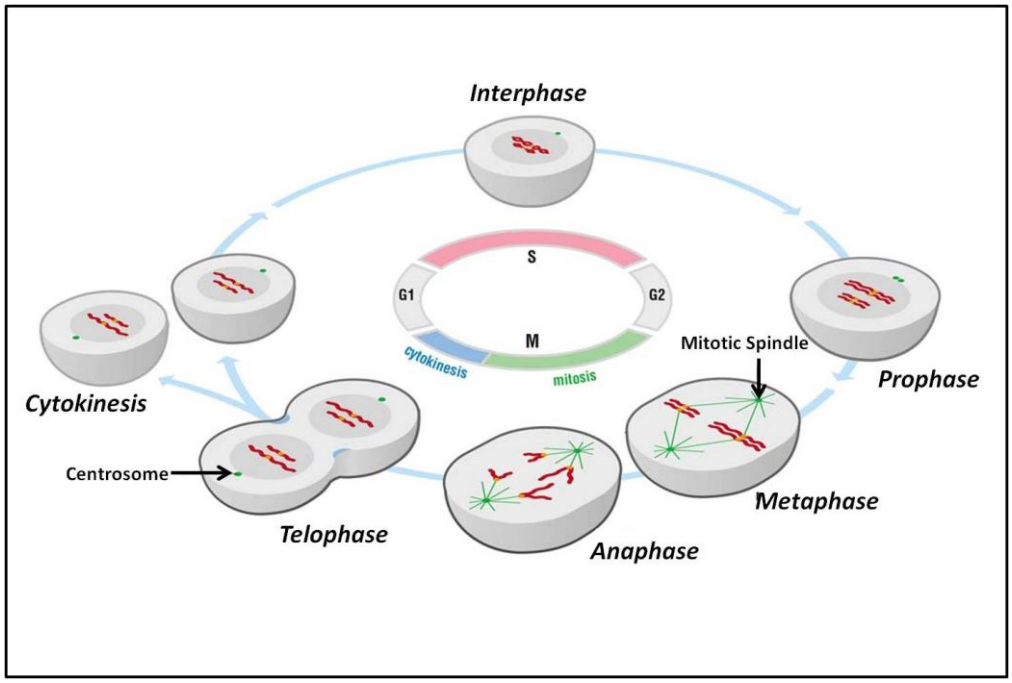

Figure 6. The cell cycle and the phases of mitosis. Chromatids are depicted in red, KT in yellow and the mitotic spindle and centrosomes in green. The figure is adapted from "the cell cycle" by David O. Morgan.

Metaphase to anaphase transition is regulated by a multiprotein complex known as "Spindle Assembly Checkpoint" (SAC), which ensures that sister chromatids segregate only when each KT is properly attached to MTs (Foley & Kapoor 2013; Musacchio & Salmon 2007). Anaphase is further divided into anaphase A and B. Respectively, during anaphase A k-fiber shrinkage causes the approach of chromosomes to spindle poles, while

during anaphase B interpolar MTs movement promotes mitotic spindle elongation enhancing sister chromatids separation (Brust-Mascher et al. 2004). The telophase is the last stage of mitosis and occurs when the chromatin re-condenses and the NE reforms around the two daughter nuclei. During this stage, MTs re-organize in a thick beam in between daughter nuclei called central spindle. This structure will mediate the distribution of the cytoplasm into daughter cells, a process known as cytokinesis. In particular, cytokinesis requires the formation of an actin-myosin-II ring positioned at the cell equator. The contraction of the ring causes formation of a deep bottleneck at the center of dividing cell, leading to abscission, which determines the final separation of the two daughter cells (Agromayor & Martin-Serrano 2013).

2.2.2 Endoplasmic Reticulum dynamics and Nuclear Envelope Breakdown

In organisms that divide by open mitosis, the Nuclear Envelope (NE) is disassembled at early prophase to allow capturing of chromosomes by MTs. The NE is formed by an Outer Nuclear Membrane which is in continuity with the ER and an Inner Nuclear Membrane (ONM and INM) both of which hold the Nuclear Pore Complexes (NPCs), whose main function in interphase is to transport molecules inside and outside the nucleus. The INM houses proteins that make contact with the chromatin and the nuclear lamina, and is mainly constituted by LaminA and LaminB polymers (Figure 7) (Güttinger et al. 2009; Burke & Ellenberg 2002).

The initiation of NEBD is controlled by different kinases. CDK1 is directly involved in phosphorylation of Lamins and mutations in LaminA and B phosphorylation sites lead to a block in nuclear lamina disassembly (Heald, R. & McKeon, 1990). Some nucleoporins are also phosphorylated by CDK1 (Favreau et al. 1996; Glavy et al. 2007; Blethrow et al. 2008). The M-phase Promoting Factor (MPF) kinase $p34^{Cdc2}$ has also been shown to phosphorylate nulear lamins and nucleoporins (NUP) (Collas 1999, Favreau et al. 1996).

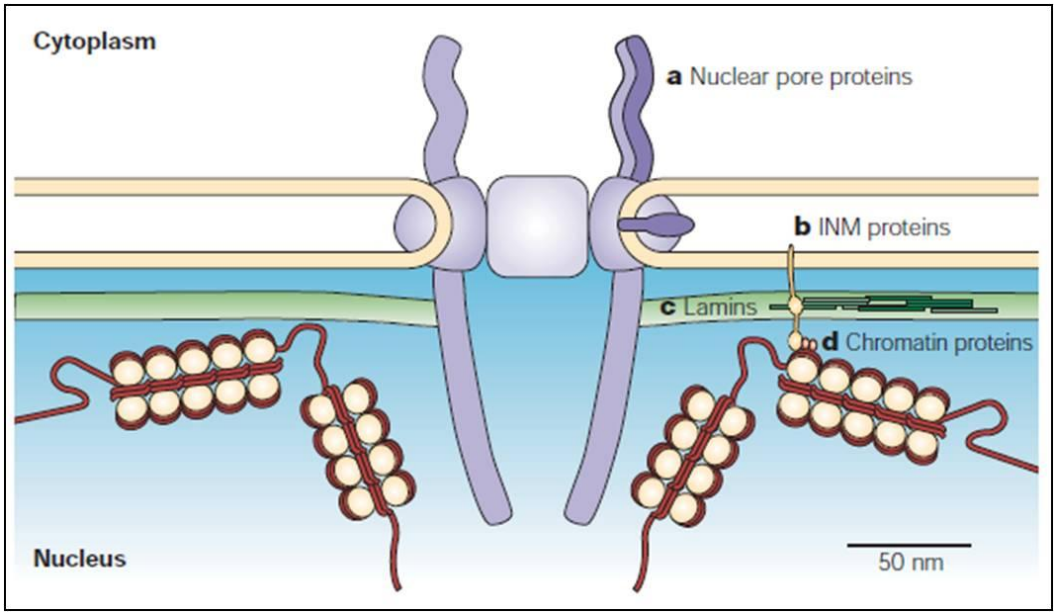

Figure 7. Nuclear Envelope (NE) organization. Adapted from Burke & Ellenberg 2002.

Protein kinase C (PKC), Aurora B and Polo-like kinase 1 (PLK1) contribute to NEBD in multiple species but little is known about their targets. Upon phosphorylation, Lamins depolymerize and NPCs become unstable and disassemble.

The other essential mechanism for NEBD depends on newly formed MTs elongating from asters and attaching to the ONM. This event, together with the fact that centrosomes initiate to move toward cell poles, exerts forces causing the invagination of the NE in proximity of centrosomes (Salina et al. 2002, Mühlhäusser & Kutay 2007). These processes are mediated by the motor protein dynein (Salina et al. 2002). Invagination of NE and detachment of NPCs causes interruptions in the ONM and INM, which contribute to destabilize the NE and LaminA/B depolimerization (Figure 8).

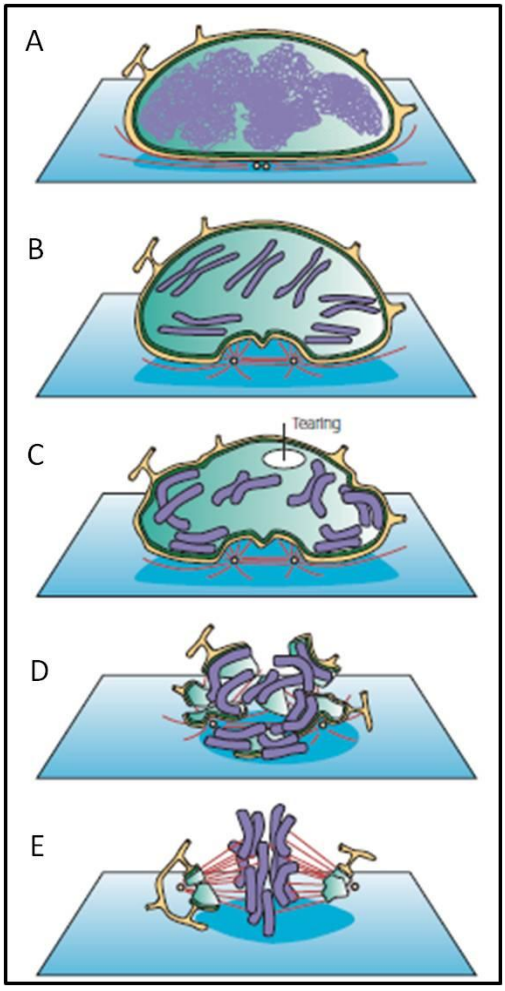

Figure 8. Nuclear Envelope (NE) disassembly in mammalian cells. (A) The nucleus in interphase is surrounded by the NE (green) which is in continuity with the ER (yellow). (B) During early prophase the newly formed centrosomes originate MTs and induce NE invagination. (C) Centrosome and protofilaments movements exert pulling forces on the surface of the nucleus inducing the formation of internal holes. (D) ONM, INM and Nuclear lamina depolymerize and NPCs re-localize at the ER membrane or at KTs. Then, MTs anchor KTs of chromosomes. (E) ER tubules remain in proximity of chromosomes and spindle poles till the onset of anaphase, when NE components start to organize for NE reassembling. Adapted from Burke & Ellenberg 2002.

Some eukaryotes, such as *Drosophila* and *Thricomonas vaginalis* respectively, divide with a semi open and closed mitosis. In these organisms, the NE remains partly or fully intact and the MTOC assembles directly on, or in close proximity of the NE. In *Thricomonas vaginalis* chromosomes attach directly to NE with their KTs (Kiseleva et al. 2001, Gómez-Conde et al. 2000), while in other organisms which divide

through a closed mitosis, such as *S. cerevisiae*, the spindle is formed inside the nucleus (McIntosh & O'Toole 1999).

It is still debated how NE membranes are organized during mitosis. Evidence in Xenopus embryos indicate that the NE fragments in vesicles which are spread throughout the cell, while studies in mammalian cells suggest that NE proteins are incorporated within the ER membranes which remain intact during mitosis (Vigers 1991, Ellenberg et al. 1997, Daigle 2001, Yang et al. 1997). Importantly, NE re-shaping correlates with association of NUP with KTs and with the mitotic spindle. In addition, NUPs have been reported to actively function in diverse mitotic events. For example, the RNA export1 (RAE1) is in complex with NUP98 during interphase for RNA export and during mitosis interacts with NuMA (Nuclear Mitotic Apparatus protein) to regulate spindle formation (Powers et al. 1997, Pritchard et al. 1999, Blower et al. 2005). The NUP107-160 complex is found in proximity of the mitotic spindle and its depletion correlates with prolonged pro-metaphase, defects in chromosome congression and a delay in anaphase onset (Zuccolo et al. 2007). Although the molecular mechanism is not completely clear, lack of NUP107-160 destabilizes KT-MT attachments by preventing KT recruitment of CENP-F, which is involved in a dynein-dependent MTs attachment (Zuccolo et al. 2007). In addition, for unknown reasons, also the SAC proteins Mad1-Mad2 and their regulators Mps1 and $p31^{comet}$ resides at NPCs during interphase and at KT during mitosis (Tighe et al. 2008).

2.2.3 Golgi Apparatus fragmentation at the onset of mitosis

Golgi Apparatus fragmentation at the onset of mitosis occurs in two sequential steps. During prophase, the pericentriolar Golgi stacks break down into smaller pieces forming the so-called Golgi blobs, a process regulated by MAPK kinase 1 (MEK1) and PLK1 (Acharya et al. 1998; Colanzi et al. 2003). Subsequently, in between metaphase and

anaphase the Golgi blobs are subjected to a further fragmentation, which generates small vesicles dispersed in the cytoplasm, known as mitotic Golgi haze (Nelson 2000). Over the past years, several groups have focused in understanding if Golgi hazes associate or are absorbed into the ER during mitosis (Zaal et al. 1999; Shima et al. 1997; Jesch et al. 2001; Prescott et al. 2001; Colanzi et al. 2000). Golgi fragmentation has been considered a mechanism for equal partitioning of the Golgi Apparatus into daughter cells. However, it has been demonstrated that Golgi Apparatus fragmentation is also necessary for entering mitosis. In fact, block of GRASP65 activity, not only impedes Golgi Apparatus fragmentation but also arrests cells in G2, suggesting the existence of a DNA-independent mechanism to initiate mitosis (Sutterlin et al. 2002). Consistent with these observations, some Golgi resident proteins play a role during mitosis. For example, *in vitro* assays with Xenopus Laevis extracts showed that proteins important for the formation of COPI vesicles contribute to NEBD, although this has not been proven *in vivo* (Cotter et al. 2007). In addition, ZW10, a component of the RZZ complex at the outer KT, is required for retrograde transport of COPI vesicles in interphase. In particular, at the Golgi Apparatus ZW10 assembles in the NRZ complex, composed of RINT1 (Rad50-interacting protein), NAG (neuroblastoma-amplified gene) and the SNAREs Syx18 and p31 (Andag & Schmitt 2003).The yeast counterpart of the NRZ complex is Dsl1 complex. It is constituted by the homolog of ZW10, Dsl1p which interacts in a tight complex with Tip20p, the homolog of RINT1, with sec39, structural and functional related to NAG and with the SNAREs Ufe1p (the yeast Syx18), Use1p, and Sec20p (Whyte & Munro 2002). Both in yeast and higher eukaryotes, these complexes are involved in COPI vesicles retrograde transport from the Golgi Apparatus to the ER (Figure 9) (Arasaki et al. 2006; Hirose et al. 2004; Sun et al. 2007; Andag & Schmitt 2003; Kraynack et al. 2005; Ren et al. 2010; Tripathi et al. 2009).

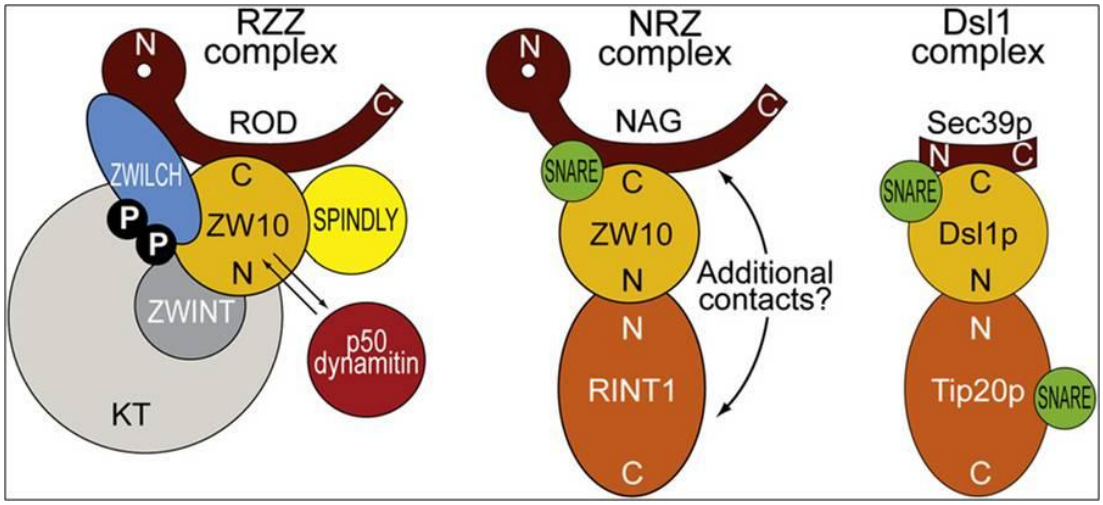

Figure 9. RZZ and NRZ in mammals assemble at the outer KT and at COPI coated vesicles respectively. The yeast Dsl1 complex is structurally and functionally related to the NRZ complex. To note, ZW10, the mammalian counterpart of Dsl1, is found in all the three complexes. Adapted from Civril et al. 2010.

2.2.4 Formation of the mitotic spindle

In most vertebrate cells, the formation of the mitotic spindle is mainly driven by the centrosomes, which serve as MT-organizing center (MTOC). Centrosomes are formed by two centrioles. Each centriole consists of nine triplets of MTs organized to form a cylinder. The two centrioles are positioned perpendicularly to each other and are immersed in the so called periocentriolar material (PCM). A key component of the PCM is the γ-tubulin ring complex (γTuRC), which contains a special version of tubulin called γ-tubulin. γ-tubulin ring structures provide anchoring for the minus-end of MTs (Moritz et al. 2000). A single MT is formed by 13 parallel protofilaments constituted by heterodimers of α- and β-tubulin, which organize to form a cylinder. Protofilaments maintain a polarized structure with α-tubulin and β-tubulin at the opposite ends. In particular, β-tubulin is exposed to the plus-end, which polymerizes quickly, while α-tubulin localizes at the minus-end, which instead polymerizes slowly. γ-tubulin rings at centrosomes specifically anchor the minus-ends of each protofilament while the plus-ends orientate toward the cytoplasm. At the plus-end, MTs are continuously polymerized and depolymerized in a process called “dynamic

instability", which is regulated by GTP/GDP loading on β-tubulin. In particular, GTP attached to β-tubulin is hydrolyzed each time an α/β tubulin heterodimer is added at the plus-end of a filament. As a consequence, α/β tubulin heterodimers are bound to GDP for the entire length of a MT, with the exception of the plus-end, which is associated with GTP**.** On the contrary, when a MT needs to depolymerize, the GTP at the plus-end is hydrolyzed without adding any heterodimer, a mechanism necessary for MTs shortening (Figure 10) (Cheeseman & Desai 2008, Kline-smith & Walczak 2004).

It has been demonstrated that in organisms or cells lacking centrosomes, MTs nucleation originates at the level of centromeres and KTs in a process named inside-out spindle formation (Maiato et al. 2004). In this context, chromatin mediates the formation of an acentrosomal spindle by recruitment of the GTPase RAN and the GEF (Guanine Nucleotide Exchange Factor) RCC1, creating a gradient of Ran-GTP with higher concentration around the chromosomes than in the cytoplasm (Karsenti & Vernos 2001; Carazo-salas et al. 2001; Gadde & Heald 2004; Bastiaens et al. 2006). Ran-GTP allows the import of factors necessary for MTs nucleation such as NuMA and TPX2 (Ems-mcclung et al. 2004). Subsequently, dynein and kinesin regulate MTs orientation. Newly formed MTs are not oriented. Only later-on minus-ends are exposed toward the cell poles, where they are anchored by regulatory proteins such as Asp and NuMa (Khodjakov et al. 2000). Recent studies show that MTs nucleation from chromatin exists also in cells containing centrosomes. Indeed, the mitotic spindle can be generated also if centrosomes are removed by microsurgery or if their formation is suppressed using mutants or depleting essential components of centrosomes. For example in *Drosophila* neuroblasts or ganglion mother cells mutant for *asterless*, a protein that regulate centrosomes formation, the mitotic spindle forms in absence of spindle poles bodies (Bonaccorsi et al. 2000). It has been reported that Ran-GTP is also able to activate γ-TuRC at centrosomes. In this study, it has been found that depletion of GCP-WD, a component of γ-TuRC, abrogates spindle

formation completely, suggesting that the protein is part of the γ-TuRC both at centrosomes and centromeres (Lüders et al. 2006).

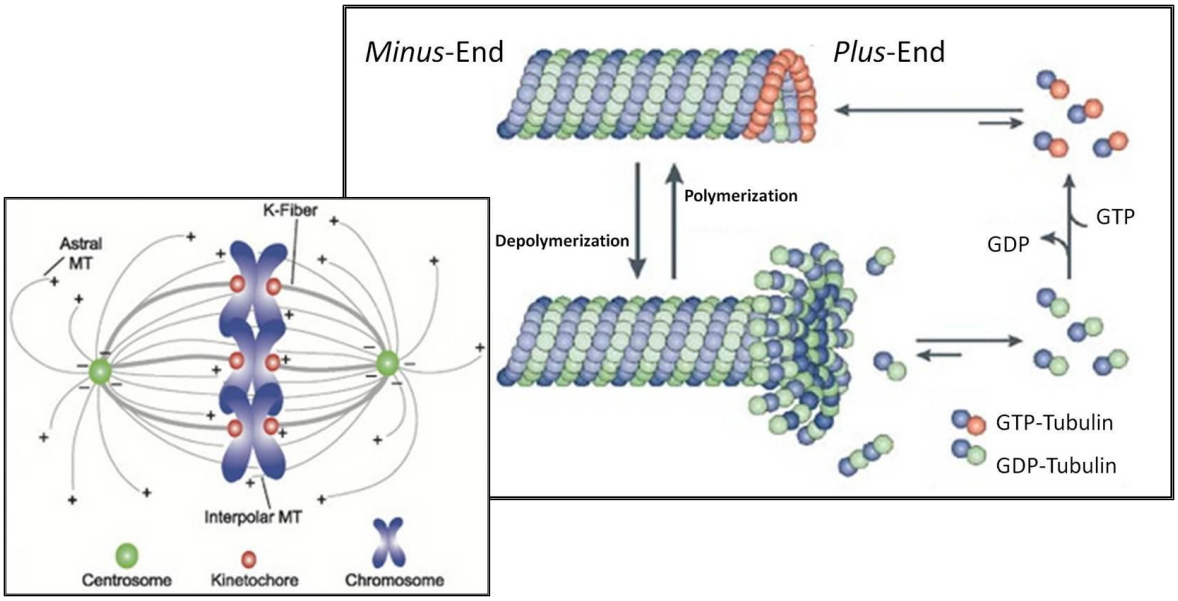

Figure 10. Polarized k-fibers in the mitotic spindle are oriented with plus-ends at KTs and minus-ends at spindle poles (left). Adapted from (Cheeseman & Desai 2008). GTP-bound tubulin promotes MT polymerization while, GDP-bound tubulin leads to MT deploy merization (right). Adapted from Kline-smith & Walczak 2004.

2.2.5 Chromosomes movement by MT motor proteins

Spindle orientation and chromosomes movement along the mitotic spindle are all regulated by motor proteins. They are divided into two classes: the kinesins, which move toward MT plus-ends (with the exception of Kinesin 14), and cytoplasmic dynein that together with the adaptor dynactin moves toward the MT minus-ends (Gatlin & Bloom 2010, Kardon & Vale 2009). Both kind of motor proteins act as dimers and contain residues for dimerization, a motif to anchor MTs, and an ATP-binding site. Some of the functions of the motor proteins involved in mitosis are the following: The kinesin-5/BimC family (Eg5 in human) controls spindle pole separation (Gadde & Heald 2004, Gatlin & Bloom 2010); the kinesin-14 (HSET in human) a minus-end-directed kinesin, is important to direct MT minus-ends toward spindle poles (Mountain et al. 1999; Sharp et al. 2000); the kinesin-10

(chromokinesin Kid in human) is required to push chromosome arms towards the equator (Levesque & Compton 2001); CENP-E localizes at KTs and transports mono-oriented chromosomes to the metaphase plate (Guruharsha et al. 2011, Kapoor et al., 2006); the kinesin Kif18a, localizes to the plus-ends at KT-MTs attachment sites and promotes chromosome congression by depolymerizing k-fibers (Mayr et al. 2007; Stumpff et al. 2009).

2.2.6 The KT structure and formation

The KT is a large multiprotein structure assembled on centromeric chromatin that allows the interaction between chromosomes and mitotic spindles during cell division. In particular, the KT can be divided into two main regions called inner and outer plates. In mammals, the inner plate is constituted by CENP-A, a centromere specific Histone H3 variant (CID in *Drosophila*) and the CCAN (Constitutive Centromere Associated Protein Network) proteins (Foltz et al. 2006; Izuta et al. 2006). CENP-A binds centromeric DNA throughout the cell cycle and at early prophase recruits CCAN proteins to allow the formation of the inner KT platform. The CCAN complex comprises CENP-A, CENP-M, CENP-N, CENP-T, CENP-C, CENP-U, CENP-I, CENP-L, CENP-O, CENP-P, CENP-K, CENP-R, CENP-Q AND CENP-S (Foltz et al. 2006, Okada et al. 2006). The exact function of all these proteins is debated. It has been proposed that CENP-T together with CENP-C might act as a platform for anchoring outer KT complexes (Gascoigne et al. 2012, Petrovic et al. 2010). In *Drosophila* the CCAN complex is not present and the only conserved centromeric-bound protein is CID, the homolog of CENP-A, which together with CENP-C mediates the recruitment of outer KT components (Figure 11) (Blower & Karpen 2001).

The outer kinetochore platform is instead important to anchor MTs and is constituted by three main complexes, the Mis12, Knl-1 (Spc105 in *Drosophila*) and Ndc80 complex,

which together are known as KMN network (Cheeseman & Desai 2008). In mammals, but not in *Drosophila*, KNL-1 anchors ZWINT-1 (ZW10 interacting protein). The KMN network forms a bridge between the inner region at the KT and the so-called fibrous corona which contains the proteins of the RZZ complex ROD, ZW10 and ZWILCH, the regulators of the SAC MAD1, MAD2, BUB1, BUBR1, BUB3, MPS1, the motor protein adaptor Spindly, PLK1, which regulates MTs attachment and finally a number of MTs Associated Proteins, MAPs (Van Hooser & Heald 2001, Wigge & Kilmartin 2001Cheeseman & Desai 2008, Liu et al. 2006, DeLuca et al. 2003).

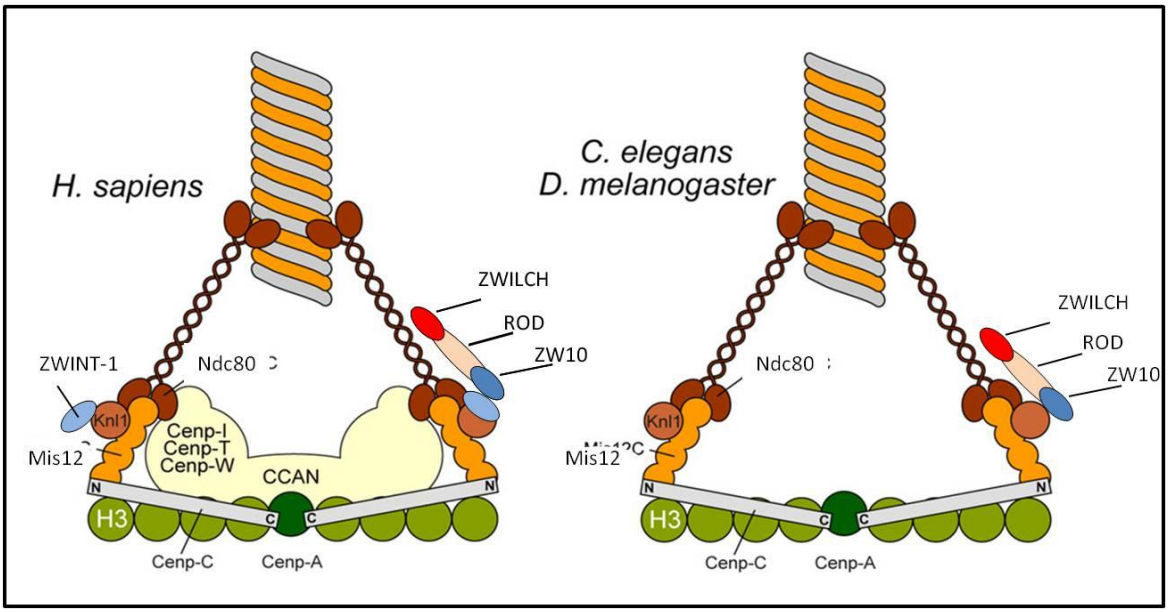

Figure 11. Schematic of the main components of inner and outer KT plates in *H.Sapiens* and *D. melanogaster*/*C.elegans*. In *Drosophila* the RZZ complex is present, but it is not known which proteins anchor it to the KT outer plate. Adapted from Screpanti et al. 2011.

2.2.7 The outer KT plate and KT-MT attachment

One of the key function of KTs is to provide a platform for MTs anchoring. Initially, MTs interact with KTs laterally and then, the lateral attachments are converted into ends-on attachments. Importantly, KTs are able to maintain the ends-on attachment by continuously polymerizing and depolymerizing MTs, a phenomenon called load-bearing attachment

(Santaguida & Musacchio 2009; Tanaka & Desai 2008). Impairment of any of the KMN members, by RNAi-mediated depletion or antibody microinjection, results in severe attachment defects, which are referred as KT-*null* phenotype (Cheeseman et al. 2004, DeLuca et al. 2005, Desai et al. 2003, Kline et al. 2006, Vorozhko et al. 2008).

The players of the KT-MT attachment are the Mis12, Ndc80, SKA complexes and Knl-1/ZWINT-1.

The Mis12 complex, in mammals is composed of four subunits, namely MIS12, MIS13/DSL1, MIS14/NSL1 and NNF1. Although the Mis12 complex itself does not directly bind MTs, it serves as a scaffold to support the entire KMN network with MIS13/DSL1 and MIS14/NSL1 interacting respectively with KNL-1 and the SPC24-SPC25 dimer of Ndc80 complex (Cheeseman et al. 2006, Kline et al. 2006, Petrovic et al. 2010). The MIS12 complex also binds directly to centromeric proteins, such as CENP-C, providing a direct linkage between outer and inner KT components (Screpanti et al. 2011). As in mammals, the *Drosophila* Mis12 complex is important to stabilize the Ndc80 complex to the inner KT plate via Cenp-C and it is composed of five subunits which include Mis12, Nnf-R1,Nnf-R2, Nsl-1 and Dsl-1 (Przewloka et al. 2007).

The Ndc80 complex, is well-conserved in yeast, *Drosophila* and mammal and is constituted in mammals by four proteins: HEC1 (Ndc80 in *Drosophila*), NUF2, SPC24 and SPC25. HEC1 with NUF2 and SPC24 with SPC25 form two heterodimers that associate to KTs before the NEBD (Wang et al. 2008). The Ndc80 complex extends across the inner and outer KT plate and is organized in a long coiled-coil region that separates two globular domains at each extremity of the complex (Figure 12) (Ciferri et al. 2005, Ciferri et al. 2008, Kim et al. 2011, Joglekar & DeLuca 2009).

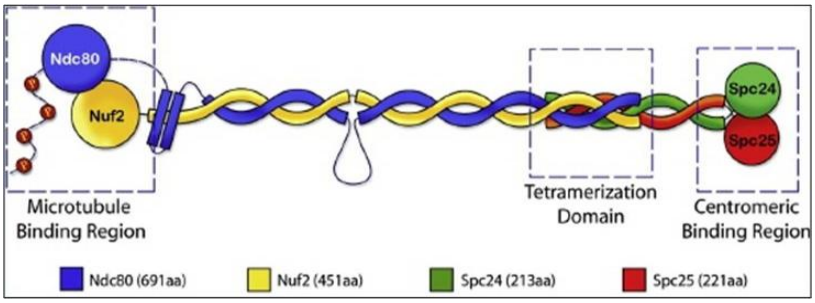

Figure 12. The structure of the Ndc80 complex. Adapted from Wang et al. 2008.

KNL-1, is a large multidomain and multifunctional scaffolding protein that recruits several outer KT proteins. Indeed, via its N-Terminal domain, KNL-1 directly interacts with ZWINT-1, the SAC proteins, Bub1 and BubR1, and with CENP-F, a centromeric protein which acts mainly in regulation of MT-KT binding (Liao H 1995, Ma L 2006). In *C.elegans*, it has been shown that Knl-1 recruits also the Ndc80 and RZZ complexes (Cheeseman et al., 2008, Essex et al., 2009, Gassmann et al., 2008). However, evidence in mammals demonstrate that KNL-1 is not necessary for NDC80 complex recruitment (Cheeseman et al., 2008, Kiyomitsu et al., 2007). In *in vitro* binding assays, KNL-1 weakly associates to MTs. However, *in vivo* in *C. elegans*, it has been demonstrated that mutants lacking the first 500 residues of Knl-1 display alteration in MT-KT binding, with MT binding predicted to occur in the nine residues at the N-terminus of the protein (Espeut et al., 2012). Consistent with this evidence, depletion of KNL-1 is associated with formation of unstable k-fibers and chromosome mis-segregation (Cheeseman et al., 2008, Kiyomitsu et al., 2007, Schittenhelm et al., 2009). In *Drosophila*, the KNL-1 homolog Spc105 has a prominent role in binding MTs. Depletion of Spc105 in S2 cells disrupts lateral KT-MT attachment, while *in vivo* MT-KT interactions are partially functional allowing movement of chromosomes toward the spindle poles (Feijao T 2013). In agreement with the evidence in mammals, Spc105-depleted *Drosophila* cells do not activate the SAC due to defects in SAC protein localization to KTs (Feijao T 2013).

In mammals, KNL-1 binds ZWINT-1, which has been initially identified in yeast as a ZW10 interacting protein (Petrovic 2010). Subsequent studies revealed that ZWINT-1 binds both ZW10 and HEC1 (Ndc80 in *Drosophila*) through its N-terminal domain (Lin et al., 2006, Wang et al., 2004), while it interacts with KNL-1 partly through its coiled-coil motif and the C-terminal domain (Wang et al., 2004). Recently, ZWINT-1 has been identified as a substrate for the kinase AURORA B (Kasuboski et al., 2011). According to this study, ZWINT-1 phosphorylation is important for RZZ complex recruitment (Kasuboski et al., 2011). One of the major function of RZZ complex is to bind the SAC proteins MAD1 and MAD2. Thus, lack of ZWINT-1 indirectly abolishes MAD1 and MAD2 recruitment (Kasuboski et al., 2011). Consistent with this, ZWINT-1 depleted mammalian cells treated with Nocodazole to induce the SAC fail to arrest mitosis, causing chromosomes mis-segregation and generation of multinucleated cells (Wang et al., 2004).

Recently, the Spindle and Kinetochore Associated (SKA) complex has been demonstrated in mammalian cells, but not in yeast and *Drosophila*, to also bind MTs at KTs. The SKA complex is formed by the association of three coiled-coil protein SKA1, SKA2 and SKA3. Originally, the three proteins were identified in distinct protein interaction analysis, however *in vitro* reconstruction with recombinant proteins and two hybrid yeast interaction assays now confirm that these proteins belong to a single complex (Sauer et al., 2005, Hanisch et al., 2006, Gaitanos et al., 2009, Welburn et al., 2009, Gaitanos et al., 2009, Theis et al., 2009, Welburn et al., 2009). *In vivo*, depletion of any of the SKA complex components reduces expression of the others, suggesting that they are interdependent (Gaitanos et al., 2009, Hanisch et al., 2006, Welburn et al., 2009). Recently, resolution of the structure of the SKA complex allowed to understand how it acts at the KT-MT interface (Jeyaprakash 2012). Ten copies of SKA complex interact to form a flexible symmetric oligomeric structure, which wraps the plus-end of a MT filament at two sides to stabilizes laterally MT-KT binding (Figure 13) (Jeyaprakash 2012). SKA complex localization at KT depends on the presence of MTs and KMN proteins, however,

to date, no physical interactions have been shown among SKA and other KT proteins (Gaitanos et al., 2009, Hanisch et al., 2006, Raaijmakers et al., Welburn et al., 2009, Chan YW 2012).

Interestingly, the yeast DASH complex, which is also present in *Drosophila*, forms a ring around protofilaments and interacts with them perpendicularly, perhaps substituting SKA complex function in these organisms (Figure 13) (Gestaut 2008, Westermann 2006, Miranda 2005, Wang 2007, Gaitanos et al., 2009, Hanisch et al., 2006, Welburn et al., 2009).

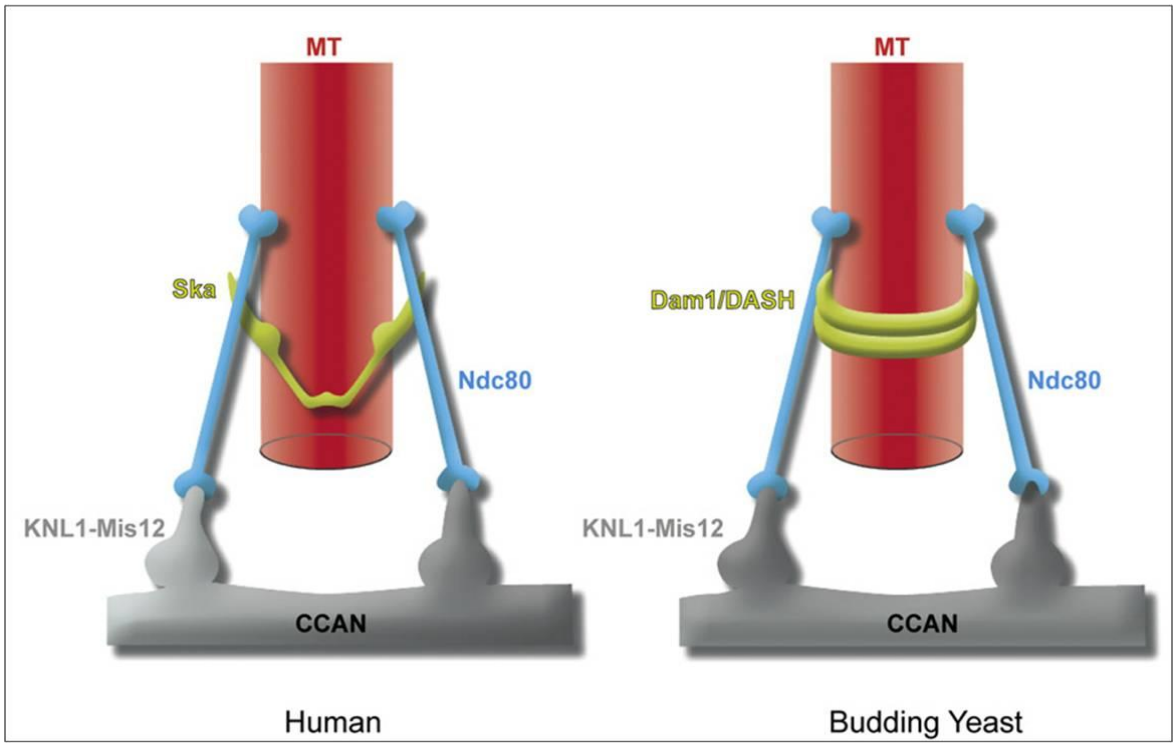

Figure 13. SKA complex in mammals and DASH complex in yeast and *Drosophila* stabilize KT-MT attachment binding laterally MTs. Adapted from Jeyaprakash AA 2012.

2.2.8 Aurora B and its role in sensing KT-MT tension

Aurora B kinase is an essential mitotic regulator controlling multiple functions and stages of mitosis. The Aurora B kinase is part of the Chromosomal Passenger Complex (CPC), together with INCENP (inner centromere protein) and the BIR domain-containing proteins

SURVIVIN and BOREALIN. From prophase to metaphase the CPC is localized at the inner centromere, the region located between the two sister-KTs. Later, in anaphase and telophase, the CPC re-localizes from the centromere to the central spindle midbody.

Among Aurora B functions is the ability to sense KT-MT attachment and to signal the presence of incorrect attachments between MT and KT (Ruchaud et al., 2007). During prophase, Aurora B phosphorilates HEC1, MIS13/DSL1, KNL-1 and SKA1. When phosphorylated, these proteins are unable to stably bind MTs (Biggins et al., 1999, Cheeseman et al., 2006, Ciferri et al., 2008, DeLuca et al., 2006, DeLuca et al., 2011b, Guimaraes et al., 2008, Welburn et al., 2009, Chan YW 2012). A study using a well characterized Aurora B activity FRET sensor has shown that substrate phosphorylation by Aurora B depends on the physical distance between Aurora B (at inner centromere) and its substrates (at KT). When sister chromatids are bi-orientated and tension is maximal, the distance between Aurora B substrates and the inner centromere increases, and consequently Aurora B cannot phosphorylate them efficiently; this leads to stabilization of MT-KT attachment. On the contrary, when the tension is minimum in the absence of bi-orentation, as in the case of prophase, Aurora B efficiently phosphorylates its substrates, therefore destabilizing KT-MT attachment (Fuller et al., 2008, Liu et al., 2009). Importantly, Aurora B can regulate KT-MT destabilization when MT are not properly attached to KTs. Indeed, as bi-orientated attachment, (i.e.: when sister KTs acquire amphitelic attachments) (Figure 14) is the requirement for correct segregation of sister chromatids, syntelic and merotelic attachments need to be corrected before cells entering anaphase. Synthelic and merotelic attachments correlate with low tension at KT, a condition in which Aurora B efficiently phosphorilates KT proteins to destabilize the erroneous attachment and, in case, allow the formation of new correct KT-MT bindings. Consistent with this, syntelic and merotelic attachments are frequently observed in cells with compromised Aurora B activity (Cimini et al., 2006, Ditchfield et al., 2003b, Hauf et al., 2003).

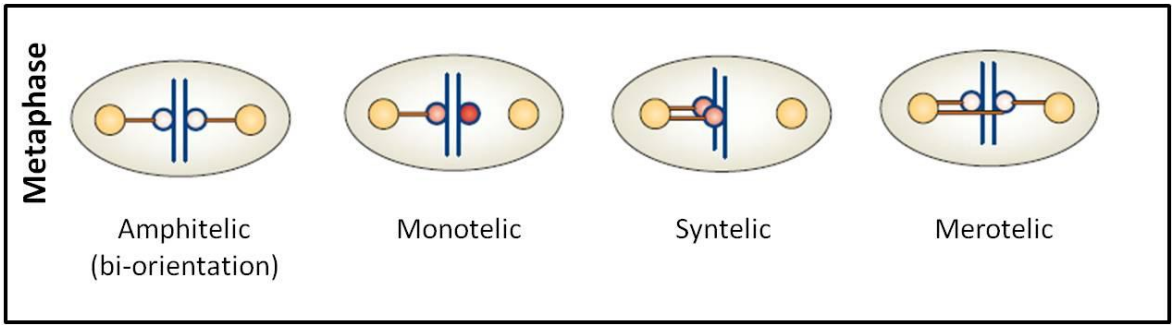

Figure 14. Correct (Amphitelic) and erroneous (Monotelic, Syntelic and Merotelic) MTs to KT attachments. Adapted from Musacchio A and Salmon ED 2007

2.2.9 The RZZ complex and Spindly at the outer KT

In both mammals and *Drosophila*, the RZZ complex localizes at KT during pro-metaphase after NEBD; it consists of three subunits, ROD, ZW10 and ZWILCH. Each subunit dimerizes and assembles to form a structure with ROD in the center and ZW10 and ZWILCH at the extremities, where they do not appear to interact with each other (Civril et al. 2010). The RZZ complex is required to recruit MAD1-MAD2, Spindly and dynein/dynactin complex at KT (Karess 2005, Buffin et al. 2005). Thus, depletion of RZZ components results in very reduced levels of SAC proteins at KTs. In *Drosophila*, Zw10 or Rod depleted cells do not arrest in metaphase in response to mitotic spindle damage and separate sister chromatids prematurely. Such impairment correlates with high frequency of aneuploidy in daughter cells (Basto et al. 2000). While the RZZ complex does not anchor MTs directly, RZZ depleted cells display defect in chromosomes congression and alignment. These defects are due to the lack of dynein at the KT of RZZ depleted cells. Indeed, dynein is important to exert a pulling force at the KT of mono-oriented chromosomes that promotes chromosome oscillation and movement toward the metaphase plate (Li et al. 2007). Another set of data show that dynein accelerates the establishment of KT-MT attachments (Gassmann et al. 2008, Vorozhko et al. 2008). The RZZ components

Zw10 and Rod are removed from KT by dynein, which during metaphase transports these two proteins from KT to the midbody (Whyte et al. 2008, Scaërou et al. 2001). Recently, it has been proposed that in mammals ZW10 and ROD release from KT at metaphase requires ZWINT-1 dephosphorylation (Figure 15) (Kasuboski et al. 2011).

SPINDLY acts as an adaptor for dynein/dynactin complex localization at KT during cell division. The RZZ complex is required to recruit SPINDLY at KT (Figure 15). Only few conserved residues are important for SPINDLY mediated recruitment of dynein/dynactin complex to KTs (Chan et al. 2009). Lack of SPINDLY affects dynein/dynactin recruitment at KTs without altering their localization at the centrosomes. In mammals, SPINDLY depleted cells display a delay in chromosomes alignment, a decreased inter KT distance and poorly organized k-fibers (Chan et al. 2009), suggesting that the MT-KT attachment is affected in cells lacking SPINDLY, possibly due to the lack of dynein at KT, as previously discussed.

The role of SPINDLY as regulator of SAC is controversial. In mammals, SPINDLY is not required for SAC proteins removal from KT. Indeed MAD1 and MAD2 are not accumulated at KTs in SPINDLY-depleted cells. Thus, a dynein independent SAC removal mechanism has been suggested to occur in SPINDLY-depleted cells (Chan et al. 2009, Gassmann et al., 2010). These data are in contrast with previous observations showing that in *Drosophila* and *C.elegans* Spindly depleted cells accumulate checkpoint proteins at KT (Vergnolle & Taylor 2007, Varma et al. 2008, Sivaram et al. 2009, Griffis et al. 2007, Wojcik et al. 2001).

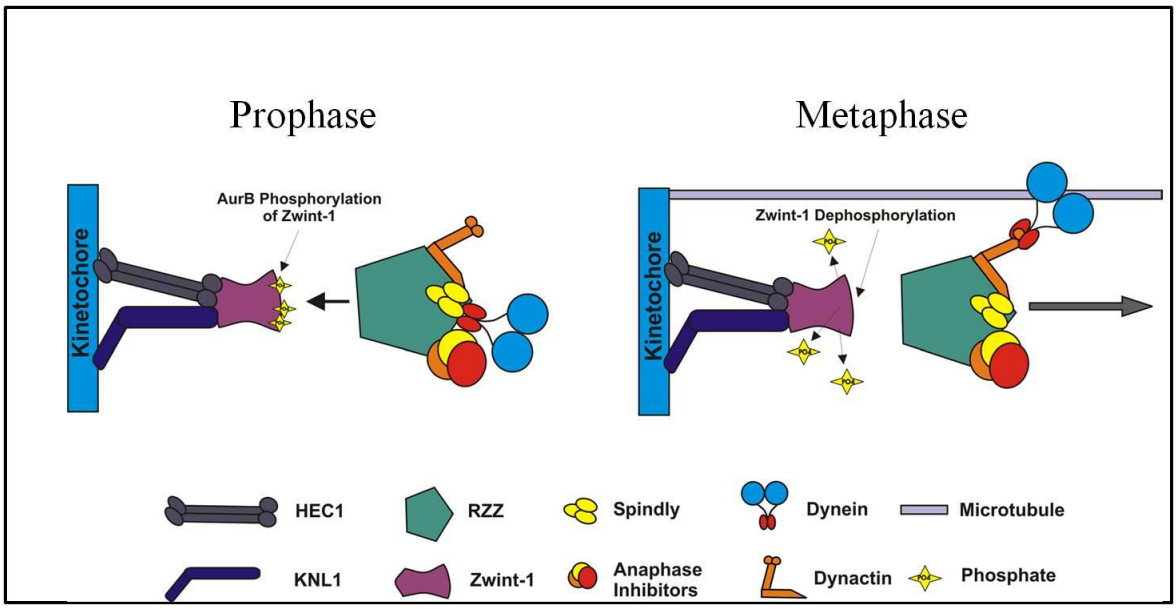

Figure 15. ZWINT-1 phosphorylation by Aurora B recruits at KTs the RZZ complex and consequently SAC proteins, SPINDLY and dynein/dynactin complex. Removal of RZZ proteins from KT through SPINDLY/dynein/dynactin requires ZWINT-1 dephosphorilation. Adapted from Kasuboski JM 2011 Kasuboski et al. 2011 .

2.2.10 The SAC and the onset of anaphase

The SAC is a surveillance mechanism evolved in eukaryotes to ensure proper segregation of chromosomes during mitosis. It prevents the onset of anaphase unless chromosomes are stably attached to bi-orientated MTs. Two major classes of SAC components in all eukaryotes are the MAD (mitotic arrest deficient) and the BUB (budding uninhibited by benimidazole) genes. MAD genes include MAD1, MAD2 and MAD3 (BUBR1 in humans) while BUB genes include BUB1 and BUB3. MAD2 is highly enriched at unattached KTs and the attachment to MTs leads to the loss of MAD2 from KTs (Howell et al. 2004, Waters et al. 1998). Importantly, a single unattached KT is sufficient to activate the SAC and delay anaphase (Rieder et al. 1990). Also the checkpoint proteins MAD2, BUBR1 and BUB3 are highly dynamic at KTs (Howell, Moree, Farrar, Stewart, Fang & Salmon 2004). In the last decade, it emerged that the SAC machinery also senses the tension generated across sister KTs (Pinsky & Biggins 2005), Zhou et al. 2002). In general, if MTs are not attached to KTs, tension at KTs is very low and cells arrest in pro-metaphase. However, if tension is applied on unattached KTs with a micro needle to pull a chromosome toward the

spindle pole anaphase begins (Nicklas & Ward 1994). Such "tension sensitive system" is supported by the observation that SAC proteins are recruited to attached but otherwise tensionless KTs (Skoufias et al. 2001). Whether lack of tension has a direct effect on the SAC and how SAC senses tension is still unclear (Nicklas et al 1995). A possibility is that the SAC is controlled by Aurora B that, as mentioned in the previous section, in condition of tensionless KTs can lead to destabilization of MT attachment.

The final target of the active SAC is Cdc20, a cofactor of the Anaphase-Promoting Complex/Cyclosome (APC/C). The current model of SAC signaling is that unattached KTs catalyze the formation of an inhibitory complex called MCC (mitotic checkpoint complex), which inhibits the ability of Cdc20 to activate the APC/C. MCC consists of MAD1/MAD2, BUBR1, BUB3 and Cdc20 (Fraschini et al. 2001), (Sudakin et al. 2001). When KTs are attached by MTs and chromosomes are bi-oriented at the metaphase plate, the SAC is silenced, Cdc20 is releaved from inhibition by the MCC and anaphase can occur.

Among others, two major mechanisms have been described that inactivate the SAC. The first of these mechanisms involves the dynein/dynactin complex in the removal of SAC proteins from correctly attached KTs (see above). Another mechanism is based on MAD2 sequestration by a specific binding protein, called $p31^{comet}$, which localizes to KTs in a MAD2-dependent manner. Depletion of $p31^{comet}$ leads to prolonged metaphase arrest while over-expression of $p31^{comet}$ bypasses the SAC (Fava et al. 2011, Mapelli et al. 2007, Wang et al. 2004, Yang et al. 2007). Upon inactivation of the SAC, APC/C-Cdc20 becomes active and promotes degradation of SECURIN, an inhibitor of SEPARASE, the protease which cleaves sister chromatids. Activation of SEPARASE results in the separation of sister chromatids and in the onset of anaphase. Activation of APC/C-Cdc20 also promotes the degradation of CYCLIN B, which initiates the inactivation of CDK1 and the exit from mitosis (Figure 16) (Bharadwaj & Yu 2004, Musacchio and Salmon, 2007).

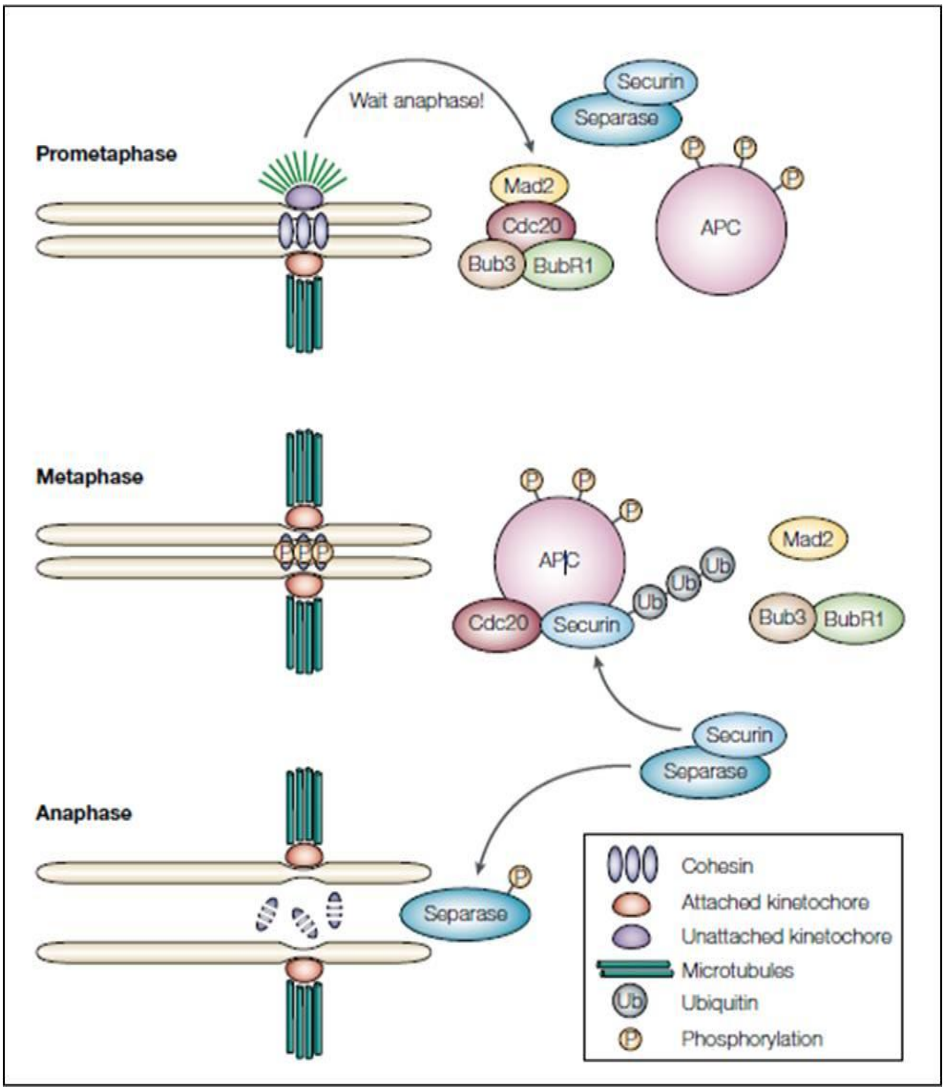

Figure 16. SAC proteins are recruited at KT during prophase and persist at KT until chromosomes align at the metaphase plate. Then SAC components are removed, promoting the activation of the polyubiquitinated APC/C complex, which sequesters and degrades Securin. Separase, which was inhibited by Securin, can now cleave coesins allowing sister chromatids separation. Adapted from Musacchio & Hardwick 2002.

2.3 Endocytosis and autophagy in mitotic cells

Whether endocytosis functions during mitosis remains debated. It has been demonstrated that clathrin mediated endocytosis is blocked in mitotic cells (Royle et al. 2012; Fielding et al. 2012). However, recently it has been shown that in physiological conditions, the uptake of destran or TfR in HeLa cells does not change in interphase compared to mitotic cells if mitosis is unperturbed (Tachenova-Grigolova et al. 2013).

Also the functionality of autophagy during mitosis is debated. It has been suggested recently that during mitosis autophagosome engulfs primarily mitochondria in a process called mitophagy (Liu et al. 2014). However, the kinase Vps34, which regulates PIP3 formation during phagophore assembly is phosphorylated and inhibited by CDK1 during mitosis. Inactive Vps34 is expected to lead to reduction of PIP3 levels thus suppressing autophagic cascade (for review Rubinsztein & Nixon 2010).

2.3.1 Trafficking proteins with moonlighting role during cells division

Proteins involved in various trafficking steps appear to play diverse moonlighting functions during mitosis. These include Epsin15, Clathrin, Rab5, ESCRT and Beclin1 proteins.

Epsin

Epsin is an endocytic adapter protein directly binding and deforming membranes via its Epsin NH2-terminal homology (ENTH) domain. It was shown using HeLa cells that Epsin regulates spindle morphology thanks to the ability to curve membranes. Spindle assembly has been proposed to require a highly interconnected membrane-like network, called spindle matrix, which would form an elastic support for spindle function. The impairment of Epsin is proposed to lead to a disorganized spindle matrix that exhibits uneven elasticity and deformability when subjected to forces by the MTs resulting in defects in spindle morphology (Liu & Zheng 2009).

Clathrin

Clathrin is involved in the generation of coated vesicles that transfer membranes and proteins around the cell. It forms a triskelion structure, composed of three heavy chains and three light chains. During mitosis, clathrin concentrates at the mitotic spindle where it binds directly to MTs and strengthens connections between MTs (Royle et al. 2005). Importantly, no membranes are involved in this process. Recent studies in HeLa cells

revealed that Clathrin exerts this function in combination with other two proteins not directly linked to mitosis or endocytosis. These are transforming acidic coiled-coil protein 3 (TACC3) and colonic and hepatic tumor over-expressed gene (ch-TOG) (Hood et al. 2013). Consistent with this, Clathrin depletion results in destabilization of k-fibers, prolonged activation of the SAC and defects in chromosomes segregation that can lead to polyploidy (Hood et al. 2013) .

RAB5

Rab5 is a small GTPase that regulates the formation of EE, their transport along MTs and their fusion to target organelles. It has been recently demonstrated using *Drosophila* S2 cells that Rab5 is required for chromosomes alignment during mitosis. In fact, Rab5 associates with the nuclear lamina and with a protein complex called mushroom body defect (Mud). Mud is the *Drosophila* counterpart of NuMa in mammals, which is known to be important for spindle formation and maintenance (see previous section). Evidence suggests that Rab5 is required for disassembly of the NEBD, for accumulation of Mud at the spindle poles and for distribution of key components for spindle structure maintenance (Audhya et al. 2007; Capalbo et al. 2011; Serio et al. 2011). Consistent with this, in human cells depletion of Rab5 affects the localization of CENP-F and phenocopies CENP-F depletions (Serio et al. 2011).

Endosomal sorting complex required for transport-III (ESCRT-III)

Endosomal sorting complex required for transport-III (ESCRT-III) complex is involved in protein sorting at early endosome/MVB compartemts. Evidences suggests that ESCRT-III complex interacts with the CPC. In humans, the CPC component Aurora B has been reported to phosphorylate the ESCRT-III subunit CHMP4C, preventing assembly within the other ESCRT-III complex. Such inhibitory event impairs formation of ESCRT-III polymers, preventing its association to membranes during formation of the cleavage furrow at cytokinesis (Capalbo et al. 2012). Cleavage furrow formation is thought to require also the RE. This process is mediated by RAB11, the GTPase associated with RE in mammals

and *C. elegans* (Wilson et al. 2005). In addition, RAB11 is also required during cellularization a process related to furrow formation in *Drosophila* and Xenopus embryos (Pelissier et al. 2003). In mammals, RAB11-REs recruit specific factors that drive membrane fusion, among which are FIP3 class II (Pelissier et al. 2003) and possibly ARF6 (Hickson et al. 2003). The tethering of RAB11/FIP3 at the membrane is mediated by exocyst (Gromley et al. 2005). A recent publication revealed that in murine oocytes Rab11 is also essential for the spindle position during asymmetric cell division, regulating actin cytoskeleton dynamics by RAB11 recruitment of Miosin-Vb on actin filaments, a process that allow correct positioning of asymmetric spindle (Holubcová et al. 2013).

Beclin1

Recently, it has been reported that Beclin1, which complexes with Vps34 during the initiation of autophagy, localizes at KTs during mitosis. Beclin1 is recruited at KT in a MTs dependent manners. At KT Beclin1 interacts with ZWINT-1 and appears to act downstream it. Indeed, Beclin1 depletion leads to partial recruitment of ZW10, CENP-E and CENP-F to KTs. Importantly, Beclin1 function at KT could be independent of its function during autophagy. Consistent with this, depletion of a panel of proteins specifically acting during autophagy do not cause mitotic alteration (Frémont et al. 2013).

2.4 NE re-assembly

During late anaphase the NE re-assembles. Chromosomes are moved towards the spindle poles, a process correlated with MTs shortening (Mora-Bermúdez et al. 2007). In the meanwhile, AURORA B phosphorylates diverse substrates, among which Condensin I complex and Histone H3, which then control chromosomes compaction. These events are followed by the NUP107-160 complex association to chromatin, which form the so-called NPC-"prepores", and by binding of ER membrane tubules to the chromatin surface (Pyrpasopoulou et al. 1996). The molecular mechanism that controls the initial attachment

of ER to chromatin is unknown. Despite this, during telophase, INM proteins contact DNA, supporting attachment of membrane sheets to chromatin. The layer of nuclear lamins reforms completely only at the end of telophase, when the nuclear import functions becomes stabilized. Holes in between the ONM and INM are closed by an anular membrane fusion, a non canonical membrane fusion event. At present, the molecular mechanism involved in NPC assembly and anular fusion are not well understood (for review Burke, B. & Ellenberg J 2002).

3. AIM OF THE PROJECT

Using *Drosophila* as animal model, we aimed first to investigate the role of Snap29 during epithelial tissue development, analyzing the function of Snap29 in membrane fusion and mitosis. Then, using mammalian cells, we planned to investigate whether the role of Snap29 during mitosis is conserved in mammals.

4. MATERIAL AND METHODS

4.1 Fly strains, mapping and genetics

Flies were maintained on standard yeast/cornmeal/agar media. All experiments were performed at 25°C. Mosaic eye imaginal discs were generated using yw eyFLP; ubiGFP[w+] FRT42, while mutant eye discs were generated using yw, eyFLP; cl[w+], FRT42/CyO, TwiGal4, UAS-GFP. Similar lines with different FRTs, or with UbxFLP, were used to generate mutant tissue for genes located on different chromosome arms or to generate mutant wing disc tissue, as previously described (Tapon et al. 2001, Newsome et al. 2000). Other alleles used were w; FRT42D, $vps25^{A3}$ (Vaccari & Bilder 2005), yv; w; FRT42D, Syb^{09}; UAS*snap29*RNAi (Bloomington Drosophila Stock Center [BDSC] #25862), $atg13^{\Delta 81}$ (Chang & Neufeld 2009), FRT42D, $fab1^{21}$(Rusten et al. 2006), $Syx17^{LL06330}$, $Vamp7^{G7738}$, *Df(2R)BSC132* and *Df(3L)Exel8098* (all from Takáts et al. 2013), UAS-Syx17 RNAi (Vienna Drosophila Research Centre - [VDRC] # GD36596), UAS Vamp7 RNAi (VDRC# GD13317).

To identify the locus affected by B6 mutation, MENE-(2R)-E/B6 was crossed to the 2R Deficiency (Df) kit (BDSC). Such complementation mapping revealed the presence of two lethal mutations around 51A-B and 60A. Blind recombination of MENE-(2R)-E/B6 to w-; FRT42D revealed that the lethality leading to the MENE phenotype was the one at 60A. Recombinant #21 (B6-21) was used for further characterization. Briefly, submapping by Df complementation around 60A narrowed the candidate region to 60A3-5. Independent recombination mapping (Zhai et al. 2003) also showed absence of recombination with 2 viable P-elements (KG01846 [BDSC#14169] and KG04017 [BDSC#13357]) mapping to 60A3 and 60A5, confirming the presence of the mutation at 60A3-5. Direct sequencing of candidate gene exons revealed a mutation in *CG11173/Snap29*. For transgenic rescue experiments we used w; FRT42, GMR-Hid/CyO; eyGal4, UASFLP, UAS p35 (from S.

Cohen), UAS SOCS36E (a gift of M. Zeidler). Transgenic fly lines carrying mutant tagged and mutant Snap29 forms were generated by standard techniques using the attP/attB recombination system. Over expression in follicle cells was obtained using the Cy2-Gal4 (BDSC). For co-localization experiments, we used UAS GFP-Rab11, UAS-GFP-LAMP1 (a gift of H. Kramer). The *10X-STAT-GFP* and *E(spl)mβ-lacZ* transgenic flies were kindly provided by E. Bach and E. Lai, respectively. *Puc-LacZ* was kindly provided by M. Simons.

4.2 Generation of transgenic *Drosophila* lines

Sequencing of *snap29* exons was performed as previously described (Vaccari & Bilder 2005), using the following primers : Snap29 1F, Snap29 1R, Snap29 2F, Snap29 2R, Snap29 3F, Snap29 3R. CFP-Snap29, ΔSNARE1, ΔSNARE2 and NPF>AAA inserts were cloned EcoRI-XbaI into a pUASattB plasmid. To generate the CFP tagged Snap29, the CFP and the Snap29 coding sequences were amplified from a Snap29 cDNA vector (*Drosophila* Genomic Research Center (DGRC) with the following primers: CFP F EcoRI, CFP R, Snap29 F, Snap29 R XbaI. The two PCR products were then used as template for a second PCR using CFP F EcoRI and Snap29 R XbaI as primers. To generate the ΔSNARE1 insert, two regions (290 bp and 532 bp) of Snap29 cDNA were amplified with the following primers: ΔSNARE1 1F EcoRI, ΔSNARE1 1R, ΔSNARE1 2F, ΔSNARE1 2R XbaI. The two PCR products were used as templates for a second PCR using ΔSNARE1 1F EcoRI and ΔSNARE1 2R XbaI as primers. To generate the ΔSNARE2 insert, Snap29 cDNA was amplified with the following primers: ΔSNARE 2F, ΔSNARE 2R. To generate the NPF>AAA insert, two PCRs were performed using Snap29 cDNA as template and the following primers: NPF>AAA 1F EcoRI, NPF>AAA 1R, NPF>AAA 2F, NPF>AAA 2R XbaI. The two PCR products were used as a template for a second PCR with NPF>AAA 1F EcoRI and NPF>AAA 2R XbaI as primers.

4.3 Antibodies production

Production of anti-*Drosophila* Snap29 antibody. To prepare a polyclonal antibody (pAb) against the *Drosophila* Snap29, *Snap29* cDNA was amplified by PCR using the Taq Polymerase (Promega) and pUASsnap29 as a template, and GST-Snap29 BamHI and GST-Snap29 XhoI as primers. The PCR product was inserted into the prokaryotic expression vector pGEX, containing the GST sequence (pGEX-GST), using *Bam*HI and *XhoI* sites. Expression was carried out in the *Escherichia coli* BL21 strain adding IPTG 1mM. Bacteria were centrifuged and the pellet was suspended in 50mM Hepes, 200 mM NaCl, 1mM EDTA, 1% NP40, 5% glycerol, Protease Inhibitors, PI (Roche) and sonicated. The lysate was centrifuged at 13.000 *rpm* for 30 minutes and the supernatant was incubated over night with Glutathione-Sepharose Beads. The solution containing protein lysate and Glutathione-Sepharose Beads was washed three times in 1% triton PBS 1x and two times in PBS 1x. Complexes were suspended in 50 mM TRIS pH7.4, 100 mM NaCl, 1 mM EDTA, 10% glycerol, 1mM DTT and PI. In order to separate GST-Snap29 protein from beads, immunocomplexes were incubated in 100mM TRIS-HCl, 100 mM NaCl, 50 mM GSH for 10 minutes and then centrifuged for 10 seconds at 2000 rpm. This step was repeated three times. Proteins were then suspended in PBS 1x through dialysis and purified. Purification was performed under standard conditions by IFOM antibody-service facility.

Production of anti-humanSNAP29 antibody. To produce a GST-humanSNAP29 for pAb production, we generated an insert by PCR using GST-hSNAP29 and GST-hSNAP29 XhoI and pCMVSPORT6.Human-*snap29* as template. The PCR product was inserted using BamHI and XhoI into pGEX-GST. IPTG induced expression of GST-hSNAP29 and purification was performed by the IFOM antibody-service facility according to standard protocols.

In both cases, purified proteins were used for rabbit immunizations (Eurogentech). Sera affinity purification was performed by the IFOM antibody-service facility, using AminoLink® Kit (Biotechnology).

4.4 Production of siRNA-resistant human *snap29* cDNA

The siRNA3 D-011935-04-0005 (Darmacon), targeting Human-Snap29 mRNA between the nucleotides 285 and 304 (5'- GAC AAG AUG GAC CAA GAU -3'), was used to silence SNAP29 expression in mammalian cells. A Human-*Snap29* cDNA encoding an RNA strand resistant for this siRNA was generated mutagenizing the siRNA target sequence in the Human-*Snap29* cDNA in order to maintain the same amino acidic sequence of the wild type protein. The resulting mutated sequence is: 5'- GAT AAA ATG GAT CAG GAC -3'. pCMV.SPORT6-Human-*Snap29* containing *Snap29* cDNA cloned between EcoRI and XhoI was used as template for the subsequenct PCRs. We performed a first PCR using the FOR-HSNAP29 primer, containing the restriction site sequence for EcoRI and the first 18 nucleotides of the *snap29* cDNA sequence, and the REV-HSNAP29 R (Resistant) primer which contains the mutagenized siRNA target sequence. The second PCR was performed using the FOR-HSNAP29 R primer, containing the mutagenized sequence, and the REV-HSNAP29 primer containing the last 18 nucleotides of Human-*Snap29* cDNA and the XhoI restriction site sequence. The two PCR products were used as template for a third PCR performed with the FOR-HSNAP29 and REV-HSNAP29 to obtain the entire Human-*Snap29* cDNA sequence mutagenized in the indicated region. The PCR product has been subjected to EcoRI-XhoI digestions and then cloned inside the pCMV.SPORT6 to obtain the pCMV.SPORT6-HumanSNAP29-R (SNAP29 siRNA Resistant).

4.5 Cell cultures

Drosophila S2 cell line were provided by Barbara Mellone. S2 cells were cultured in Schneider's medium (GibCO) supplemented with 1% Glutamine (Euroclone) and 10% Fetal Bovine Serum (FBS) (Euroclone) at 28°C. Cells were plated to a density of 1.000.000 cells/ml every three days. U2OS-HB2-GFP-mCherry-αTubulin cell line was provided by Letizia Lanzetti (Candiolo, University of Turin). The U2OS-HB2-GFP-mCherry-αTubulin cell line stably expresses a GFP tagged Histone2B (H2B) (to mark chromosomes) and a mCherry tagged α-tubulin (to mark microtubules). U2OS cells were cultured in DMEM (GibCO) supplemented with 10% FBS at 37°C with 5% CO2 with the addition of 0,5 mg/mL G418 and 1µg/mL Puromycin. HeLa cell line was cultured in DMEM (GibCO) supplemented with 10% FBS at 37°C with 5% CO2. Cells were plated to a density of 500.000 cells/ml every two days.

To depolymerize MTs, HeLa and U2OS-HB2-GFP-mCherry-αTubulin cell lines were incubated with 300 ng/mL of Nocodazole for 16 hours. Cells were then fixed in 3.6% PFA. Alternatively, Nocodazole was removed, cells were washed four times with PBS1x and fresh medium was added to analyze cell behavior upon Nocodazole wash-out.

Cold shock assay was performed by incubating cultured cells at 4°C for 8 minutes. Subsequently, cells were fixed in 3.6% PFA and processed for immunofluorescence analysis.

4.6 Double stranded RNAs interference in S2 cells

Double stranded (ds) RNAs for Snap29 and Ndc80 interference in S2 cells were generated using the following primers: T3-Snap29, T7- Snap29, T3-Ndc80, T7 Ndc80. DsRNA were transcribed *in vitro* with the T3/T7 polymerase (Promega) according to manufacturer's instructions, annealed and incubated with the cells at a final concentration of 15ug/10^6 cells for 72 hrs.

4.7 SNAP29 siRNA mediated silencing in HeLa and U2OS-HB2-GFP-mCherry-αTubulin

250.000/350.000 cells were plated in 6 well plate and left in the incubator for 24h. The mix composed of siRNA specific for Snap29 mRNA (D-011935-04-0005, Darmacon) and RNAiMax lipofectamin was prepared following the manufacturer's instruction (Invitrogene) and then added to cells. Cells were collected at different time points after transfection. For rescue experiments, a mix composed of the pCMV.SPORT6-HumanSNAP29-R alone or mixed with the siRNA specific for Snap29 mRNA and Lipofectamin 2000 was prepared following the manufacturer's instruction (Invitrogene). Five hours after transfection fresh medium was added to transfected cells. Cells were collected 24/48 hours after transfection.

4.8 Double thymidine block in HeLa cells

40-50% confluent HeLa cells were treated with 100mM thymidine for 16 hours. Then, four washes with PBS1x were performed and fresh medium containing 12mM deoxycytidine, to favor thymidine release was added for 8 hours. Subsequently, fresh medium containing thymidin was added to cell plates, that were incubated at 37°C for 16 hours. Two thymidine pulses treatment is sufficient to arrest cells in G1/S. After the second thymidine block, all the cells were blocked in G1/S and a plate of cells was collected as time 0. Cells were then rinsed four times with PBS1x and then fresh medium was added. Cells were subsequently collected after 3, 6, 7, 8, 9 and 10 hours and processed for protein extraction, or immunofluorescence analysis. Specifically, we stained these cells for Phospho-Histone3 to measure the Mitotic Index at each time point.

4.9 Immunostainings

Imaginal discs, ovaries and fat body tissues were fixed with 4% paraformaldeyde (PFA) diluited in H_2O for 20 minutes. Then, samples were rinsed three times with 0.1% triton PBS1x for 5 minutes. For permeabilization, samples were treated for 10 minutes with 1% triton PBS1x and then the blocking solution, composed of 5% BSA in 0.1% triton PBS1x, was added for 30 minutes. Samples were incubated with primary antibodies diluted in blocking solution over night (O.N.) at 4°C. Three washes in 0.1% triton PBS1x of 5 minutes each were performed. Secondary antibodies, diluited in PBS1x, were added for two hours at room temperature (RT). Samples were then rinsed three times for 5 minutes with 0.1% triton PBS1x. Eventually, DAPI was added for 10 minutes and then washed once with 0.1% triton PBS1x. Samples were then mounted with Glycerol or Moviol (Calbiochem).

For immunofluorescence analysis HeLa or U2OS-HB2-GFP-mCherry-αTubulin cells were cultured on Poly-D-lysine or 2% gelatin covered glass supporter. Cells were fixed in 3.6% PFA for 15 minutes. After three washes with PBS1x, cells were permeabilized in 0.1% Triton PBS1x for 10 minutes. Subsequently, the blocking solution composed of 3% BSA in PBS1x was added for 30 minutes. Cells were incubated at RT for 2 hours with primary antibodies diluited in blocking solution. Cells, were then rinsed with PBS1x for three times and secondary antibodies were added for 1hour at RT. Cells were finally wash with PBS1x for three times and eventually DAPI was added. Glass supporters were mounted on a glass slide using Moviol as mounting medium.

For *Drosophila* tissues and S2 cells, primary antibodies against the following antigens were used: Rabbit anti-Snap29 1:1000, rabbit anti-Syx7 1:100 (Lu et al. 2005), rabbit anti-GM130 1:1000 (Abcam), rabbit anti-ref(2)P 1:1000 (Nezis et al. 2008), rat anti-Atg8a 1:300 (Takats S 2013), mouse anti-βGal 1:25 (Developmental Studies Hybridoma Bank - DSHB), mouse anti-FK2 1:100 (ENZO), rabbit anti-Phospho-HistoneH3 1:200 (Sigma), rabbit anti activated Caspase3 1:100 (Signal Transduction Technologies), mouse anti-

NECD 1:100 (DSHB), rat anti-α-tubulin 1:100 (AbD SeroTech), rabbit anti-Dome 1:100 (a gift from S. Noselli), chicken anti-GFP 1:1000 (Cell Signaling), Chicken anti-CID 1:1000 (gift of Barbara Mellone), Mouse anti-γ-tubulin 1:100 (Sigma Aldrich), Rat anti-INCENP 1:400 (gift of Kim McKim). For mammalian cells the following primary antibodies were used: rabbit anti-humanSNAP29 (1:500), mouse anti-HEC1 (1:1000), human anti-CENP-A (1:1000), rabbit anti-CENP-C (1:1000), mouse anti-NSL1 (1:1000), rabbit anti ZWINT-1 (1:1000), rabbit anti-ZWILCH (1:1000), rabbit anti-SPINDLY (1:1000), mouse anti-MAD2 (1:1000) (gift from Anna DeAntoni); goat anti-LaminA (1:50) (Santa Cruz), mouse anti-Golginin97 (1:100) (abcam), goat anti-EEA1 (1:50) (Santa Cruz), mouse anti KDEL (1:1000) (Streegene), mouse anti Rab11 (1:100) (BD).

Alexa conjugated secondary antibodies from Invitrogen and Rhodamine-phalloidin (Sigma) were used.

4.10 Notch trafficking assay

Notch surface staining and Notch trafficking assays were performed according to Vaccari & Bilder 2005. 30 L3 larvae were dissected in cold M3 medium (Sigma) and then incubated for 90 minutes with the NECD on the rocket at 4°C. At cold temperature, the endocytic pathway is blocked and in not-permeabilized conditions, the anti-NECD binds to the extracellular portion of Notch receptor. After 90 minutes, L3 larvae were quickly washed with M3 medium and while 10 larvae were fixed in 4% PFA, the others were incubated with M3 medium in a rocket at RT. At RT, the endocytic trafficking resumes and the Notch receptor conjugated with the NECD antibody is internalized. After 15 minutes, 10 larvae were fixed in 4% PFA while the other samples were left in the rocket for 210 minutes. This time is sufficient to allow Notch receptor degradation in lysosomes. Subsequently, the remaining 10 L3 larvae were fixed with 4% PFA. The fixed larvae were then stained with primary and secondary antibodies as previously described.

4.11 Imaging

All images are single confocal sections taken with a Confocal Microscope (Leica) using, ×40/NA 1.25, or ×63/NA 1.4 oil lenses. Images were edited with Adobe Photoshop and ImageJ and assembled with Adobe Illustrator.

The measurement of the interkinetochore distances was performed using a homemade plugin developed in ImageJ. The line selection tool was used to manually draw a straight line between the brightest spots of each kinetochore pair; we used an anti-CENPT antibody to label KT. The resulting fluorescence intensity profile was analyzed using the "Find Peak" plugin [1] to automatically find the two peaks. The peak-to-peak distance represents the interkinetochore distance. [1] : http://fiji.sc/Find_Peaks.

The measurement of the spindle pole body elongation was performed using ImageJ. The Threshold tool was used to manually set a threshold level in order to segment the image and extract the spindle pole bodies. An ellipse was fitted to each segmented spindle pole body using the Analyze Particle tool and the Set Measurement tool. The major axis of the fitted ellipse represents the spindle pole body elongation.

4.12 Protein extraction and Western Blot

Third instar larvae eye imaginal discs, S2 cells or mammalian cells were collected, homogenized and incubated for 20 minutes on ice in 1 mM Tris-HCl, 150 mM NaCl, 5 mM EDTA, 1% TritonX, 1% Deoxycholate and 0,1% SDS. Lysates were cleared by centrifugation. Supernatants were recovered and quantified, separated by SDS-PAGE and transferred to nitrocellulose by standard methods. Primary antibodies used were rabbit anti-Snap29 (this study) 1:1000, anti-ref(2)P 1:1000 (Nezis et al. 2008), anti-Ubiquitin PD41 1:1000 (Santa Cruz), anti NICD 1:1000 (DSHB), anti-β-tubulin 1:8000 (Amersham), anti-p6SK (1:2000) (a gift from Aurelio Teleman), anti-Ndc80 1:1000 (gift from Patrizia

Somma), anti-HumanSNAP29 (1:500) (this study), anti-vinculin (1: 8000) (Amersham). Secondary antibodies used were anti-rabbit and anti-mouse 1:8000 (Amersham). Immunoblots were visualized with SuperSignal West pico/femto Chemioluminescent Substrate (Thermo Scientific) using Chemidoc (Biorad).

4.13 Immunoprecipitation and LC-MS/MS analysis

S2 cells were collected and centrifuged for 10 minutes at 800 rpm at 4°C. After discarding supernatant, cell pellet was washed with PBS1X and centrifuged for 10 minutes at 800 rpm at 4°C. Cell were homogenized in JS Lysis Buffer (Hepes 50 mM pH7.4, NaCl 150 mM, Glycerol 10%, Triton X-100 1%, $MgCl_2$ 1.5 mM, 5 mM EGTA, Na pyrophosphate 0.1 M pH7.5, PMsF 0.1 M in ethanol, Na Vanadate 0.5 M pH7.5 in Hepes, NaF 0.5 M, proteases inhibitor 1:200) and incubated 20 minutes at 4°C on a wheel. Cell suspensions were centrifuged for 10 minutes at 13.200 rpm 4°C and supernatants containing total proteins were collected and quantified. Proteins (1 mg) were incubated with the antibody (1 ug) O.N. at 4°C on a wheel. The antibodies used were the anti-Snap29, anti-Ndc80 as positive control, and anti-yeast Mad2 as negative control. During this step the polyclonal antibodies bind to specific epitopes of the proteins of interest (bait), Snap29 and Ndc80. The following day, protein G-Sepharose beads (Amersham) were added to proteins complexed with the antibodies and incubated for 3 hours at 4°C. Protein G Sepharose beads display an high binding affinity for the Fc fragment of the antibody. After the incubation, samples were centrifuged for 1 minute at 3000 rpm 4°C. The supernatants contain the so-called immunocomplex formed by Protein G-Sepharose beads, antibodies, the baits and a certain number of proteins that bind the bait within the cell. The supernatant was washed 3 times with JS buffer and finally centrifuged for 1 minute at 3000 rpm 4°C. Laemli Buffer 3X was added to the samples and they were boiled 5 minutes at 98°C to allow protein denaturation. Proteins were then centrifuged for 2 minutes at 13.200 rpm to separate the protein G-

Sepharose Beads (Bottom) from the immunoprecipitate (Top). The supernatant containing only the proteins of the immunocomplexes were subjected to Western Blot as previously described. Immunoblot analysis of immunocomplexes was performed with the anti-Snap29 and the anti-Ndc80 antibodies.

For LC-MS/MS analysis, proteins were separated and processed as described (Rappsilber et al. 2003). Peptides were analyzed by liquid chromatography on an Agilent 1100 LC system (Agilent Technologies Inc.) coupled to LTQ-FT ultra (Thermo Fisher Scientific). Mass spectrometric data were analyzed for protein identification and presence of digly signature using Mascot Deamon and Proteome Discoverer 1.1 (1.1.0.263 Thermo Fisher Scientific Inc.).

4.14 Reverse Transcription (RT)-PCR

Third instar larvae eye imaginal discs were collected and RNA was extracted using TRIZOL Reagent (Invitrogen) and RNAse Mini kit (QIAGEN). Concentration and purity was determined by measuring optical density at 260 and 280 nm using a Nanodrop spectrophotometer. cDNA was generated from 1μg of RNA using the SuperScript VILO cDNA Synthesis kit (Invitrogen), according to manufacturer's protocol. 5 ng of cDNA was amplified (in triplicate) using the following primers: usnp F, usnp R, E(Spl) mβ R, Upd1 F, Upd1 R, Atg8a F, Atg8a R, Atg18.2 F, Atg18.2 R, Rpl32 F, Rpl32 R. Amplicon expression in each sample was normalized to its RpL32-RA mRNA content. The reactions were performed by IFOM-RT-qPCR service facility.

4.15 Electron microscopy and tomography

For morphological EM of *Drosophila* tissues, samples were prepared as previously described (Beznoussenko et al. 2007). Briefly, samples were fixed with 1% glutaraldehyde for 1 h and then with 1% reduced OsO4 for 1 h and embedded into Epon or gelatine. Then, constantly checking the position of section plane with the help of stained semi-thin sections, Epon or cryo-sections were prepared. Cryo-sections were then labelled with rabbit anti-Ref(2)p antibody (1:100) or with rat anti-Atg8a antibody (1:40). The primary antibody was marked with 10nm gold. The analysis of chemically fixed samples by electron tomography was performed on 200-nm-thick sections, as described previously (Beznoussenko et al. 2007). Briefly, samples were tilted from +65° to –65° at 1° intervals, with a magnification of 26,500x or 40,000x. At least 5 tomograms were analyzed per each experimental condition.

4.16 Adult Wing preparation

Adult flies were scored 2-3 days after eclosion, and only females were taken into account. Wings were dissected in isopropanol and mounted on microscopy slides using a mixture of Canadian balm (xylem-free) with methyl salicylate 1:1. Preps were dried at RT and imaged with a Nikon SMZ1500 microscope using the NCIS Elements5.0 software. Images displayed in figures are representative examples of at least 10 images per samples.

4.17 Time lapse of U2OS-HB2-GFP-mCherry-αTubulin

Time lapse of control and SNAP29 depleted U2OS-HB2-GFP-mCherry-αTubulin, treated or not with Nocodazole or after Nocodazole wash-out were recorded using a spinning disk confocal microscope (Perkin Elmer UltraVIEW VoX). Silenced cells were plated into glass-bottomed dishes (Matek) and placed onto a sample stage within an incubator chamber (Okolab) set at 37 °C in an atmosphere of 5% CO2. Images were captured with a 40× oil-immersion objective (N.A. = 1.3) using 120 and 150 ms exposure for the GFP and mCherry RFP respectively every 5 min for 8 h and keeping the laser intensity at minimum to avoid phototoxicity. Z-stacks images were collected every 1,5 μm on a cell thickness around 3 μm. Automated acquisition of 7 different fields and 17 stacks was done by using a high-precision motorized stage.

4.18 Bioinformatics

Multiple sequence analysis was performed using ClustalX using standard parameters.

4.19 List of Primers

Sequences of primers used for PCR:

Snap29 1F 5'-GATAACTCCAGACAACAACAAAG-3'

Snap29 1R 5'-CTGGGGGTTGTAGGAGAGAG-3';

Snap29 2F 5'-CTGGACTCTACCAACAAAAGC-3'

Snap29 2R 5'-ACCGGATGATTGTCGTAGC-3';

Snap 293F 5'-GCCAATAGCAACATTAACC-3'

Snap29 3R 5'-CTTAATGGCCTTGTGAAGTGC-3'

CFP F EcoRI: 5'-GATCGAATTCATGGTGAGCAAGGGCGAGGA-3'

CFP R : 5'- TAGTTATGGGCCTTGTGCAGCTCGT -3'

Snap29 F: 5'- ACGAGCTGTACAAGGCCCATAACTA -3'

Snap29 R XbaI: 5'- GATCTCTAGAGCTATTCTAAGCAATG -3'

ΔSNARE1 1F EcoRI 5'-GATCGAATTCGAAGTTTCCCTCGCC-3'

ΔSNARE1 1R 5'-CAGACCAGTCAGATGAGTTCGCTGCTCAATG-3';

ΔSNARE1 2F 5'-ATTGAGCAGCGAACTCATCTGACTGGTCTG-3'

ΔSNARE1 2R XbaI 5'-GATCTCTAGAGCTATTCTAAGCAATG-3'.

ΔSNARE 2F 5'-GATCGAATTCGAAGTTTCCCTCGCC-3'

ΔSNARE 2R 5'-GATCTCTAGAGAATGCTCGCTTGTTCACTGGTAGGTGCTGCTG-3'

NPF>AAA 1F EcoRI 5'- GATCGAATTCGAAGTTTCCCTCGCC-3'

NPF>AAA 1R 5'- CATCCATCTCTGCGGCTGCGGTGCTCCTC-3',

NPF>AAA 2F 5'- GAGGAGCACCGCAGCCGCAGAGATGGATG-3'

NPF>AAA 2R XbaI 5'-GATCTCTAGAGCTATTCTAAGCAATG-3'

GST-Snap29 BamHI 5'-GATCGGATCCGCCCATAACTACCTGC-3'

GST-Snap29 XhoI 5'- GATCCTCGAGGCTATTCTAAGCAATG-3'

GST-hSNAP29 BamHI 5'-CGCCGGATCCACCATGTCAGCTTACCCTAAAAGCTAC-3'

GST-hSNAP29 XhoI 5'-CCGCTCGAGTCAGAGTTGTCGAACTTTTCTTTCTG-3'

FOR-HSNAP29 5'-GATCGAATTCTTCAGCTTACCCTAAGAGCTAC-3'

REV-HSNAP29 R 5'-ATTTCAAGTCCTGATCCATTTTATCCACCAT-3'

FOR-HSNAP29 R 5'-ATGGTGGATAAAATGGATCAGGACTTGAAGAT

REV-HSNAP29 5'-CCGCTCGAGTCAGAGTTGTCGAACTTTTCTTTCTG-3'

Sequences of primers for T3 and T7 probes preparation:

T3-Snap29 5'- TAATACGACTCACTATAGGGAGAAACCCAGGAGGTGGGTAAG-3'

T7-Snap29 5'- AATTAACCCTCACTAAAGGGAGAATGTTATCCAGCAATTCATTTTG-3'

T3-Ndc80 5'- TAATACGACTCACTATAGGGAGAATGTCGCACCTGATGCCCCGG-3'

T7-Ndc80 5'- AATTAACCCTCACTAAAGGGAGATAAGCTCCTGATCCCACAAGG-3'

Sequences of primers used for RT-qPCR:

Snap29 F 5' –AGCAGCGAACTCTGGACTCT– 3'

Snap29 R 5' – TGTGATGTCTTCTCCAGTTGCT– 3'

E(Spl)mβ F 5' –GAGTGCCTGACCCAGGAG – 3'

E(Spl) mβ R 5' –CGGTCAGCTCCAGGATGT - 3'

Upd1 F 5' –ATGGCCGAGTCCTGGCTACTGTT – 3',

Upd1 R 5' – AACTGGATCGACTATCGCAACTTC - 3'

Atg8a F 5' -GGGATGCATCGGAATGAA- 3'

Atg8a R 5' -CGGTTTTCCTCAATTCGTTT- 3'

Atg18.2 F 5' -AAAATACAATCACCAAAGCACAAA- 3'

Atg18.2 R 5' -GTCCTGGTTGAAGTTCATTTGAT- 3'

Rpl32 F 5' –CGGATCGATATGCTAAGCTGT – 3'

Rpl32 R 5' – CGACGCACTCTGTTGTCG - 3'

5. RESULTS

5. 1 Characterization of B6 mutation in *Drosophila* epithelial organs

5.1.1 *MENE (2R)-B6-21* disrupts epithelial tissue architecture in *Drosophila*

In screen to identify genes that control epithelial architecture in *Drosophila*, we had previously isolated the MENE-(2R)-*B6-21* (B6) mutant (Vaccari et al. 2009). We studied the effect of the B6 mutation in larval eye-antennal imaginal discs which are the developing epithelial organs that give rise to the corresponding adult body parts. Compared to wild type (WT) (Fig. 17A), eye-antennal discs formed for a large part by B6 mutant cells (referred to as "mutant discs" henceforth) display altered epithelial architecture and larvae bearing them die before entry into pupariation (Fig. 17B, B', B"; Vaccari et al. 2009). Aberrant epithelial tissue development in B6 mutant discs is characterized by mispolarization of apico-basal polarity markers (Fig. 17C, D) and reduced ability to terminally differentiate in variable portions of the disc epithelium (Fig. 17E, F). Similarly, B6 mutant wing imaginal discs display altered tissue organization (data not shown). This analysis indicates that the gene carrying B6 mutation controls tissue architecture in *Drosophila* developing epithelial tissues.

5.1.2 *MENE (2R)-B6-21* is a mutant in the gene encoding *Drosophila Snap29*

To identify the gene mutated in B6, we mapped the mutation by complementation and recombination, and by candidate exon sequencing. B6 maps to the *ubisnap* gene (Flybase: Usnp/CG11173), which encodes the *Drosophila* homolog of SNAP29, Snap29 hereafter (Fig. 18A). Snap29 shares all the features of its human homolog (Fig. 19). Sequencing reveals that B6 is a nonsense mutation introducing a premature stop codon in the *Snap29* gene predicted to truncate the protein between the two SNARE domains (Fig. 18B). Discs containing mutant cells express almost normal levels of Snap29 mRNA (Fig. 18C).

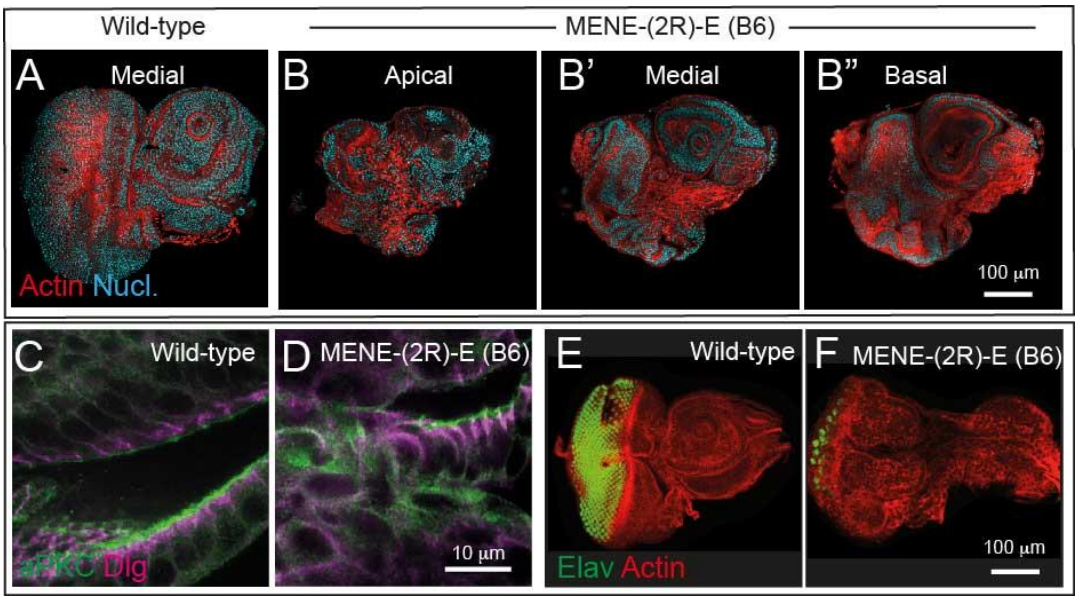

Figure 17. MENE(2R)-21-B6 mutant eye imaginal discs phenotype. (A) WT eye-antennal disc (eye disc to the left, antennal to the right) and (B-B'') apical, medial and basal sections of MENE(2R)-21-B6 mutant eye disc stained with phalloidin, to mark subcortical F-actin, and DAPI. Compared to WT, a mutant eye disc shows tissue architecture disruption. (C, D) WT and MENE(2R)-21-B6 eye discs stained with anti-aPKC and anti-Dlg, apical and lateral membrane markers respectively, and (E, F) with anti-Elav, a marker of neuronal differentiation. Compared to WT, MENE(2R)-21-B6 discs loose apico-basal and lateral polarity and the ability to terminal differentiate.

With an anti-Snap29 antibody that we have generated, we observed by western Blot analysis that discs containing mutant cells also express a Snap29 form of predicted size for the truncated protein (Snap29^{B6} henceforth; Fig. 18D). To determine which domain of Snap29 is important for function, we attempted to rescue the phenotype of Snap29^{B6} mutant discs by ectopic expression of full–length Snap29 or of mutated forms of Snap29 (Fig. 18E–O). When expressed in Snap29^{B6} mutant discs, a full-length CFP-tagged form of Snap29 (CFP- Snap29) (Fig. 18G, G') fully rescues eye-antennal discs defects and lethality, leading to development of adults with eye structures indistinguishable to that of WT animals (Fig. 18L, M, O), indicating that impairment of Snap29 function is the cause of the phenotypes observed in *Snap29^{B6}* mutant tissues. Both *Snap29^{B6}* homozygous and *Snap29^{B6}* hemizygous animals are lethal shortly after larval hatching, indicating that *Snap29^{B6}* is likely to be a strong loss of function *Snap29* allele. Surprisingly, a Snap29

form with a mutated NPF motif (NPF>AAA) can rescues pupal lethality, yielding escaper adults with various degrees of eye defects (Fig. 18H, H', N, O). These data suggest that the NPF motif can be dispensable for Snap29 function, at least upon over-expression of the mutant form. In contrast, Snap29 forms lacking either the first or the second SNARE domain (ΔSNARE1 and ΔSNARE2 respectively) are unable to rescue *Snap29*^{B6} mutant discs, when overexpressed at comparable levels to other forms (Fig. 18H, H', O), indicating that the presence of both SNARE domains is required for function. Mutant forms of Snap29 do not appear to possess dominant negative activity when overexpressed at equal levels in otherwise WT discs (Fig. 18I, J, K). This is the case also of ΔSNARE2, a mutant form of Snap29 that lacks the second SNARE domain and resembles the Snap29^{B6} protein (Fig. 18H, H', J). Considering that ΔSNARE2 does not rescue *Snap29*^{B6} mutant discs, we conclude that forms lacking the C-terminal portion of the protein are inactive, suggesting that Snap29^{B6} is most likely non-functional in *Snap29*^{B6} mutants.

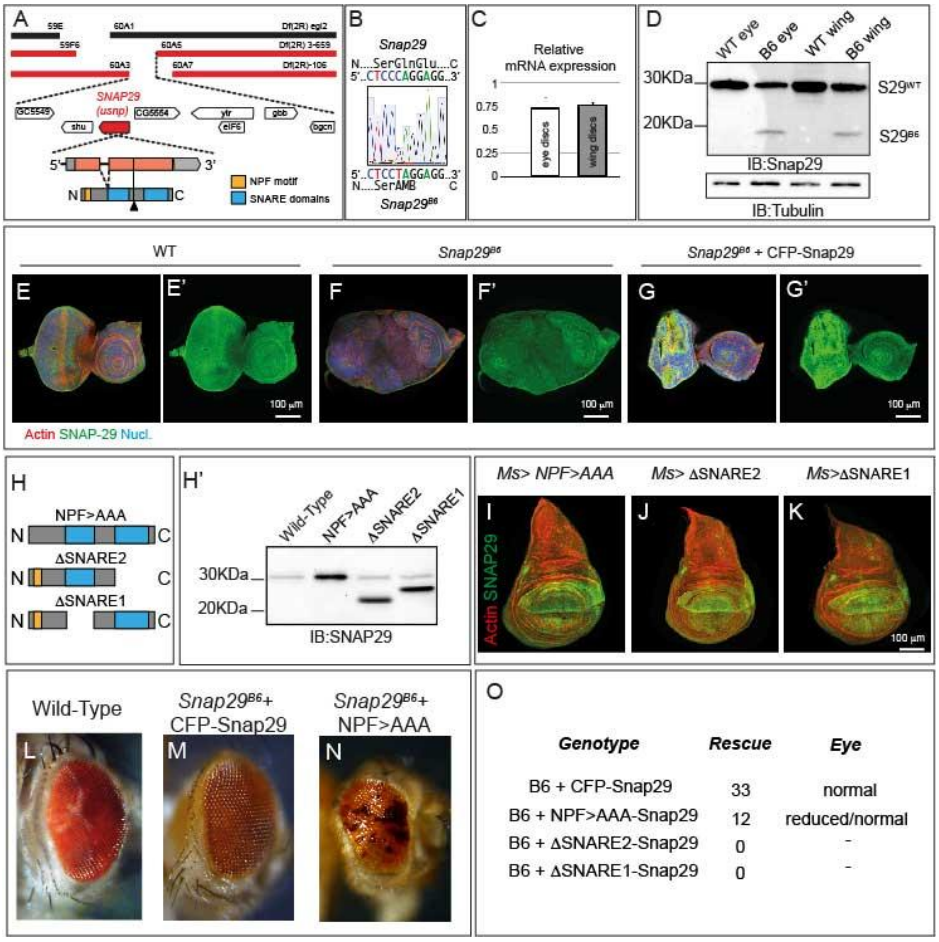

Figure 18. S*nap29* is the gene affected by MENE(2R)-E B6 mutation. (A) Schematic view of the *Snap29* locus. Df(2R)egl2 (black) complements the B6-21 mutation, while Df(2R)3-659 and Df(2R)106 (red) fail to complement it, indicating that B6-21 maps to the genetic interval 60A3-A5 on the right arm of the *Drosophila* chromosome 2. The coding sequence of *Snap29* is shown in orange, while the domains of Snap29 are indicated in yellow (NPF) and blue (SNARE motifs). A black triangle marks the approximate position of the B6 mutation. (B) Sequencing of the $Snap29^{B6}$ allele in heterozygosity with the parental chromosome on which the mutation was induced. A C-to-T change creates a premature stop codon that truncates the protein right after the first SNARE domain. (C) Expression of Snap29 mRNA is only 25% reduced in mutant eye-antennal and wing discs, relative to WT. (D) Analysis of Snap29 expression by Western blot in WT discs extracts and in extracts of discs containing $Snap29^{B6}$ mutant cells indicates that $Snap29^{B6}$ ($S29^{B6}$: 20 KDa), a truncated form of Snap29 ($S29^{WT}$: 34KDa) is present in mutant cells. (E-G) Eye-antennal discs of the indicated genotype immunostained with anti-Snap29, phalloidin and DAPI. Compared to WT, $Snap29^{B6}$ mutant discs display altered eye disc morphology, which is rescued over expressing CFP-Snap29 under the eyeless-GAL4 promoter in the eye disc. Note in F'-G' the reduced level of Snap29 expression in B6 mutants and the increased level in eye discs over expressing CFP-Snap29. (H) Cartoon of mutated NPF motif in Snap29 (NPF>AAA), and of Snap29 forms lacking the C-terminus (ΔSNARE2) and the central SNARE motif (ΔSNARE1). (H') Blotting with anti-Snap29 yields a band at 34KDa in WT discs, while discs expressing Snap29 mutant forms display comparable amount of polypeptides of the expected sizes. (I-K) Over expression of the indicated mutant Snap29 forms under ms1096-GAL4 in wing disc does not alter disc morphology.

(L-N) Adult eyes of flies with the indicated genetic background. Eye-specific ectopic expression of CFP-Snap29 or of a Snap29 form with a mutated NPF motif (NPF>AAA) yield adults with normal (CFP-Snap29), or reduced eyes (NPF>AAA). Mutant cells expressing the rescue construct give rise to orange photoreceptors, while the WT cells give rise to dark red ones. (O) Table of rescue experiments, with number of animal rescued to adulthood by over expression of the listed construct in *Snap29*^{B6} mutant eyes over two crosses, and description of resulting eye phenotypes.

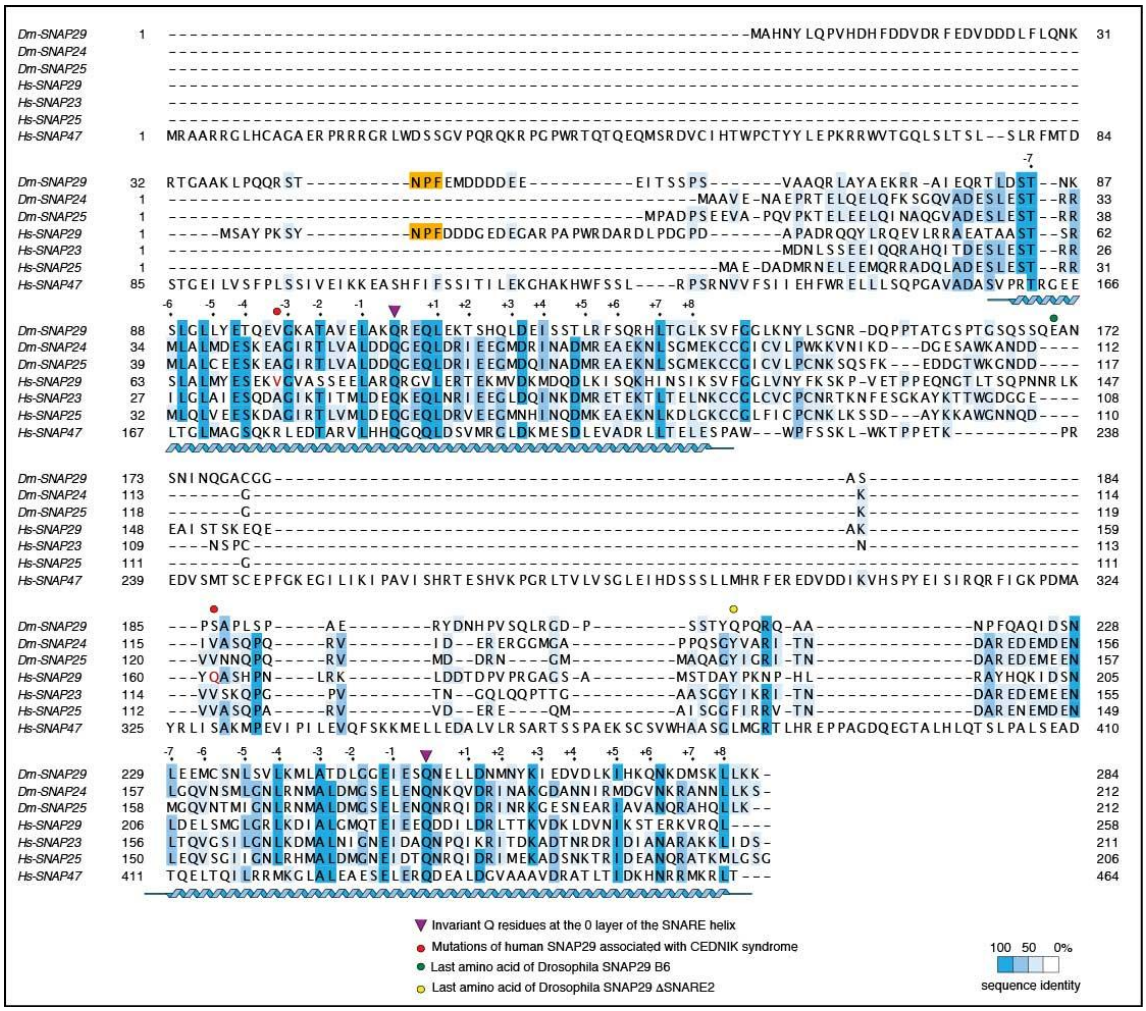

Figure 19. Conservation, structure and mutations of Snap29. Multiple sequence alignment of *Drosophila* and humans SNAP29 paralogs with residues are colored according to their conservation. Helices corresponding to the two Q-SNARE domains are displayed at the bottom of the alignment, with the canonical domain layering numbered at the top. Conserved 'NPF' triplets at the N-terminus of SNAP29 are highlighted in orange. Mutations of Human SNAP29 associated with CEDNIK syndrome is depicted with a red circle.

5.1.3 Snap29 localizes to multiple organelles in interphase and to KTs in mitosis

We then studied the subcellular localization of Snap29 in epithelial cells. In mosaic imaginal discs containing *Snap29*^{B6} mutant cells (referred to as "mosaic discs" henceforth) anti-Snap29 marks cytoplasmic puncta and such signal is reduced in clones of *Snap29*^{B6} mutant cells (Fig. 20A, A'). Similar localization was observed in the follicular epithelium (FE) of the adult ovary (Fig. 20B). Cytoplasmic puncta are also observed by expression of a functional CFP-Snap29, which in addition localizes to the PM (Fig. 20C). To assess to which intracellular organelles the puncta correspond to, we co-localized Snap29 or CFP-Snap29 with markers of various trafficking compartments. Consistent with previous findings, we observe partial co-localization with markers of the Golgi Apparatus, of the early and recycling endosomal compartment and of the late endosome and lysosome (Fig. 20D-G). In agreement with these data, in the analysis of Snap29 interactors by mass spectrometry, we repeatedly identified a set of SNARE proteins that consists of the plasma membrane Qa-SNAREs Syntaxin1A (Syx1A) and Syntaxin4 (Syx4), of the endosomal Qa-SNARE Syx7, and of the R-SNAREs Sec22, Synaptobrevin (Syb) and Vamp7. We have also found the SNARE-specific factors dNSF2, αSnap and γSnap and a limited set of other proteins (Fig. 21A; Table 1). These data are consistent with large-scale protein complex identification approaches (Guruharsha et al. 2011), and suggest that Snap29 associates with multiple SNARE complexes and thus multiple trafficking compartments.

Surprisingly, during mitosis Snap29 assumes a different localization. Indeed, it co-localizes with the inner KT-marker CID (the *Drosophila* homolog of CENP-A) in mitotic cells in the FE (Fig. 20H-I) and in epithelial imaginal discs (Fig. 20J). In support of the localization data, we have found by mass specrometry analysis that among the proteins immunoprecipited with Snap29 are the outer KT components Ndc80, Spc105 (the *Drosophila* KNL-1), Nuf2, Mis12, Kmn1 (the *Drosophila* Dsl1 homolog), and Kmn2 (the

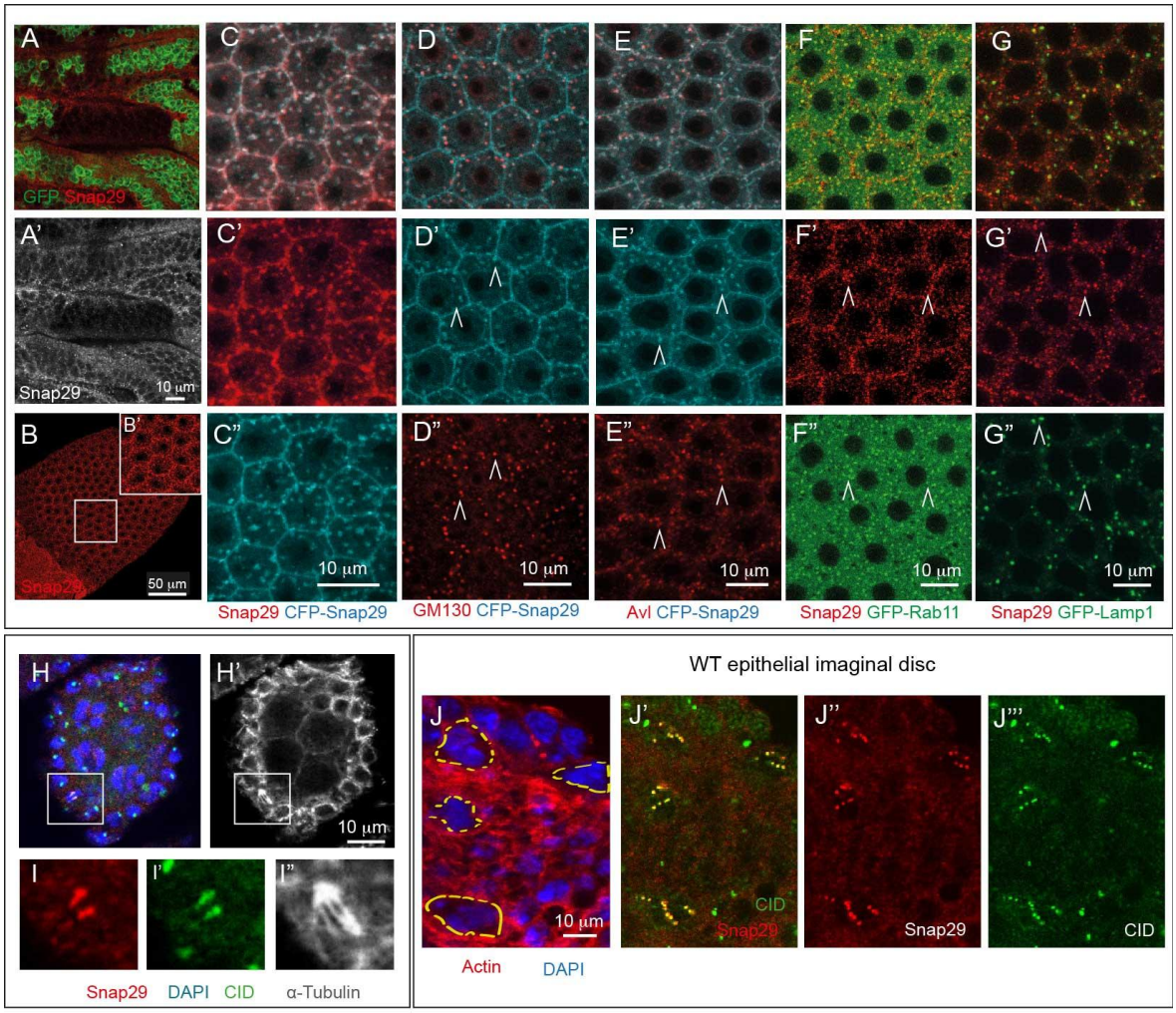

Figure 20. Snap29 localization in interphase and mitotic cells in *Drosophila* epithelial tissues**.** (A) High magnification of a clone of *Snap29* mutant cells in a mosaic wing disc stained to detect Snap29 (Single channel in A'). Nuclear GFP marks surrounding WT cells. In these, Snap29 is found in intracellular puncta. In *Snap29*^{B6} mutant cells, which express truncated Snap29, staining levels are strongly reduced, indicating that the antibody signal is specific. (B) As in discs cells, Snap29 localizes to intracellular puncta in adult follicular epithelial cells. A single medial confocal cross-section is shown. The inset (B') shows a higher magnification of the boxed area. (C-G) Co-localization of Snap29 or CFP-Snap29 with markers of various trafficking compartments in follicular cells. Single medial confocal cross-sections (as in B') are shown. Over expression of CFP-Snap29 increases the portion of Snap29 at the plasma membrane (compare Snap29 expression of C-E with F-G). Snap29 partially co-localizes with markers of Golgi Apparatus (GM130), early endosome (Avl), recycling endosome (GFP-Rab11) and forming lysosomes (GFP-Lamp1). Example of co-localizing signals are highlighted by arrowheads. (H, H') Single medial confocal cross-section of an early stage egg chamber stained for Snap29, the inner KT marker CID, DAPI and α-tubulin, to mark mitotic spindle. (I-I'') High magnification of the boxed area in H, H' showing a dividing cells in anaphase. (J) Eye disc epithelium containing four mitotic cells, circled with yellow dashed line, stained for actin, DAPI and (J'-J''') for CID and Snap29. Snap29 co-localizes *in vivo* with the KT marker CID (J').

Spc24 homolog) (Fig 21B, Table1). These results strongly suggest a possible new role for Snap29 at the KT during cell division.

Prompted by *Snap29*^{B6} phenotype in the eye immaginal disc, we next investigated the mechanism by which Snap29 sustains signaling and tissue architecture during epithelial tissue development. To this end, according with our preliminary results, we studied the role of Snap29 in membrane trafficking and in cell division.

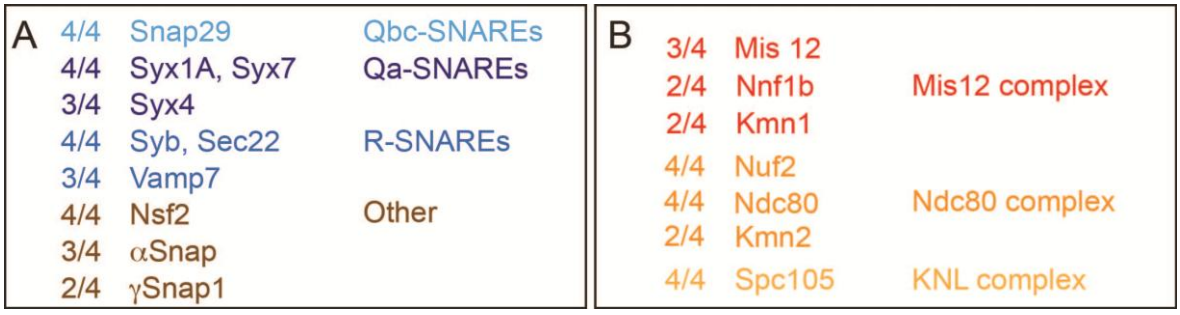

Figure 21. Snap29 interactors analysis by Mass Spectrometry**.** (A) Membrane fusion and (B) KT proteins co-immunoprecipitated with Snap29 in at least 2 out of 4 experiments using two independently-raised anti-Snap29 antibody. The proportion of immunoprecipitations containing each protein is indicated.

5.2 Snap29 is a regulator of autophagy and trafficking pathways in *Drosophila* epithelial tissues

5.2.1 *Snap29* mutant tissue displays altered autophagy and Golgi apparatus organization

To understand the function of Snap29 in epithelial tissue, in collaboration with our EM facility, we analyzed the ultrastructure of *Snap29*^{B6} mutant discs by electron microscopy (Fig. 22). Compared to WT, *Snap29*^{B6} mutant tissue displays a striking accumulation of double membrane vesicular organelles (Fig. 22A-B). Accumulated double membrane organelles present diameters ranging from 0.5 μm to 5 μm with most of them averaging 0.7 μm and contain a wide array of intact cellular structures, such as mitochondria, ER or

vesicles (Fig. 22B, arrows). By immuno-EM, we find that these organelles are positive for ref(2)P, a selective autophagy target, and for Atg8a, a master regulator of autophagy, indicating that they are autophagosomes (Fig. 22D, arrows). In WT eye disc cells, autophagic structures are very rare and tomographic analysis reveals that the few found are late stage amphisomes or autolysosomes, as judged by their single and double limiting membrane and by their partly degraded luminal content (Fig. 22E; movie 1). In contrast, the vast majority of the autophagosomes accumulated in *Snap29*^{B6} mutant cells are completely delimited by double membrane filled with a continuous protein-poor space. In addition, the accumulated autophagosomes in *Snap29*^{B6} mutant cells contain cytosolic structures in their lumen that are perfectly preserved, indicating that no degradation occurs in these organelles (Fig. 22F; movie 2). The outer and inner limiting membranes of the accumulated autophagosomes is often convoluted and folded on a limited part of the organelle surface, and accumulated autophagosomes were often found close to each other (Fig. 22G; movie 3), or close to multilamellar organelles that could be lysosomes (Fig. 22H; movie 4). Rarely, amphisomes were found in *Snap29*^{B6} mutant cells, suggesting that fusion of autophagosomes with MVBs can still occur to a certain degree. In this case, signs of content degradation, such as broken membranes, are apparent (Fig. 22I; movie 5). In addition to intracellular accumulation of autophagosomes, *Snap29*^{B6} mutant cells present a prominent apical extracellular accumulation of large vesicles, possessing a single delimiting membrane and displaying approximately the size of the autophagosomes accumulated intracellularly (Fig. 22B, arrowhead). Importantly, tomographic analysis reveals that these also can contain intact non-digested cellular structures, and are often found juxtaposed to the apical membrane, or can be found at various stages of fusion with the apical plasma membrane (Fig. 22J, movie 6), indicating that they might represent exocytosed autophagic structures. Occasionally, we observed the presence of very large (> 2 μm in diameter) cytoplasmic bodies surrounded by a double membrane containing smaller autophagosomes and other organelles (Fig. 22C-D, K). Similar giant structures

could be also found outside of the cells apically (Fig. 22C, L). While these aberrant organelles could occur by multiple rounds of autophagic sequestration, the presence of apoptotic cells in *Snap29*^{B6} mutant discs suggests that they could be apoptotic bodies, possibly engulfed by epithelial cells. Finally, compared to WT cells, *Snap29*^{B6} mutant cells show a prominent disorganization of the cisternae of the Golgi apparatus (Fig. 22M-N). Tomographic reconstructions show that while in WT cells the Golgi cisternae are typically stacked (movie 7), in *Snap29*^{B6} mutant cells the cisternae are highly perforated and their number is decreased (movie 8). Also, while in WT cells the length of individual cisternae is uniform, in *Snap29*^{B6} mutant cells their size is highly variable (movie 8). Taken together, these data indicate that *Snap29*^{B6} is required to prevent accumulation of autophagosomes and to maintain a correct Golgi apparatus morphology.

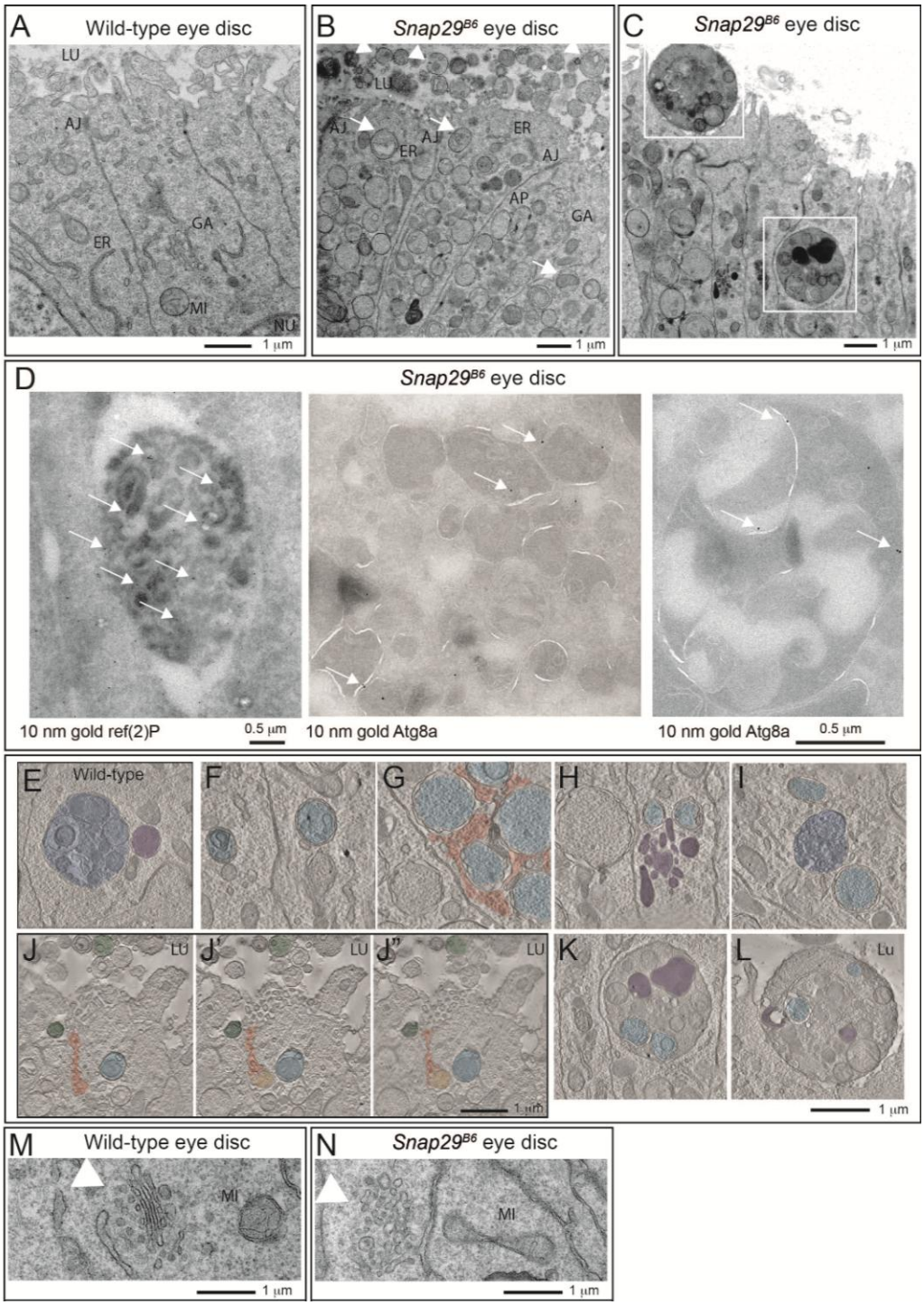

Figure 22. *snap29* mutant tissue electro microscopy analysis. (A-B) Electron micrograph of a section of eye disc tissue of the indicated genotype. A portion of the apical part of 3-5 epithelial cells above the level of the basal nuclei is shown. While double membrane organelles are very rarely observed in WT cells, mutant cells are packed with them. In B, examples of double membrane organelle containing other organelles are indicated with white arrows, while examples of organelles with a single membrane containing with vesicles or organelles in the apical lumen are indicated by white arrowheads. (C) Example of a thick 200 nm section of mutant tissue used for tomography reconstructions. Gold particles have been added for image registration. White boxes highlight a intracellular giant body containing autophagosomes, lysosomes and mitocondria (bottom box), and a similar apical extracellular organelle (top box). Corresponding higher magnification

images are shown in L-M and relative tomograms are presented as supplementary data. (D) ref(2)P and Atg8a label autophagosomes in *Snap29*^{B6} mutant cells by immuno-EM, as indicated by white arrows. A large double membrane structure marked with Atg8a is also shown in the rightmost panel. (E) Example of amphisome (blue) in a WT cell close to a multilamellar organelle that could be a lysosome (pink). (F-I) Examples of autophagic organelles accumulated in mutant cells: Autophagosomes completely enclosed by a double membrane (F, light blue). Autophagosomes clustered together enclosed by folded membranes in part connected (G, light blue). The cytoplasmic space between them is shaded in red. Autophagosomes (H, light blue) close to a cluster of multilamellar organelles that could be lysosomes (H, pink). A rarely occurring amphisome (I, blue) in between two autophagosomes (I, light blue). (J-J") Three representative planes of a tomographic reconstruction showing intracellular autophagosomes (one highlighted in light blue), exocytosed autophagosomes (two highlighted in green), and one autophagosome in the process of being exocytosed (green) the lumen connecting to the apical extracellular space is highlighted in red. (K-L) Examples of large structures inside (K) and outside (L) mutant cells. Autophagosomes internal to these structures are highlighted in light blue and electrondense lysosomal material is shaded in pink. Tomograms of panels E-L are presented as supplementary data. (M-N) Examples of Golgi apparatus organization. Note the absence of stack organization in the Golgi apparatus of a mutant cell. Labels are as follows: Lu: Apical lumen, AJ: Adherens Junctions, ER: Endoplasmic Reticulum, Go: Golgi apparatus, Mi: Mitocondrium, Nu: Nucleus.

5.2.2 Snap29 controls fusion of autophagosomes to degradative organelles

In agreement with the EM analysis on mutant discs, in mosaic discs containing clones of *Snap29*^{B6} cells, mutant cells also display accumulation of ref(2)P, when compared to surrounding GFP-positive WT cells (Fig. 23A-B, D). Similar ref(2)P accumulation is seen in cells mutant for *Vps25* (Fig. 23C-D), which is a tumor suppressor gene whose impairment blocks endosomal sorting and causes autophagosomes accumulation (Vaccari & Bilder 2005). As expected from failure of autophagy to clear ubiquitinated protein aggregates marked by ref(2)P, *Snap29*^{B6} mutant discs display moderate accumulation of ubiquitin, when compared to WT or *Vps25* mutant discs (Fig. 23B-C, E). Accumulation of autophagosomes and ref(2)P in mutant cells could be due to a block in the autophagy flux or to induction of autophagy, or both. To distinguish between these possibilities, we tested S6k phosphorylation and expression of *Atg* genes, as it has been shown that, in conditions of starvation-induced autophagy, levels of phospho-S6k are low and expression of certain *Atg* genes is high (Ravikumar et al. 2010, Wu et al. 2009). Compared to WT discs, mutant

discs possess high levels of phospho-S6k and low Atg8a and Atg18.2 expression, suggesting that accumulation of autophagosomes in mutant cells is not due to induction of autophagy (Fig. 23F-G). To test whether a block in autophagosome fusion to degradative organelles is the cause of autophagosome accumulation, in collaboration with T.E. Rusten and H. Stenmak, we analyzed the localization pattern of mCherry-Atg8a, a marker of autophagosomes and autophagolysosomes in the fat body, a tissue used as model to study autophagy. In agreement with previous analysis (Pircs et al. 2012) mCherry-Atg8 marks distinct punta in starved WT cells, indicating that autophagolysosomes are properly formed. Instead, when Snap29 is depleted as in the GFP positive cells, starved cells show a broadly accumulation of mCherry signal and the punctuate mCherry positive structure decreases suggesting that autophagolysosomes are not formed. In addition, Snap29 depleted cells under starvation show accumulation of ref(2)P when compared to WT cells (Fig. 23H, I). Consistent with our EM findings, these data suggest that Snap29 is required for fusion of autophagosomes with degradative endocytic organelles. If Snap29 regulates fusion of autophagosomes with lysosomes, it should be found associated to these organelles. In FE of animals expressing GFP-Lamp1, a marker of late endosomes and forming lysosomes, Snap29 puncta only rarely overlap with GFP-lamp1 puncta (Fig. 23J). However, they are sometimes found in close proximity of clusters of Atg8a puncta surrounding GFP-Lamp1 positive structures (Fig. 23K), indicating that Snap29 could transiently associate to autophagosomes to mediate lysosomal fusion. Consistent with this and with recent data in literature (Takas et al. 2013), which indicate that Snap29 controls autophagosome to lysosome fusion together with Syx17 and Vamp7, we find that Snap29 genetically interacts with these two SNAREs. Indeed, Snap29 depletion phenotype in the posterior half of developing wing imaginal discs leads to a reduction of adult wing tissue that is enhanced by depletion of Syx17 (Fig. 23L–N) or Vamp7 (Fig.23O, P, Q).

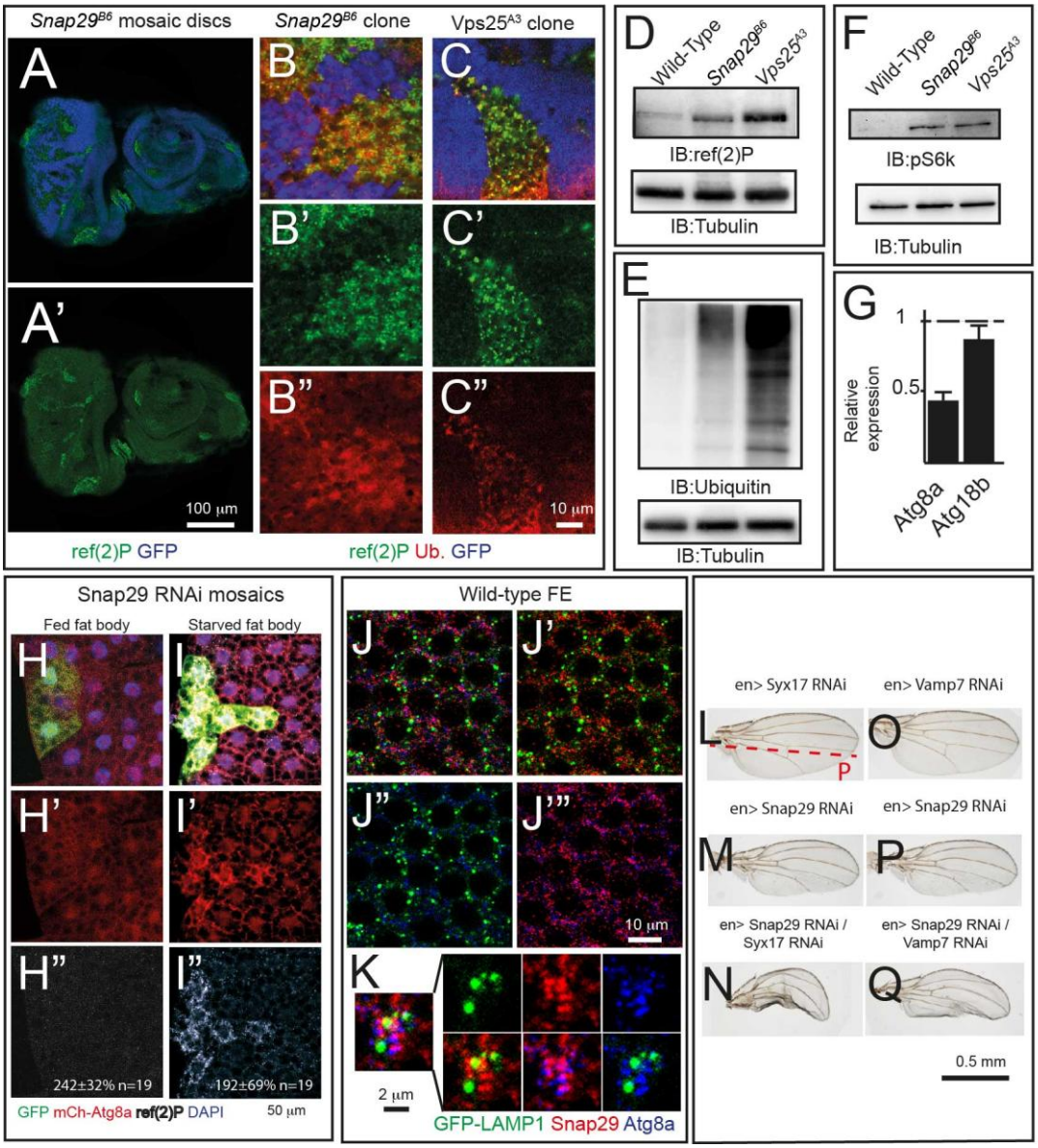

Figure 23. *snap29* mutant cells fail to complete autophagy**.** (A-B) Clones of *Snap29*^{B6} or (C) *Vps25*^{A3} mutant cells in mosaic eye-antennal discs accumulate high levels of Ref(2)P and ubiquitin, compared to surrounding WT cells. B-C show a high magnification image of an anterior portion of an eye discs. Single ref(2)P and Ubiquitin channels are shown. (D-F) Immunoblots of protein extracts from eye-antennal discs of the indicated genotypes to detect (D) ref(2)P, (E) Ubiquitin and (F) pS6K. Compared to protein extracts of WT discs, discs mutant for *Snap29* and for the autophagy and trafficking regulator *Vps25* accumulate ref(2)P, Ubiquitin and pS6K. Loading controls are shown below each blot. (G) Relative expression of Atg8a or Atg18.2 by Q-PCR analysis of mRNA extracts from WT and mutant discs. Mutant discs do not show induction of expression of Atg genes. (H-I) Clones of cells expressing Snap29 RNAi (green) in fat body cells of (H) fed or (I) 4hr starved larvae. Compared to WT cells, starved cells depleted of Snap29 display ref(2)P accumulation, and lack of punctate mCherry-Atg8astructured. H'-I'' are the single mCherry-Atg8a channels, while H''-I'' are the single ref(2)P channels. Relative abundance of ref(2)P in depleted versus non-depleted cells in starved fat body samples is shown in I''. (J) A single medial confocal cross-section of the *Drosophila* FE of a stage 9 egg chamber. FE cells over expressing GFP-Lamp1 are stained for Snap29 and Atg8a. J', J'', J''' show

respectively the Lamp1 and Snap29, the Lamp1 and Atg8a, and the Snap29 and Atg8a merged channels. A high magnification of a typical cluster formed by GFP-Lamp1, Snap29 and Atg8a-positive vesicles is shown in K. The three proteins are in close proximity. (L-Q) Wings of animals of the indicated genotypes. Expression of engrailed-GAL4 (en>) occurs in the posterior part (P) of the developing wing discs, demarcated in adult wings by the red line in L. Knock-down of Snap29 results in mild reduction of wing size, a phenotype that is enhanced by down regulation of Syx17 and Vamp7, indicating that the corresponding genes genetically interact with *snap29*.

5.2.3 Snap29 is a negative regulator of autophagosomes secretion

Since we found presence of organelles with the morphology of autophagosomes in the apical lumen of $Snap29^{B6}$ mutant discs (Fig. 22B, C, J, L), we hypothesized that Snap29 could negatively regulate secretion at the plasma membrane. Consistent with this, we observe that secreted organelles in mutant cells are ref(2)P and Atg8a positive (Fig. 24A-E). Secretion of autophagosomes could be an indirect consequence of intracellular accumulation of autophagosomes. To assess whether this is the case, we tested whether secretion of autophagosomes is also present in discs mutant for *Syx17* and *Vamp7*. Surprisingly, both by immunofluorescence and EM, we find that, while *Syx17* and *Vamp7* mutant tissues display accumulation of autophagosomes intracellularly, they are devoid of secreted autophagosomes (Fig. 24F-I). Interestingly, no giant autophagosomes are found in *Syx17* and *Vamp7* mutant discs (Fig. 24H-I). Taken together, these data indicate that autophagosome secretion is unlikely a consequence of impaired fusion of autophagosomes with lysosomes and suggest that Snap29 might negatively regulate fusion at the plasma membrane independent of Syx17 and Vamp7.

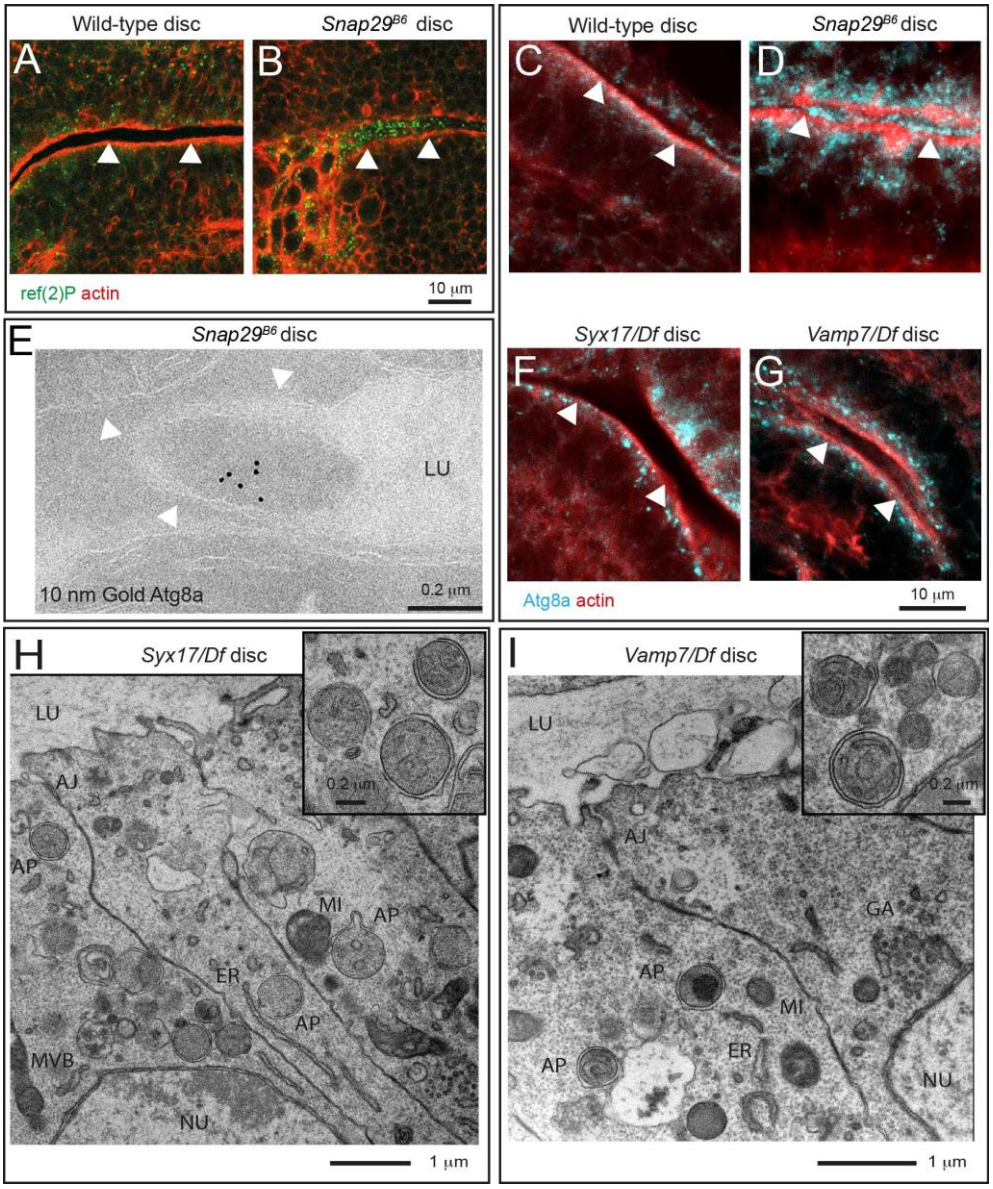

Figure 24. Autophagosomes are secreted in *Snap29* mutant discs. (A-D) Cross sections of WT and *snap29*^{B6} mutant wing discs (A-B), or eye discs (C-D) stained as indicated. ref(2)P and Atg8a accumulate inside mutant cells and above the apical lumen of s*nap29*^{B6} mutant discs. White arrowheads highlight the apical plasma membrane of the tissue above which is the lumen between two epithelial folds. (E) Immuno EM of s*nap29*^{B6} mutant disc reveals Atg8a labeling of a large vesicle in the extracellular lumen. The white arrowheads indicate the apical plasma membrane. (F-I) Immunofluoresce and EM analysis of sections of eye discs mutant for *Syx17* or *Vamp7*. Atg8 and autophagosomes accumulate within mutant cells, but they are not present in the extracellular lumen.

5.2.4 Snap29 regulates Notch and Domeless receptors secretion and degradation

In order to investigate whether or not Snap29 role in regulation of vesicle fusion at the plasma membrane is specific for autophagosomes or it is instead extended to other

vesicles, we decide to monitor the level at the plasma membrane of Notch and Domeless receptors in *Snap29*^{B6} mutant cells compared to WT (Fig. 25A–D). We found that both receptors are increased at the plasma membrane of mutant cells. To understand whether the increased levels are due to increased secretion rather than decreased endocytosis, we monitored Notch endocytosis through a trafficking assay (see materials and methods). We confirmed that Notch receptor accumulates at the apical membrane of *Snap29* mutant cells in not permeabilized conditions (Fig. 25E, E'). 15 minutes after internalization Notch localizes in Syx7 positive vesicles in mutant and control cells (Fig. 25F, F'), indicating that endocytosis is not impaired in *Snap29*^{B6} cells. However, 210 minutes after internalization, we observed that Notch-containing vesicles fail to be degraded in *Snap29* mutant compared to control cells (Fig. 25G–H), suggesting that a mutation in *Snap29* might also impaired a late step of endocytosis. We confirmed that Notch accumulates in *Snap29*^{B6} mutant cells by Western Blot analysis. As positive control, we used protein extracts from *Vps25* mutant discs, which are known to accumulate Notch (Fig. 25I) (Vaccari & Bilder 2005). Overall, these results suggest that Snap29 is important to control apical secretion and a late step of endosomal degradation.

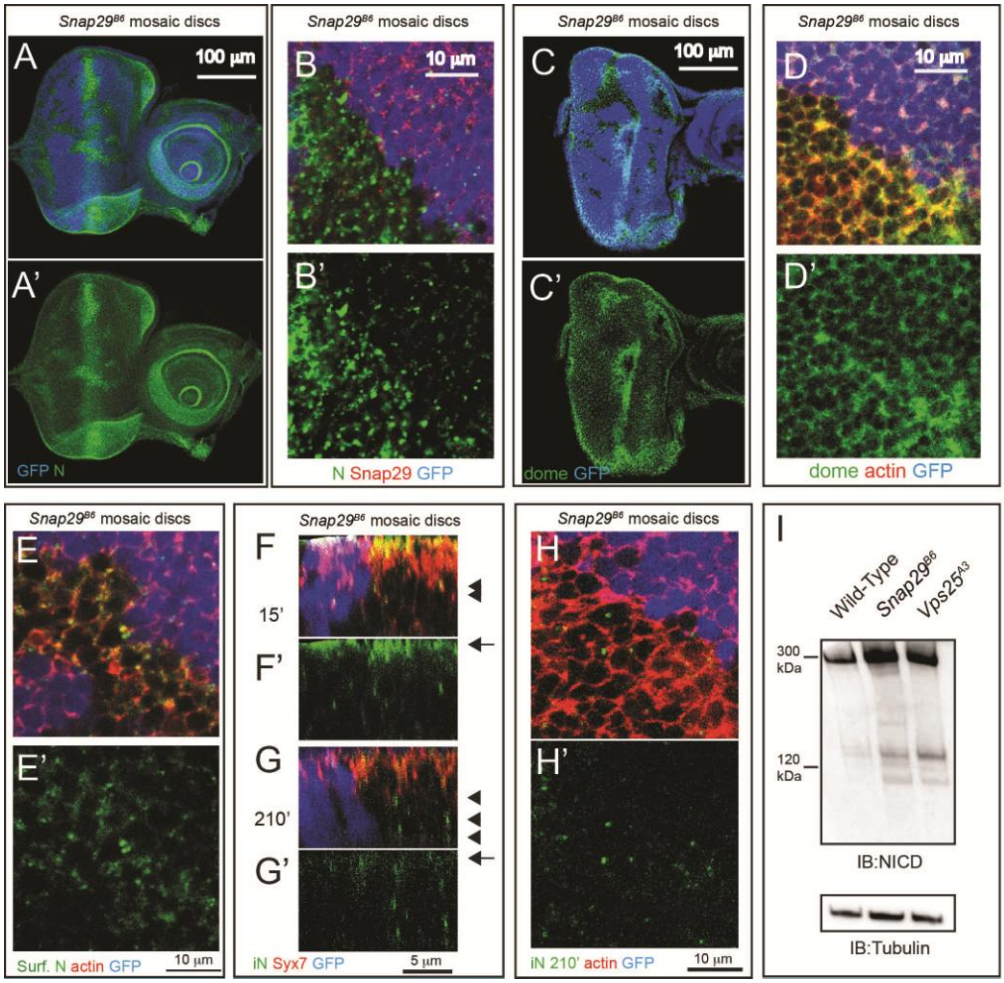

Figure 25. *Snap29* mutant cells display altered Notch and Domeless trafficking. (A, C) Clones of *Snap29*^{B6} mutant cells in mosaic eye-antennal discs accumulate high levels of Notch and Domeless receptor, compared to surrounding WT cells. (B) High magnification of a cross section of a mosaic disc show that Snap29 signal strongly decreases in *Snap29*^{B6} mutant cells, while both Notch and Domeless receptors accumulate at the plasma membrane and within cells. A'-B' and C'-D' are single channel for Notch and Domeless receptors respectively. (E) Labeling of non-permeabilized *Snap29*^{B6} mosaic eye-antennal discs with an anti- NECD. Compared to WT cells marked by expression of GFP, clones of mutant cells in the eye disc display higher Notch surface levels (Surf. Notch). E' shows the single confocal channel for anti-Notch. (F-G) Z-sections of eye disc epithelia subjected to 15' (F) and 210' (G) internalization of anti-NECD and staining as indicated. Similar to WT cells, Notch is present on the apical plasma membrane of mutant cells (F, arrow) and is able to access early endosomes (F, arrowhead). Notch is efficiently internalized over time in both WT and mutant cells (G, arrow); however, in mutant cells it fails to be degraded and accumulates in a Syx7-negative compartment (G, arrowhead). F'-G' shows the single confocal channel for anti-Notch. (H) Cross section of a *Snap29*^{B6} mutant clone surround with WT cells, 210' minute upon anti-NECD internalization. Compared to WT cells, mutant cells display intracellular Notch accumulations. The Actin-rich cell cortex is marked with phalloidin. G' shows the single confocal channel for anti-Notch. (I) Immunoblotting of protein extracts with an antibody recognizing the intracellular domain of Notch. Full-length Notch is approximately 300KDa while the intracellular domain is

120KDa. Both forms accumulated in *Snap29* and *Vps25* mutant discs, compared to WT. The same membrane blotted with anti-β-tubulin provides a loading control.

5.3 SNAP29 is required for KT stability and MT-KT attachment during cell division in *Drosophila* and mammalian cells

5.3.1 Snap29 localizes at the outer KT platform and is important for cell division in *Drosophila* S2 cells

As previously shown (chapter 1.3, Fig 20), Snap29 localizes at KT in mitotic cells. A detailed analysis of Snap29 localization in mitotic *Drosophila* S2 cells reveals that from prophase until anaphase Snap29 localizes to KTs (Fig. 26A-E). An high magnification of a cell in metaphase shows that Snap29 partially overlaps with CID, but never with Incenp, a centromeric chromatin marker, suggesting that Snap29 is located at the outer KT (Fig. 26K). Interestingly, S2 cells depleted of the outer KT component Ndc80 lose Snap29 localization at KT (Fig. 26M, N) indicating that Snap29 recruitment at the outer KT depends on the Ndc80 complex. In agreement with these data, we found that Snap29 and Ndc80 immunoprecipitate in the same complex (Fig. 26O). Finally, during telophase and cytokinesis Snap29 is found at centrosomes, where it co-localizes with γ-tubulin (Fig. 26E, L).

To assess whether Snap29 has a function during mitosis, we treated S2 cells with dsRNA against Snap29 for 96 hours (Fig. 26F-J). Interestingly, we find that when the level of Snap29 protein strongly decreases, mitotic chromosomes fail to align to the metaphase plate and lagging chromosomes are present during anaphase (Fig. 26H). Snap29 depleted cells conclude cytokinesis normally, but often generate daughter cells carrying mininuclei (Fig. 26J). All together, this observation allows us to conclude that Snap29 acts at the outer KT platform to control cell division in S2 *Drosophila* cells.

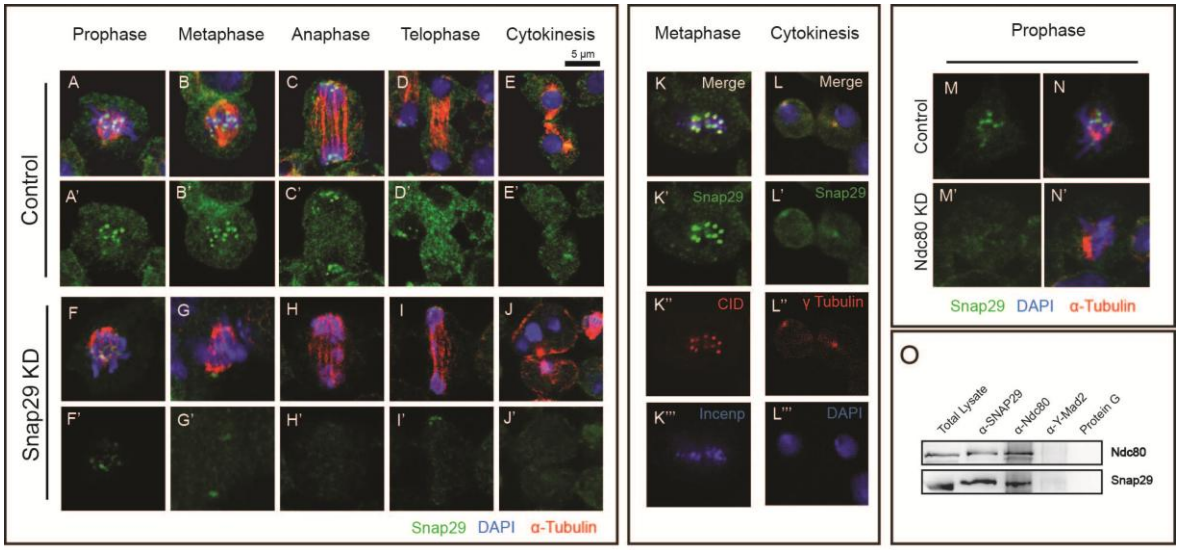

Figure 26. Snap29 is an outer KT protein which regulate cell division in *Drosophila* S2 cells. (A-E) Mitotic stages of control and (F-J) Snap29 depleted S2 cells stained to detect Snap29, α-tubulin and nuclei. (A'-E', F-J') Single confocal channel for Snap29. Snap29 localizes at KT from prophase until anaphase and is found at the spindle pole in cytokinesis. Lack of Snap29 causes cell division defects. (K) S2 cell in metaphase stained for Snap29, CID and DAPI. Single channel are showed in K', K'', K'''. Snap29 localizes toward the outer KT platform. (L) S2 cell in cytokinesis stained for Snap29, γ-tubulin and DAPI. Single channel are showed in L', L'', L'''. Snap29 co-localizes with γ-tubulin at the spindle pole during cytokinesis. (M-N) Control and Ndc80 depleted S2 cells stained to detect Snap29, α-tubulin and nuclei. In absence of Ndc80, Snap29 does not localize at KT. (O) Immuno-blotting with anti-Ndc80 and anti-Snap29 of S2 protein extract (total lysate) as positive control, Snap29 co-precipitated proteins (anti-Snap29), Ndc80 co-precipitated proteins (anti-Ndc80). Yeast Mad2 co-precipitated protein (anti-Mad2) and protein G only, are negative controls. Snap29 co-precipitates with Ndc80 and viceversa.

5.3.2 Human SNAP29 associates to centrosomes and MTs during mitotis and transiently localizes near KT during prophase

Next, we wondered whether the function of Snap29 at KT is conserved in mammals. Firstly, we analyzed the pattern of expression of SNAP29 in HeLa cells in interphase and mitosis, using a human anti-SNAP29 antibody that we generated (Fig. 27A). Interestingly, immunofluorescence analysis of SNAP29 shows that SNAP29 protein expression increases in mitotic compared to interphase cells (Fig. 27A, arrowheads vs arrows). To confirm this result we synchronized HeLa cells with a double thymidine block assay and collected proteins at different time points after the second thymidine wash-out (see materials and

methods for details). We analyzed the Mitotic Index (MI) and found that the % of mitotic cells in the population increases to 20% 10 hours after thymidine wash-out. Western Blot analysis confirms that SNAP29 expression doubles in the population enriched in mitotic cells (Fig. 27B).

Next, we analyzed the localization pattern of SNAP29 in interphase and mitotic cells. In interphase cells, we found that SNAP29 is mainly localized at the Golgi Apparatus (Fig. 28A) and EE (Fig. 28B), while rarely it associates with the ER (Fig 28C) or with RE (Fig. 28D). Surprisingly, in mitotic cells, the pattern of espression of SNAP29 is different compared to the pattern of the *Drosophila* Snap29. The human SNAP29 never fully co-localizes with CENP-A (the human homolog of the *Drosophila* CID) even though it is found in close proximity of it during prophase (Fig. 29A-A'). In addition, co-localization analysis with α-tubulin, a marker of MTs (Fig. 29B-D) and with γ-Tubulin, a marker of centrosomes (Fig. 29B'-D') shows that SNAP29 localizes at the spindle poles from prophase to telophase and that during metaphase and anaphase is mostly found along the mitotic spindle. SNAP29 localization persists at KTs upon Nocodazole treatment to depolymerize MTs and its vicinity to CENP-A is enanched (Fig. 29E-E'''), suggesting that the recruitment of SNAP29 at KTs is MT-independent. Increased levels of SNAP29 are detected by Western Blot analysis of Nocodazole-treated cell compared to the untreated ones (Fig. 29G). Interestingly, after Nocodazole wash-out, SNAP29 strongly associates with newly polymerized MTs (Fig. 29F-F'''). All together, this evidence suggests that SNAP29 might be recruited by KTs independently of MTs and that it might be removed from KTs by MTs.

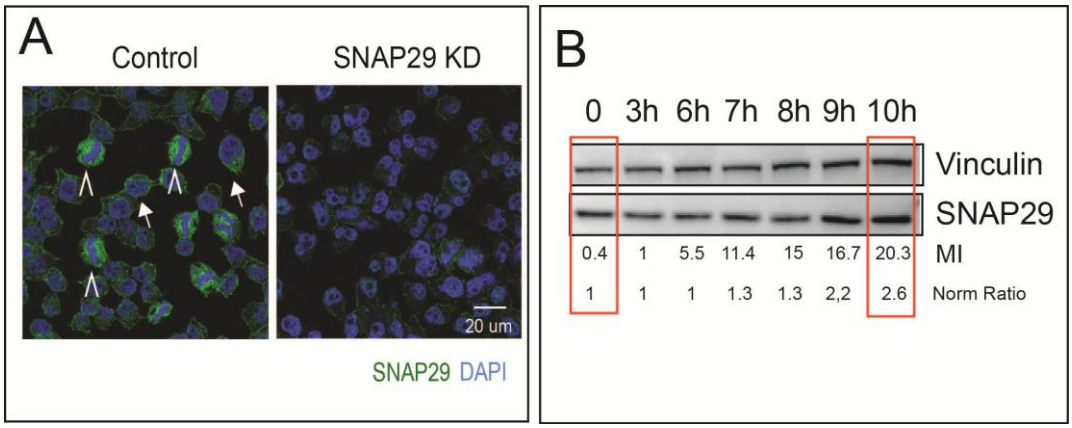

Figure 27. Human SNAP29 protein levels in mitotic and interphase HeLa cells. (A) Control and SNAP29 depleted (SNAP29 KD) HeLa cells stained for SNAP29 and DAPI. SNAP29 expression level decreases in SNAP29 depleted cells compared to control indicating the specificity of the antibody. In Control, arrowheads indicate metaphase cells, while arrows indicate interphase cells. To note that the signal of SNAP29 increases in mitotic cell compared to interphase cells. (B) Protein extracts from HeLa cells at different time points after double thymidine block are blotted with the anti-SNAP29 and with the anti-Vinculin to provide a loading control. Below each samples the Mitotic Index (MI) is reported as a ratio between the number of mitotic cells and the number of total cells. To estimate the SNAP29 expression level, SNAP29 and Vinculin pixel values are measured using Imaje J. The ratio between SNAP29 and Vinculin of each time point is then normalized for the ratio at time 0 (t0) (Norm Ratio). Compared to SNAP29 level at t0, SNAP29 protein levels increase 10h after thymidine wash out when the cell population contains more than 20% of mitotic cells. Compare the boxed red lines.

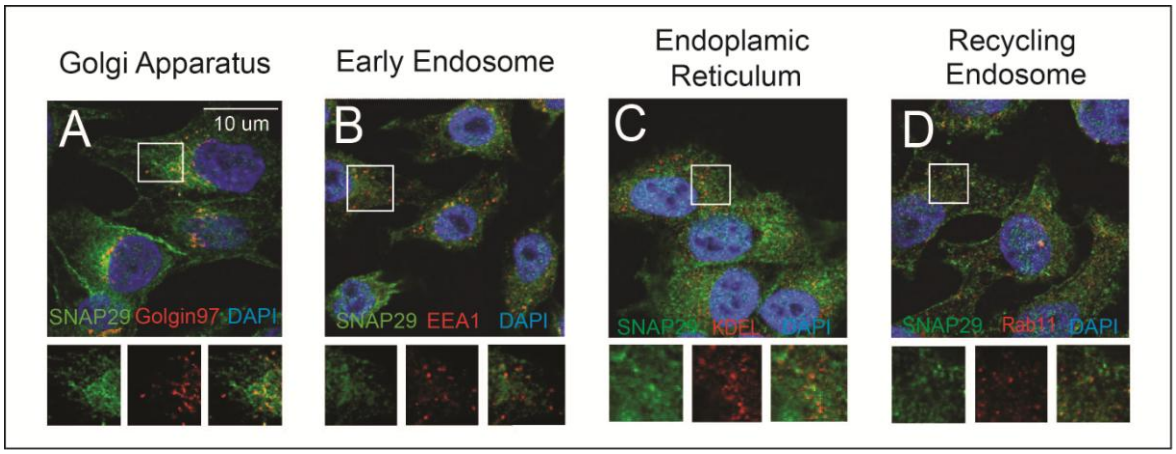

Figure 28. Analysis of SNAP29 localization in interphase cells. (A-D) Co-localization of SNAP29 with markers of trafficking compartments: (A) Golgi, (B) Early Endosome (EE), (C) Endoplasmic Reticulum (ER), (D) Recycling Endosome (RE). DAPI is added to detect nuclei. Enlargements of the boxed area and its single channels are shown below each panel. SNAP29 is mainly found at the Golgi and EE, while rarely associates with ER and RE.

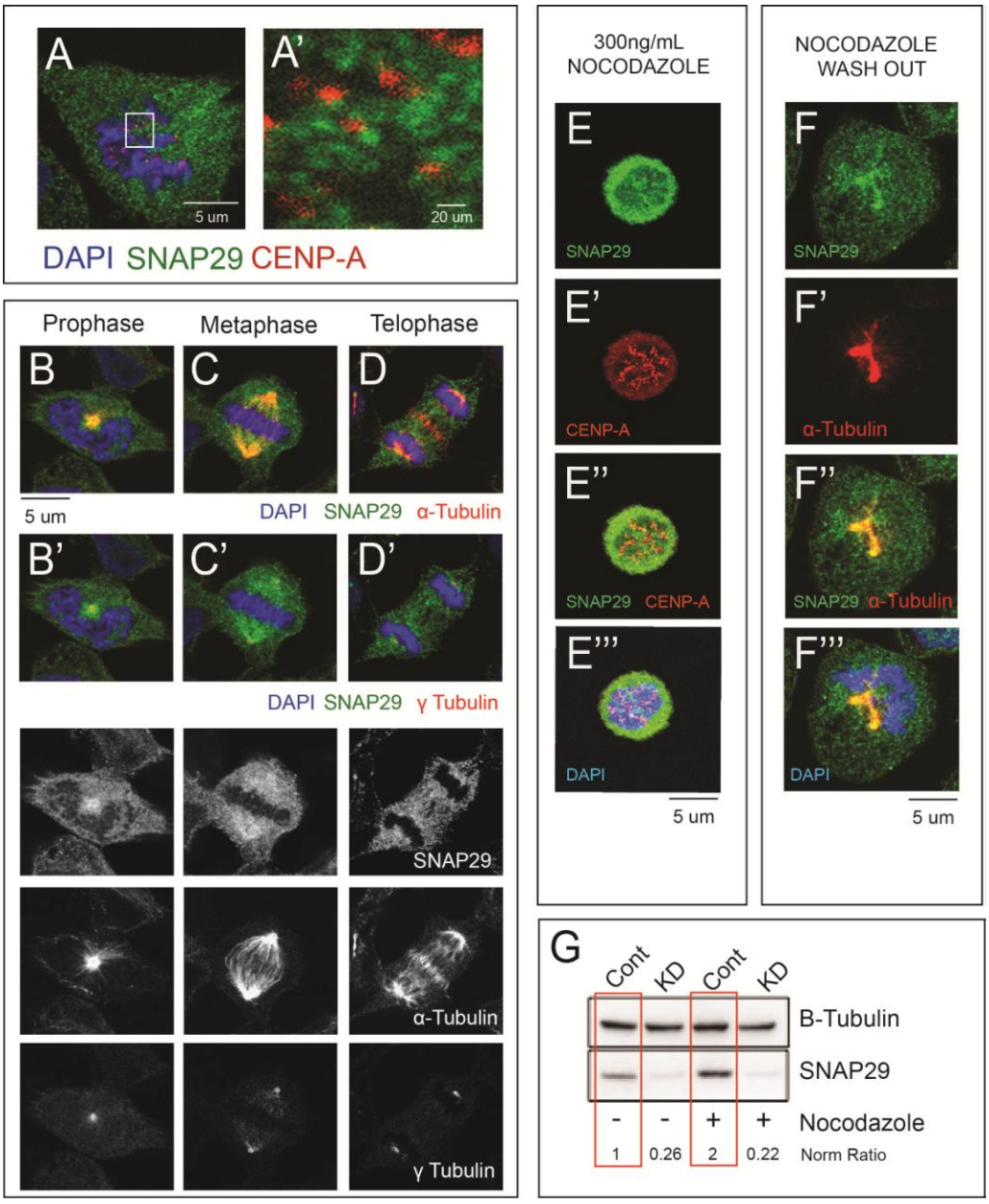

Figure 29. Analysis of SNAP29 localization in mitotic cells (A) HeLa cells in prophase stained to detect SNAP29, CENP-A and DAPI. (A') The high magnification of the boxed area in A, with the SNAP29 and CENP-A merged channels, shows that a pool of SNAP29 is close to CENP-A, but never overlaps with it. (B-D') HeLa cells in prophase, metaphase and anaphase stained to detect α-tubulin, SNAP29 and nuclei (B-D) and γ-tubulin, SNAP29 and nuclei (B'-D'). Single channels are shown below the merge. (E) HeLa cells fixed 16h after Nocodazole treatment and (F) 1h after Nocodazole wash-out, stained to detect SNAP29, CENP-A and nuclei. SNAP29 vicinity to CENP-A is enhanced when a cell is blocked in prophase, while SNAP29 associates to MTs as soon as the cell re-enters in mitosis. (G) Protein Extracts from control and SNAP29 depleted HeLa cells, treated or not with Nocodazole, are blotted with anti-SNAP29 and anti-β-Tubulin to provide a loading control. To estimate SNAP29 expression levels in different conditions, SNAP29 and Vinculin pixel values are measured using ImajeJ. The ratio between SNAP29 and Vinculin of each sample has been calculated. The ratio of untreated control cells has been

used for normalization and Norm Ratio is reported below each sample. Nocodazole treated cells show a double amount of SNAP29 protein compared to control cells (red squares).

5.3.3 SNAP29 regulates prophase to metaphase transition

To uncover a possible role of SNAP29 during cell division, we depleted SNAP29 (SNAP29KD) in HeLa cells and analyzed them 24-72 hours after siRNA-mediated Knock Down (KD). Western Blot with the anti-SNAP29 antibody confirms that SNAP29 protein levels decrease by 72%, 85% and 90% 24h, 48h and 72h after siRNA transfection, respectively (Fig. 30A). The analysis of dividing cell using phospho-HistoneH3 (pH3) as a marker of mitosis, reveals that SNAP29 depletion leads to an increase of the mitotic index (MI) to 8.6%±2.7 and 12.6%±2.8 24 and 48 hours after siRNA transfection respectively, compared to 6.1%±4.2 and 5.5%±1.6 in controls (Fig. 30B). Further analysis of mitotic stages show that compared to controls, SNAP29 KD cells 48h after siRNA transfection are arrested in pro-metaphase and very few late mitotic phases are present (Fig. 30C). Interestingly, we observe that 72h after transfection the MI is reduced to 7.2%±2.5 (Fig. 30B), the total number of cells decrease compared to control (Fig. 30B) and we do not observe anaphases, telophase and cytokinesis (Fig. 30C) suggesting that possibly cells stop to divide or that the cells that are still able to enter mitosis do not progress past pro-metaphase. In agreement with data in *Drosophila* S2 cells, the population of HeLa cells 72h after SNAP29 siRNA transfection is enriched with cells possessing one or more mininuclei (Fig. 30D). Interestingly, the mininuclei display a completely formed NE. Indeed, both MAD1 and LAMIN A surround nuclei in SNAP29 depleted cells, as it happens in control cells (Fig.30E, F), indicating that SNAP29 is not required for NE dynamics during cell division. Together, this evidence shows that SNAP29 depletion for 48h might cause prophase to metaphase delay leading to generation of multinucleated cells after 3 days of depletion. To better characterize mitotic defects in SNAP29 depleted cells, we analyzed control and SNAP29 KD U2OS cells expressing a GFP-Histone2B and mCherry-alpha-Tubulin by time-lapse microscopy (Fig. 31A). We recorded the behavior of

SNAP29 KD cells during three different intervals of time after siRNA transfection: 24-36h, 48-66h and 72-90h. At 24-36h KD cells take longer time compared to control to reach metaphase (120' versus 25' in control cells; Fig. 31A, B, F, G, movie 9 and 10), however, in most cells ultimately chromosome align at the metaphase plate and anaphase completes normally. 30% of cells remain blocked in pro-metaphase for the entire length of the observation (movie 11). At 48-66h, cells are strongly delayed at the prophase to metaphase transition (187' vs 25' in control cells). Finally, they divide without passing through a proper anaphase. Indeed, in these cells chromosomes never align to the metaphase plate. As consequence, cells divide generating daughter cells with more than one nucleus (Fig. 31C, movie 12). In some cases, one or both the daughter cells die after division (movie 13). Both the pro-metaphase delay and the generation of daughter cells with more than one nucleus are rescued by expression in KD cells of a siRNA-resistant SNAP29 (SNAP29 R) (Fig. 31E, F, G and movie 14), whose over expression *per se* does not have an effect on mitosis (Fig. 31D, F, G and movie 15). In agreement with the cell behavior of mitotic SNAP29KD cells at 48-66h, at 72-90h, multinucleated cells are present. These are still able to initiate mitosis, but die immediately after (movie 16). Indeed, we scored an increase in cell death equal to 19.6% and 49.6% at 48-66h and 72-90h respectively. Interestingly, upon SNAP29 depletion, cells mostly form an actin-rich ring, suggesting that cytokinesis is not defective (Fig. 31F). This evidence suggests that SNAP29 plays a role during mitosis and that the presence of more than one nucleus in a SNAP29 depleted cell is not due to cytokinesis defects.

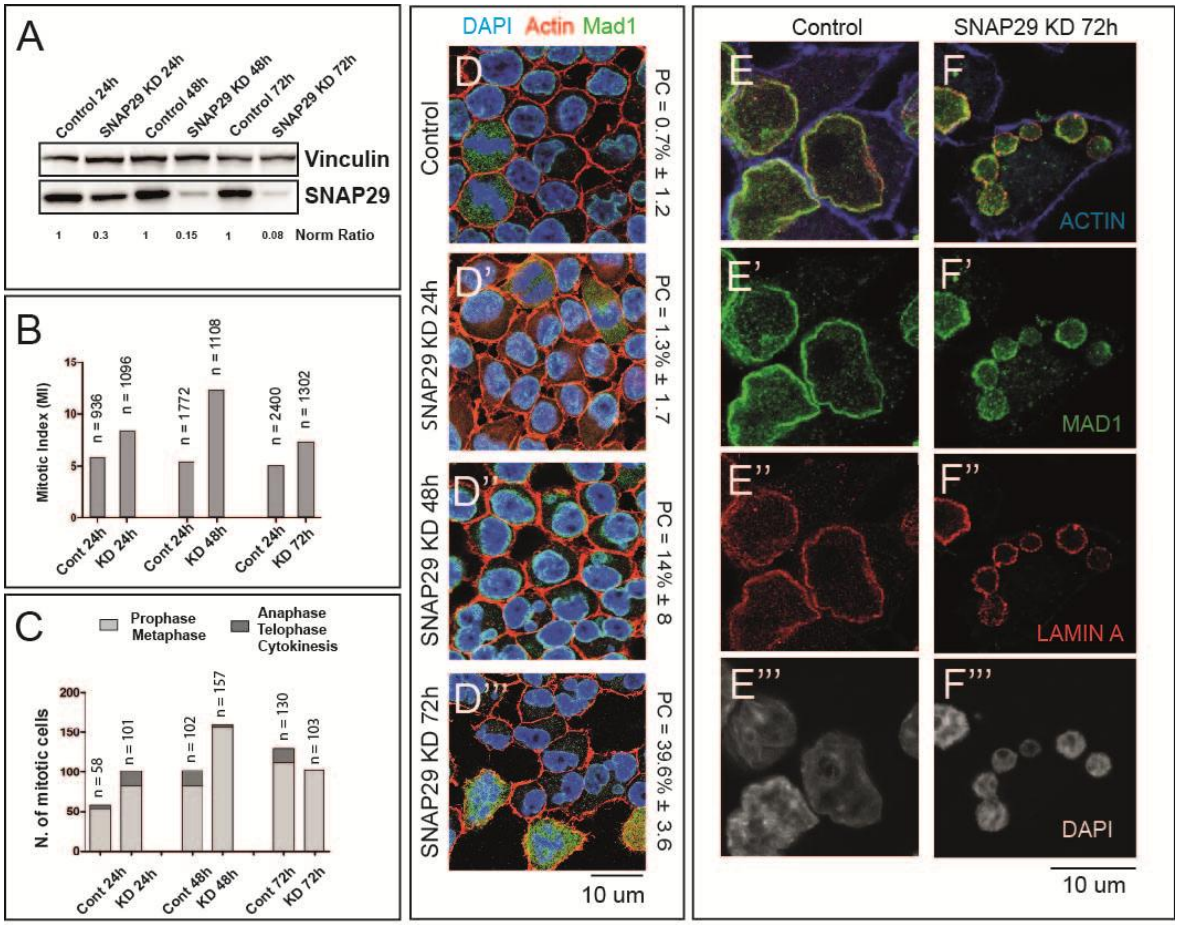

Figure 30. SNAP29 depletion in HeLa cells causes cell division impairment and leads to generation of multinucleated cells. (A) Protein extracts from control and HeLa cells treated with siRNA specific for SNAP29 for 24, 48 and 72 hours, are blotted with anti-SNAP29 and anti-β-Tubulin to provide a loading control. The Norm Ratio represents here Snap29 protein level in depleted cells relative to controls at each time point. (B) Measure of the MI in control (Cont) and SNAP29 depleted (KD) HeLa cells. For each condition the number of cell counted is reported (n). The MI increases upon 48h of SNAP29 depletion while it decreases 72h after SNAP29 depletion (compare KD48h with KD72h). (C) Quantification of the different mitotic phases in control and SNAP29 HeLa cells 24, 48 and 72 hours after siRNA transfection. After 48h of SNAP29 depletion, cells are mostly blocked in prophase, and few late mitotic cells are scored. After 72h the number of prophase cell is comparable with that of controls, but no late mitosis stages are detected. For each condition the number of counted mitotic cells is reported (n). (D) Control and 24h, 48h and 72h SNAP29 depleted cells stained with DAPI, anti-MAD1 and phalloidin to mark ACTIN. The number of plurinucleated cell (PC) counted is reported below each figure. 72h after SNAP29 depletion, the number of cells carrying mininucleai increases. (E) Control and (F) 72h SNAP29 depleted cells stained to detect nuclei, LAMIN A and MAD1, to mark NE. (E'-E''', F'-F''') Single channels are shown. In the example, a SNAP29 KD cell shows six mininuclei surrounded with a NE.

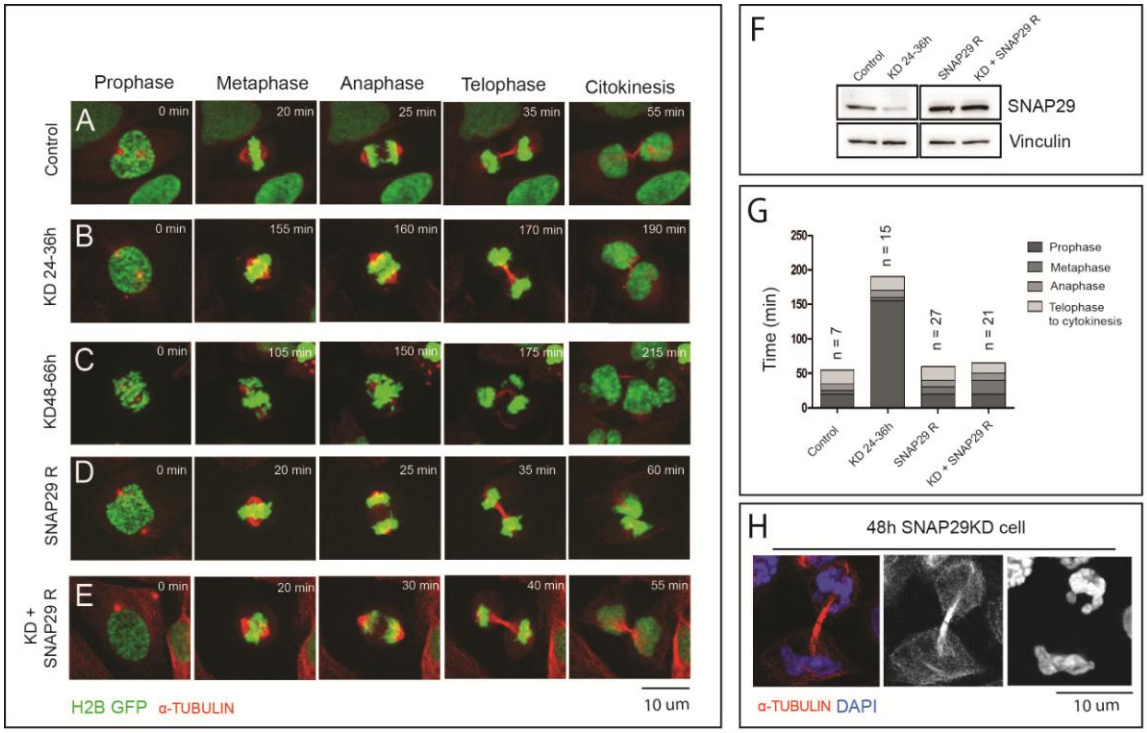

Figure 31. Lack of SNAP29 causes pro-metaphase delay. (A-E) Time-lapse imaging of U2OS cells expressing GFP-H2B and mcherry-α-tubulin. Control cells (A), SNAP29 depleted cell from 24h to 36h (B) and from 48h to 66h (C), cells over expressing a siRNA resistant form of SNAP29 (R-SNAP29) (D), SNAP29 depleted cells over expressing R-SNAP29 (E). 24-36h SNAP29 depleted cells spend more than two hours to align chromosomes at the metaphase plate and then divide normally, while 48-66h SNAP29 depleted cell never form a metaphase plate and then divide generating cells with more than one nucleus. Over expression of the R-SNAP29 rescues the pro-metaphase delay and the generation of multinucleated cells. (F) Protein extracts from U2OS-GFPH2B-mcherry-α-tubulin with the indicated background. In SNAP29KD over-expressing the R-SNAP29, SNAP29 level is comparable with that of the R-SNAP29 over expression. (G) Quantification of the time spent by U2OS-GFPH2B-mcherry-α-tubulin cells into different mitotic stages for each condition. n is the number of mitotic cells counted. (H) A 48h SNAP29 KD cell stained with anti-α-tubulin and DAPI, highlights the formation of the actin midbody during cytokinesis, suggesting that this mitotic step is not altered in SNAP29 KD cells.

5.3.4 SNAP29 controls KT stability in HeLa cells

To investigate whether SNAP29 is important for KT stability, we depleted SNAP29 in HeLa cells and analyzed KT components such as CENP-A, CENP-T, and HEC1 and NSL1, which represent respectively the inner KT, the NDC80 and MIS12 outer KT complexes (Fig. 32A-D). We found that such KT components are all present at the KT of

SNAP29 KD cells indicating that the outer KT platform is not altered when SNAP29 is lost. Importantly, compared to control, we find that localization of ZWINT-1 and ZWILCH, belonging to the RZZ complex, are strongly reduced at the KT of SNAP29 KD cells, compared to control (Fig. 32E, F). Strikingly, in depleted cells, ZWINT-1 is totally absent, while ZWILCH is increased at the edge of the metaphase plate compared to control cells, suggesting that the former might be degraded while the latter might fail to be recruited to KT in absence of SNAP29. Taken together, our results suggest that SNAP29 plays a conserved crucial role in formation or stabilization of the KT platform and is required for RZZ recruitment at prophase.

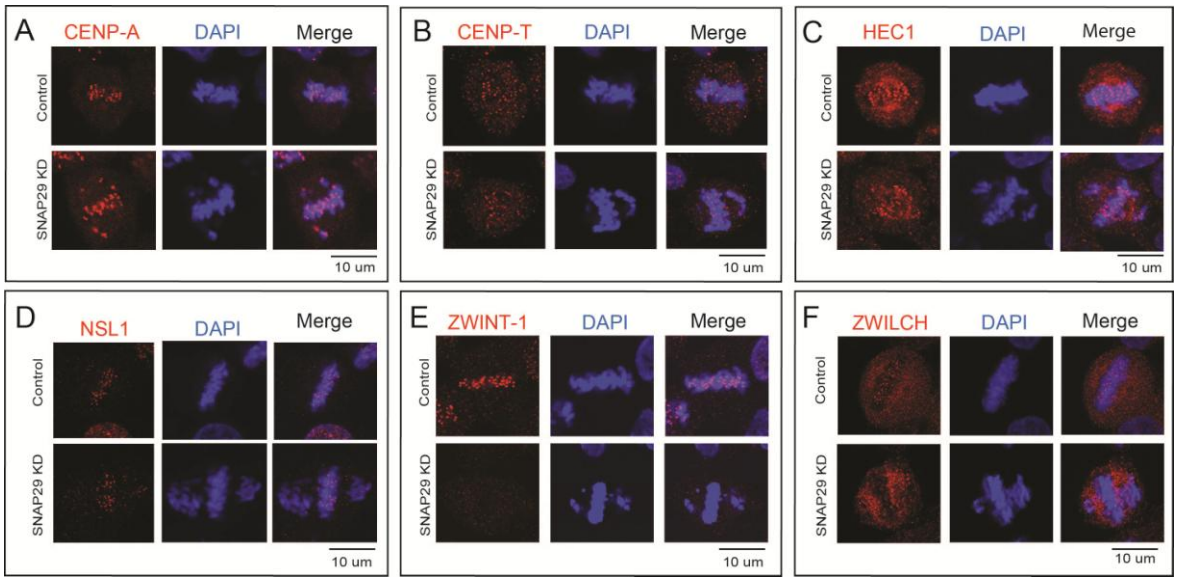

Figure 32. SNAP29 regulates KT stability. **(**A-F) Control and SNAP29 depleted HeLa cells stained for DAPI and for markers of outer KT platform such as CENP-A, CENP-T, HEC1 and NSL1 and RZZ complex components, ZWINT-1 and ZWILCH. Lack of SNAP29 causes impairment in the recruitment of ZWINT-1 and ZWILCH.

5.3.5 Depletion of SNAP29 impairs MTs attachment to the KT platform

Lack of ZWINT-1 and of the RZZ complex is often associated to altered spindle formation and chromosome mis-segregation (Karess 2005, Buffin et al. 2005). To understand whether this is the case in absence of SNAP29, we analyzed mitotic spindles and

chromosome segregation in HeLa cells. Compared to WT (Fig. 33A), metaphase cells depleted of SNAP29 show multiple spindle defects (Fig. 33A'-A'''). In particular, we observed the presence of monopolar spindles (24%) (Fig 33A'), bipolar spindles (26%) (Fig. 33A'') and cells with bipolar abnormally elongated spindles (49%) (Fig. 33A'''), which are 30% longer than that of control cells in metaphase (Fig. 33B). Only 1% of SNAP29KD cells display a tripolar spindles (not shown). SNAP29KD cells with a bipolar spindles maintain the ability to organize a metaphase plate, although some chromosomes often fail to congregate into to the spindle mid-zone and remain in proximity of the poles or are dispersed around. On the contrary, in cells with an abnormal elongated spindle, chromosomes fail to reach the metaphase plate. We measured inter-kinetochore distance (iKTD) of unaligned chromosomes in SNAP29 KD and we found that it is 50% less than that of metaphase control cells (Fig. 33C-D), when tension is maximum between inner and outer KT components (Maresca & Salmon 2009). Indeed, the iKTD in SNAP29 KD cells is comparable to that measured in control cells at early prophase, when MT attachment to KT is not yet stable (Fig. 33C-D). Cold shock assay confirm that unaligned chromosomes in SNAP29KD cells are not anchored by MTs, compared to control (Fig 33E-F). All together, this evidence suggests that SNAP29 is fundamental for MTs attachment to KTs and therefore for a correct spindle organization.

5.3.6 SNAP29 depleted cells overcome SAC arrest

The RZZ complex has been shown to be important for recruitment of SAC components during prophase (Karess 2005, Buffinet et al. 2005). Thus, we asked whether SNAP29 KD cells are able to recruit SAC components to KTs. To this end, we stained SNAP29 depleted HeLa cells with MAD1 and we found that MAD1 is recruited to chromosomes in prophase albeit to a reduced level (Fig. 34A, A'). To confirm that the SAC machinery is active in depleted cells and might mediate the pro-metaphase delay observed upon depletion of

SNAP29, we treated control and SNAP29 KD U2OS-GFP-H2B-mCherry-α-tubulin cells with 300ng/mL Nocodazole for 16 hours and performed a time laps for the following 16h (movies 17 and 18).

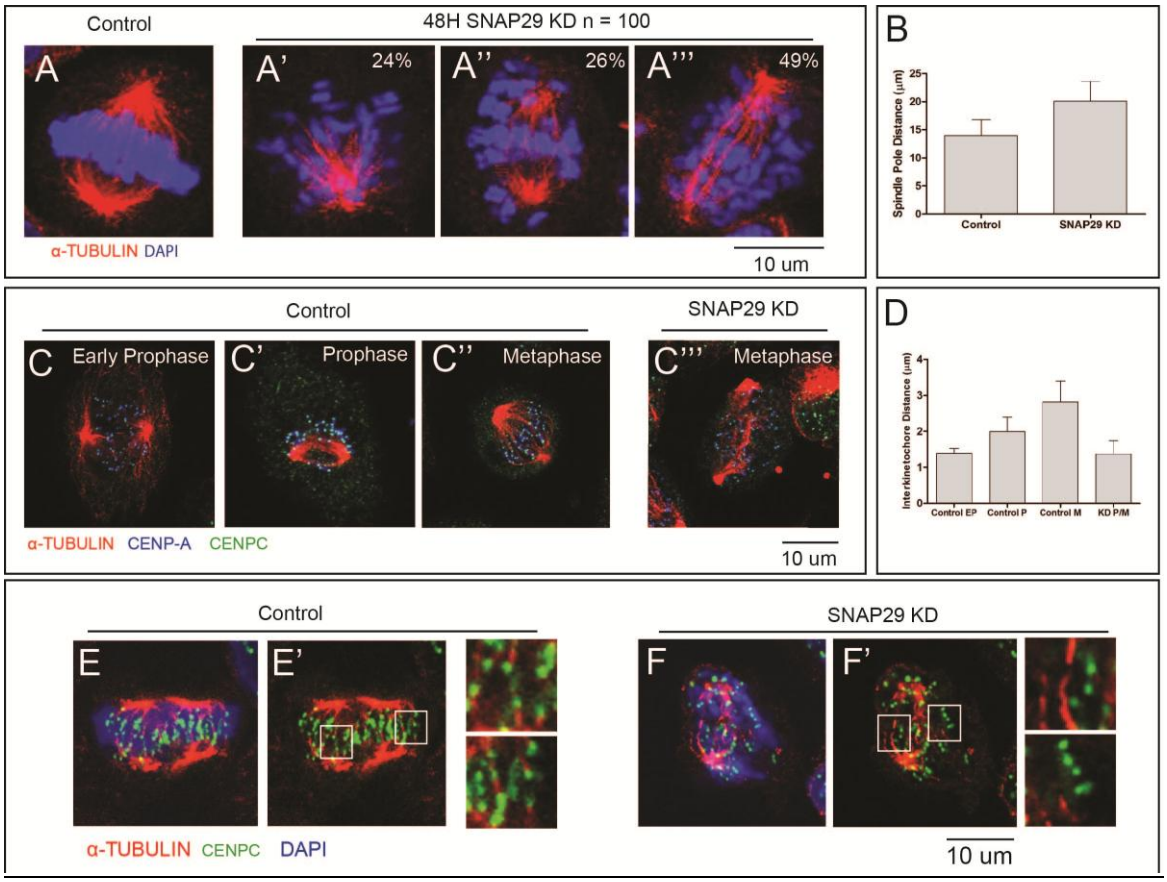

Figure 33. SNAP29 is required for anchoring MTs to the outer KT platform. (A) Metaphase of control and (A'-A''') 48h SNAP29-depleted HeLa cells stained to mark DNA and α-tubulin. We analyzed 100 metaphase-defective cells and express in % the observed phenotypic categories: A', monopolar; A'', Bipolar; A'''Bipolar with abnormally elongated spindle. (B) Quantification of the Spindle Pole Distance in control and SNAP29 depleted cells. SNAP29KD cells show elongated spindles. (C-C'') Early prophase, prophase and metaphase of a control cells and (C''') metaphase of a SNAP29 depleted cells, stained to detect α-tubulin, CENP-A and CENP-C. The distance between two CENP-C positive dots has been used to measure the iKD. (D) Quantification of the iKD in the indicated conditions. In SNAP29 KD cells the iKD is comparable with that of an Early Prophase, indicating that on average no tension is present at KT in SNAP29 KD cells. EP: Early Prophase. P: Prophase. M: Metaphase. KD P/M: SNAP29 KD pro-metaphase. (E) Metaphase of control and (F) SNAP29 depleted cells subjected to cold shock, stained with anti-α-tubulin, anti-CENP-C and DAPI. In E' and F' the α-tubulin/CENP-C merge is shown. The boxed areas are enlarged in E' and F' to highlight that in SNAP29 KD cells, KTs are not attached to MTs.

We do not observe any SNAP29KD cells progressing pro-metaphase, suggesting that the SAC is active in SNAP29 depleted cells. According to this, we found that, as in the control, MAD1 is placed at the KT platform in SNAP29KD U2OS cells treated with Nocodazole (Fig. 34 C,C'), in condition in which ZWINT-1 levels are strongly reduced at the KT of SNAP29KD cells compared to control (Fig. 34B, B'). This evidence indicates that although ZWINT-1 is decreased in SNAP29KD cells, MAD1 is still recruited at KT and it likely mediates together with other SAC components, the prophase to metaphase delay observed in SNAP29 KD cells. When MTs are stably bound to KT at metaphase, SAC proteins are removed with the help of SPINDLY, the adapter of dynein/dynactin complex (Barisic and Geley 2014). We analyzed SPINDLY localization in control and SNAP29 KD cells in prophase and found that compared to control (Fig. 34D), SPINDLY is less recruited in SNAP29 KD cells (Fig. 34D'). Consistent with this, SPINDLY is also decreased at the KTs of Nocodazole treated SNAP29 KD U2OS cells compared to control (Fig. 34E, E'). Next, we analyzed the localization of MAD1 and SPINDLY, in control and SNAP29 KD cells in metaphase (Fig. 34F, G). MAD1 and SPINDLY are both absent at the KT of aligned chromosomes but are still present at the KT of the not aligned one (Fig. 34F', G'). This is in agreement with the fact that when MTs are not well attached to KTs SPINDLY cannot recruit dynein/dynactin complex to remove them and as a consequence MAD1 is retained at KTs. In support of these data, we also find that MAD1 and SPINDLY persist at KTs of U2OS-GFP-H2B-mCherry-α-tubulin SNAP29 depleted cells after Nocodazole wash-out (Fig. 34H-J'). Importantly, we observe that upon Nocodazole wash-out, SNAP29 KD cells spend more time (267 ± 158 min) compared to control cells to assemble a metaphase plate (88 ± 155min). Eventually, they proceed into anaphase, as the control cells do (movies 19 and 20), generating multinucleated cells (60,9% vs 2.38% in the control). These data indicate that SNAP29 KD cells are able to overcome mitotic arrest with MAD1 at KTs, suggesting that the SAC response of depleted cells is weakened.

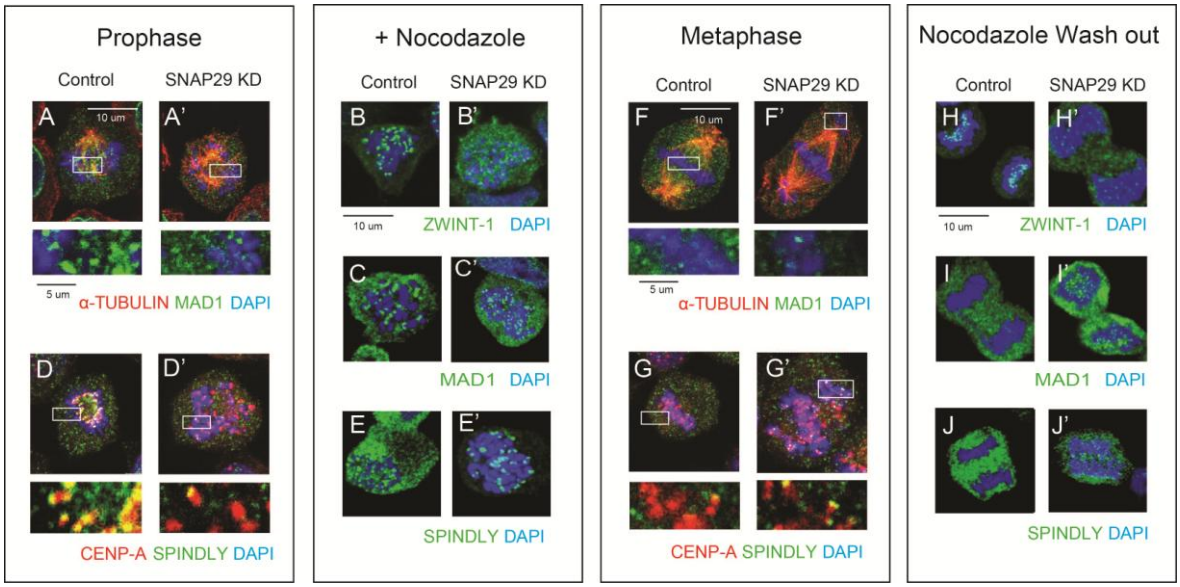

Figure 34. SNAP29 depleted cells overcome the SAC arrest. (A, A', F, F') Prophases and metaphases of control and SNAP29 KD HeLa cells stained with DAPI, anti-MAD1 and anti α-tubulin. (D, D', G, G') Prophases and metaphases of control and SNAP29 KD HeLa cells stained with DAPI, anti-SPINDLY and anti-CENP-A. In prophases, MAD1 and SPINDLY are present in SNAP29 KD cells but show decrease level compare to control cells. In metaphases, MAD1 and SPINDLY are both present at the unaligned chromosomes. Below each panel enlargements of the white boxed squares are shown. (B, C, E) Nocodazole treated control and (B', C', E') SNAP29 KD U2OS cells stained with DAPI, anti-ZWINT-1, anti-MAD1 and anti-SPINDLY respectively. In SNAP29 KD cells, MAD1 and SPINDLY are present at KTs even though the levels of ZWINT-1 are decreased compared to control. (H, J, I) Anaphases of control and (H', J', I') SNAP29KD cells upon Nocodazole wash-out, stained with DAPI, anti-ZWINT-1, anti-MAD1, and anti-SPINDLY respectively. MAD1 and SPINDLY are present at KT of SNAP29KD cells in anaphase, while in control cells they have been removed.

5.4 The *in vivo* relevance of the trafficking and cell division functions of SNAP29 for epithelial architecture

5.4.1 Autophagosome accumulation does not cause the epithelial tissue defects observed in *Snap29*^{B6} mutant eye disc

To understand whether autophagy is required for establishment and mantainance of epithelial architecture, we monitored tissue morphology and Notch and ref(2)P localization in eye imaginal discs carrying mutations in genes controlling autophagic or endolysosomal

pathways. These were: *Atg13*, which is required for initiation of autophagy (Chang & Neufeld 2009), *Vamp7* and *Syx17*, which act with Snap29 in fusion between autophagosomes and lysosomes (Takats et al. 2013), and *fab1*, which controls fusion between amphisomes and lysosomes or late endosomes and lysosomes (Rusten et al. 2006). In WT discs, Notch localizes to the apical plasma membrane and in endosomal puncta, while little signal of ref(2)P is detected, consistent with low levels of constitutive autophagy (Fig. 35A). In $Snap29^{B6}$ mutant discs, Notch and ref(2)P accumulate at the apical membrane and the tissue architecture is altered as previously shown (Fig 18B). $Atg13^{\Delta 81}$, *Vamp7* and *Syx17* mutant discs accumulate ref(2)P only (Fig. 35C-E), while $fab1^{21}$ mutant discs accumulate both ref(2)P and Notch (Fig. 35F). The subcellular localization of both markers is different in these samples (fig. 35I, J, K, L), when compared to $Snap29^{B6}$ mutant cells, in which Notch accumulates apically and ref(2)P in the apical portion below the cell cortex (Fig. 35H). Importantly, no disc morphology alterations are observed in $Atg13^{\Delta 81}$, *Vamp7*, *Syx17* and $fab1^{21}$ mutant discs, suggesting that neither impairment of autophagosomes formation or block of autophagosome fusion to lysosome impair tissue architecture. Taken together, our genetic analysis strongly suggests that the impairment in the autophagosome lysosome fusion observed in $Snap29^{B6}$ mutant cells is not causing the tissue architecture alteration of $Snap29^{B6}$ mutant eye discs.

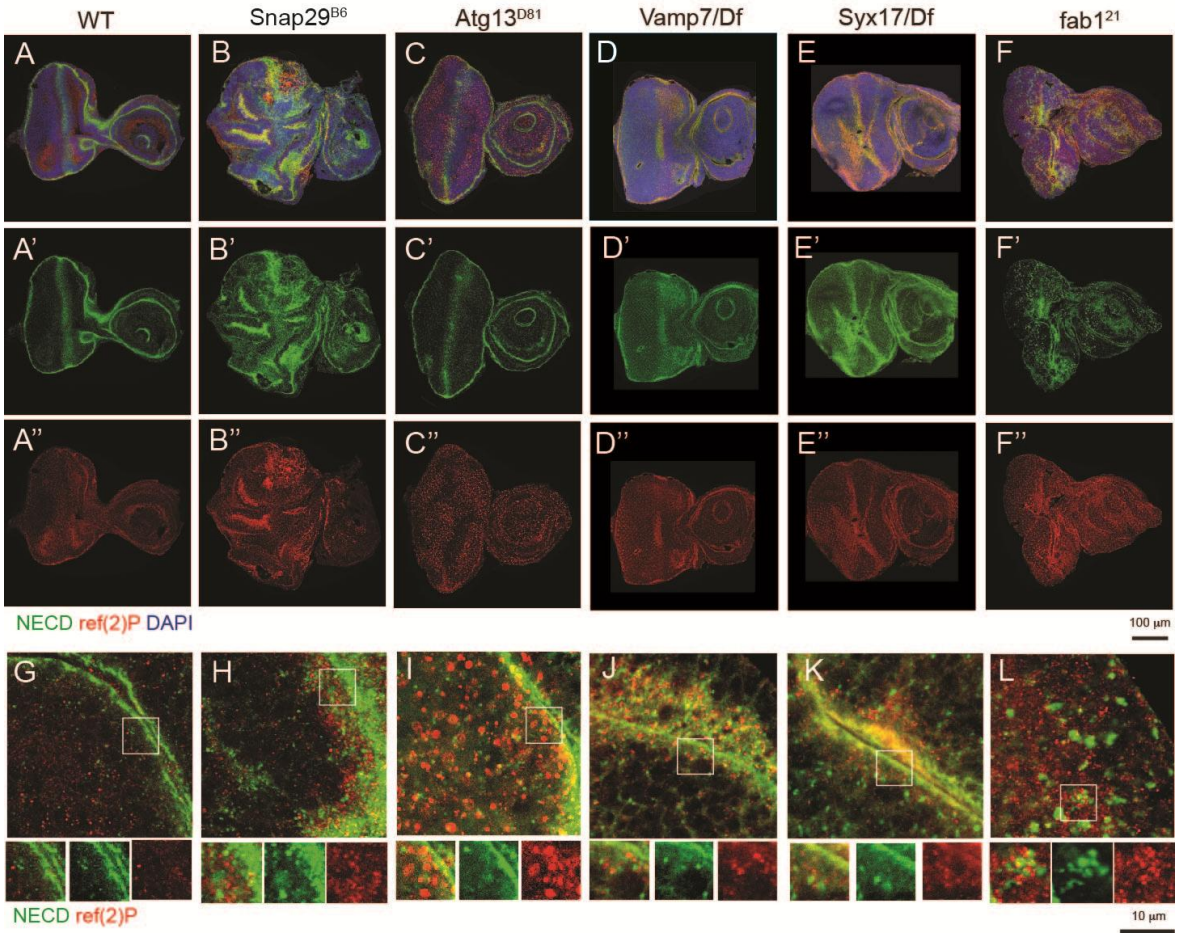

Figure 35. ref(2)p accumulation and autophagy pathway alteration do not correlate with tissue architecture defects. (A-F) WT and mutant discs of the indicated genotype immunostained to detect Notch, ref(2)P and nuclei. A'-F'' show the Notch and ref(2)P channels, respectively. Compared to WT (A), discs mutant for (B) *snap29* display epithelial architecture defects, and strong ref(2)P and Notch accumulation. (C, D, E) *Atg13*, *Vamp7*, *Syx17* mutant discs display accumulation of ref(2)P, no Notch accumulation and normal organ morphology. (F) *Fab1* mutant discs show both ref(2)P and Notch accumulation, but not tissue morphology alteration. (G-L) High magnification of a cross-section of anterior portion of discs. Enlargements of the boxed area and its single channels are shown below each panel. Note the distinct patterns of accumulation of Notch, or ref(2)P, in the different mutants.

5.4.2 Epithelial tissue disruption in *Snap29^{B6}* mutant epithelial discs is sustained by JAK/STAT signaling pathway

Loss of epithelial architecture in imaginal discs is often associated to altered signal transduction. In particular, elevated JNK and JAK/STAT signaling contribute to aberrant

architecture of mutant organs (Wu et al. 2011). To assess whether this is the case in B6 mutant eye discs, we monitored expression of a panel of targets of conserved signaling pathways controlling proliferation and differentiation of disc cells. We found that expression of Notch and EGFR target genes is mildly reduced in B6 mutant discs, relative to WT. In contrast, expression of JAK/STAT and JNK signaling targets is elevated by several folds (Fig. 36A). Consistent with this, expression of the Notch reporter E(spl)-*mbeta* is decreased in B6 mutant discs and its pattern of expression is completely altered compared to WT (Fig. 36B, C). On the contrary, expression of the JAK/STAT and JNK reporters, STAT-GFP and puc-lacZ, respectively, in B6 mutant discs is strongly increased, when compared to WT discs (Fig. 36D-G). We next investigated whether inhibition of JNK and JAK/STAT pathways rescue $Snap29^{B6}$ phenotype. We did not detect any changes in $Snap29^{B6}$ mutant discs when the JNK dominant negative form (JNK^{DN}) was ectopically over expressed in $Snap29^{B6}$ discs (data not shown). In contrast, over expression of the negative regulator of JAK/STAT signaling SOC36E rescues lethality of animals bearing B6 mutation (Snap29B6>Soc36E) (Fig. 36L-M). Animals rescued present very reduced eyes, bearing few photoreceptors originating from mutant cells (Fig. 36M). In addition, $Snap29^{B6}$ tissues display some region positive for cleaved Caspase3, an apoptotic marker (Fig. 36H, I). However, the block of apoptosis doesn't meliorate $Snap29^{B6}$ phenotype, and on the contrary, it causes an increase in tissue size (Fig. 36J, K). Together, this data indicate that JAK/STAT signaling contributes to epithelial tissue alteration in $Snap29^{B6}$ mutant tissue and that apoptosis clears a portion of defective cells from the mutant tissue.

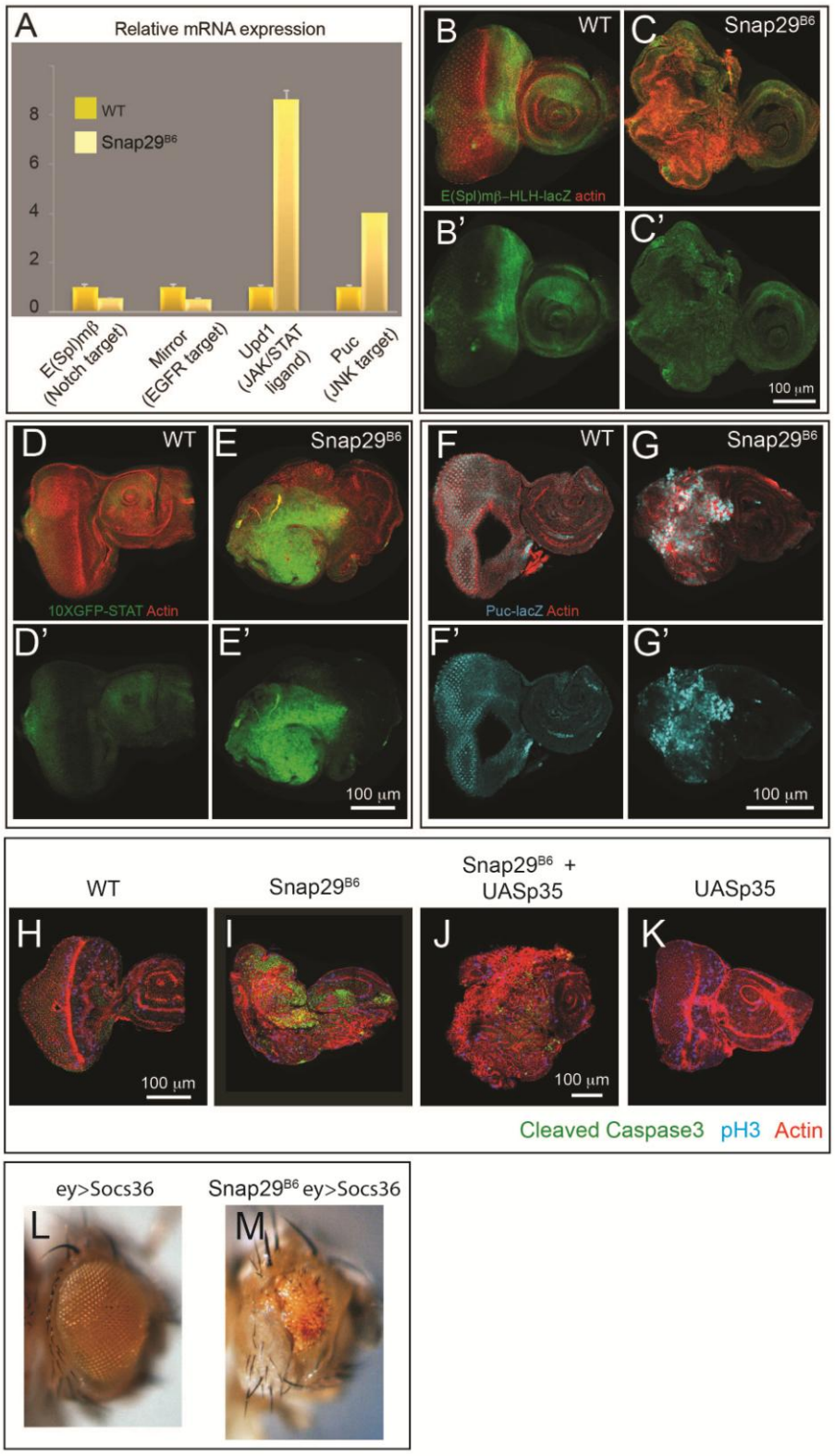

Figure 36. Analysis of Notch, JNK, JAK/STAT pathways and of apoptosis. (A) Expression of target genes of the indicated signaling pathway in eye disc extracts. mRNA levels of Notch and EGFR targets decrease in *Snap29* mutant eye-antennal disc extract, while the mRNA of the JAK/STAT ligand Upd1 and of the JNK target puc are greatly elevated, compared to WT. (B-C) WT and *Snap29* mutant eye discs expressing E(Spl)mβ-lacz, a Notch signaling reporter, stained as indicated. S*nap29* mutant discs display a

reduction of Notch signaling compared to WT. B'-C' show single anti-β-Gal channels. (D) WT and (E) *Snap29* mutant eye disc expressing GFP-STAT are stained to detect cortical actin. (F) WT and (G) *Snap29* mutant eye disc expressing puc-lacz are stained to detect cortical actin and with the anti-β-Gal antibody. The expression of STAT-GFP and puc reporters are increased in mutant discs compared to WT discs. D'-E' are the single GFP channels. F'-G' are single anti- β-Gal channels. (H-K) Eye-antennal disc of the indicated genotype are stained to detect actin, pH3 and Cleaved-Caspase3. Apoptotic cell are present in *Snap29* mutant disc. Block of apoptosis by expression of the inhibitor p35, reduces the number of apoptotic cells, and it worsens disc morphology.
(L, M) Adult eyes of flies of the indicated genotypes. (L) Eye specific ectopic expression of SOCS36E, a JAK/STAT signaling inhibitor, does not impair eye development. (M) SOCS36E expression in *Snap29* mutant eye discs rescues in part eye development and yields adults with reduced eyes. In M, mutant cells expressing the SOCS36E give rise to orange photoreceptors, while the few WT cell to the dark red ones.

5.4.3 Cell division is affected in *Snap29^{B6}* mutant discs

Because of SNAP29 function in stabilizing the KT platform, we wondered whether *Snap29^{B6}* phenotype could also depend on an impairment in cell division during development. Thus, we next analyzed cell division in *Snap29^{B6}* mutant discs. Cell division in third instar eye discs of WT animals mostly occurs at the morphogenetic furrow, consisting in few rows of cells forming photoreceptors, as shown by immunolocalization of phosopho-Histone-H3 (pH3)-positive cells (Fig. 37A). As result of epithelial tissue alteration in *Snap29^{B6}* mutant eye discs, pH3-positive cells loose the typical distribution along the morphogenetic furrow (Fig. 37B). However, pH3 positive cells in mutant discs are not statistically more abundant compared to that of control discs (Fig. 37B). However, parts of the mutant tissue with very altered epithelial architecture display a noticeably high number of pH3-positive cells, suggesting that some *Snap29^{B6}* mutant cells might containing more dividing cells. These areas are characterized by large cells which contain fragmented nuclei positive for pH3 and cells with disorganized nuclei (Fig. 37C-E). To recognize different mitotic stages *in vivo* we stained tissues to detect Incenp, which relocalizes from the centromeric region to the midzone during anaphase (Fig. 37F-N). Interestingly, compared to control, *Snap29^{B6}* tissues display an higher amount of cells in

pro-metaphase compared to control, indicating that mutant cells might be delayed (Fig. 37L).

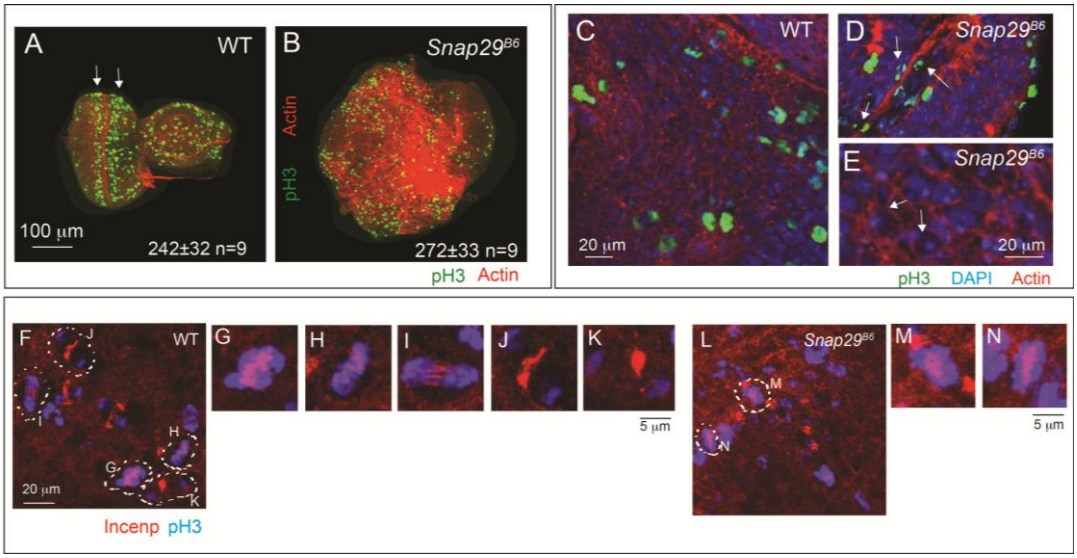

Figure 37. Cell division defects contributes to alter the phenotype in *Snap29*^{B6} discs. (A) WT and (B) *Snap29* mutant eye-antennal discs stained with anti-phospho-HistoneH3 (pH3) to detect dividing cells. Compared to WT tissue, in which cell division is mostly limited to the differentiating photoreceptors along the morphogenetic furrow, mutant eye discs display areas containing several pH3-positive cells, suggesting that mutant cells are enriched in dividing cells. The average number of pH3-positive cells in samples of the indicated genotype is showed. P-value (Wilcoxon-Mann Whitney Test) is 0.0625. (C) Closed up of regions of WT and (D, E) *Snap29* mutant eye discs stained to detect pH3, actin and DNA. Compared to WT, mutant cells display fragmented pH3 positive nuclei (D, arrows) and giant cell containing disorganized nuclei (E, arrowheads). (F-K) WT and (L-N) mutant eye discs stained to detect DNA and Incenp. A dashed line circled different mitotic stages. Each mitotic stage is magnified (G: prophase, H: metaphase, I: anaphase, J: telophase, K: citokynesis, M and N: pro-metaphase). WT eye disc display all the mitotic stages, while *Snap29*^{B6} mutant tissue is enriched in cells in prophase or metaphase.

5.5 Snap29 function in autophagy and cell division are independent

To assess whether Snap29 function at KT *in vivo* depends by SNAREs, we analyze Snap29 localization in discs mutants for *Syx17* and *Vamp7*, the SNARE protein interactors of Snap29 in autophagosome to lysosome fusion (Takas et al. 2013), and in *Syb* mutant discs, which is another known interactor of Snap29 (Table1). Interestingly, we did not find changes in Snap29 localization at KTs in these mutants, compared to control, suggesting that Snap29 function at KTs is Syx17-, Vamp7- and Syb- independent (Fig38A-E).

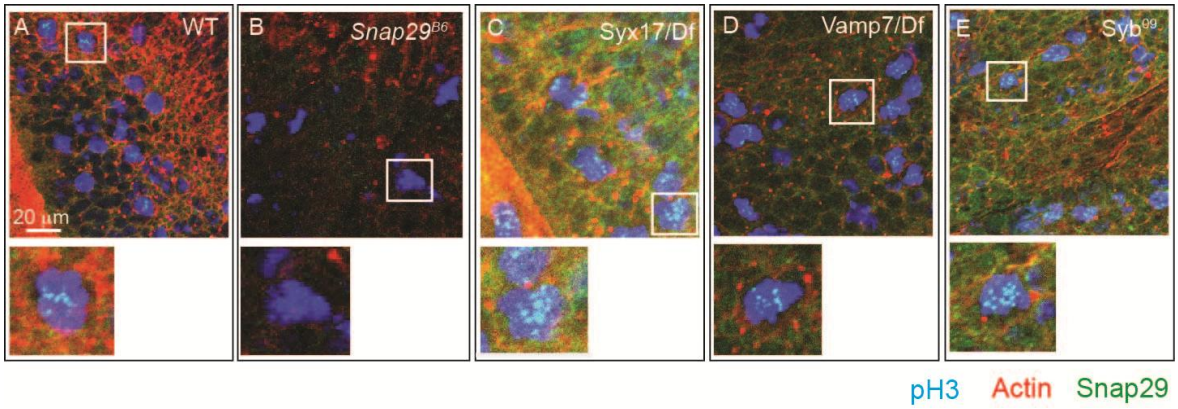

Figure 38. Analysis of Snap29 localization in epithelial tissues depleted for Syx17, Vamp7 and Syb. **(**A-E) WT, Syx17, Vamp7 and Syb mutant eye discs, stained to detect Actin, pH3 and Snap29. Enlargment of boxed areas show Snap29 localization at KTs in cells at prophase.

6. DISCUSSION

Our analysis of the first *Drosophila* loss of function mutant in *Snap29,* the human SNAP29 homolog, indicates that it acts at key steps of autophagy, secretion and endolysosomal trafficking. In addition, our data support a model by which SNAP29 in human and *Drosophila* cells exerts an important role during cell division. In particular, we found that the human SNAP29 is required to anchor ZWINT-1 and the RZZ complex component ZWILCH at KTs, and to guarantee a stable KT-MT attachment. The implications of our findings on the understanding of SNAP29 function and their impact on the biology of developing epithelial organs, cancer and CEDNIK is discussed in detail below.

6.1 Functions of Snap29 during interphase

6.1.2 The role of Snap29 in membrane fusion during trafficking in *Drosophila*

The identity of SNARE proteins regulating the subsequent steps of fusion required for autophagosome formation and maturation into autolysosomes is a long-standing question, on which significant progress has been reported recently (Nair & Klionsky 2014; Moreau et al. 2013; Hamasaki, Shibutani, et al. 2013; Itakura et al. 2012a). It is established that SNAREs participates at least in two key steps of autophagy. The first is the phagophore elongation and the second is the fusion between autophagosomes and lysosomes (Moreau et al. 2013, Itakura et al. 2012a). Recently, it has been demonstrated in HeLa cells and in *Drosophila* organs that Syx17, Vamp8 (or the *Drosophila* homolog Vamp7) and SNAP29 form a SNARE complex necessary for autophagosome to lysosome fusion (Itakura et al. 2012, Takáts et al. 2013, Hamasaki, Furuta, et al. 2013). Additionally, a defect in autophagosome clearance has also been shown in *C. elegans* in which Snap29 has been

deleted (Sato et al. 2011, Kang et al. 2011). Finally, a recent publication shows that SNAP29 binding to Syx17 is blocked by the viral Phoshoprotein (P) expressed by HPIV3, which requires autophagy for infection (Ding et al. 2014). In agreement with these observations, our ultrastructural analysis shows clearly accumulation of almost exclusively fully formed autophagosomes with preserved luminal content in *Snap29*^{B6}, *Syx17* and *Vamp7* mutant epithelial tissues. In addition, we detected a genetic interaction between *Snap29* and *Syx17*, and *Snap29* and *Vamp7*. All together, these data strongly support the possibility that Snap29 is required with Syx17 and Vamp7 for fusion of autophagosomes with lysosomes.

An aspect that demands further investigation is whether Snap29 acts elsewhere in the endo-lysosomal system. We find contrasting evidence for this. On one hand, we find partial co-localization of Snap29 with the endosomal Qa-SNARE Syx7, and repeatedly find Syx7 in our immunoprecipitation experiments. In addition, in our uptake assay in mutant cells the endocytic cargo Notch accumulates in an endosomal compartment. On the other end, such compartment is Syx7 negative. Since accumulation of Notch in a Syx7-positive endosomes has been reported to promote ectopic Notch activation (Vaccari & Bilder 2005), and we have found reduced Notch signaling in *Snap29* mutant discs, the point of Notch accumulation could be a post-sorting compartment, such as the late endosome/MVB, or the lysosome. Despite this, we do not observe MVB accumulation in *Snap29* mutant discs. A possible explanation for this is that impairment in the degradation of Notch containing vesicles in *Snap29* mutant cells, is an indirect consequence of autophagy alteration rather than of a block of late endosomes/MVBs fusion with lysosomes.

6.1.2 Snap29 might function as a negative regulator of membrane fusion

We observed traits in *Snap29* mutant cells that could be the result of excess or inappropriate membrane fusion events, rather than of reduced fusion. These are the presence of giant autophagosomes, multilamellar membranes and the secretion of autophagosomes extra-cellularly. The giant autophagosomes might be the result of homotypic fusion between autophagosomes, a described phenomenon which occurs often in physiologic conditions and might intensify when the lysosomal degradative function is blocked (Jahreiss et al. 2008). Nevertheless, it is unlikely that homotypic fusion is indirect in $Snap29^{B6}$ mutant cells, because in *Syx17* and *Vamp7* mutant discs similar giant autophagosomes are not observed. Interestingly, in a recent publication a role in homotypic fusion during phagophore expansion have been reported for the SNAREs VAMP7, SYX8 and SYX7 (Moreau et al. 2011). It is interesting to note that Syx7 is found to interact with both *Drosophila* and Human SNAP29 (this study and our preliminary data on SNAP29 interactors) and we showed that Snap29 partially co-localizes with Syx7. Nevertheless, we didn't find Snap29 functioning during early steps of endocytosis. Thus, we hypothesize that Snap29 could associate to Syx7 or other SNAREs to negatively regulate the homotypic fusion during the expansion of phagophore or between two autophagosomes. Also the secretion of autophagosomes extra-cellularly appears to be a direct consequence of impairment in Snap29 functionality, since no autophagosome secretion has been observed in *Syx17* and *Vamp7* mutant discs. We hypothesize that the presence of autophagosomes in the extracellular space could arise from failure to inhibit fusion during secretion. Inhibitory SNAREs have been postulated to occur naturally to control Golgi stack fusion patterns (Varlamov 2004), while bacteria encode inhibitory SNAREs containing two SNARE domains that if expressed in mammalian cells can act with Syx7 and Vamp8 (the homologs of *Drosophila* Syx7 and Vamp7) to inhibit secretion of lysosomes (Paumet et al. 2009). Interestingly, negative regulation of fusion by Snap29 at the plasma membrane has been observed in rat neurons (Su et al. 2001a; Pan et al. 2005).

A direct role of Snap29 in inhibition of membrane fusion at the plasma membrane during secretion could account also for the elevated Notch and Domeless levels on the surface of mutant cells. Consistent with this possibility, we find that Snap29 interacts with Syx1A and Syx4, the SNAREs that control exocytosis in neuronal and non neuronal cells respectively, and localizes to the plasma membrane upon over-expression. Interestingly, an unconventional secretion route involving autophagy regulators has been recently described (Manjithaya et al. 2010; Bruns et al. 2011; Duran et al. 2010). Finally, considering that Snap29 might be important to inhibit secretory vesicle fusion at the PM in physiologic conditions and that the protein P of HPIV3 binds the SNARE motifs of SNAP29 (Ding et al. 2014), it would be interesting to know whether HPIV3 infected cells display autophagosomes in the extracellular space. It is tempting to speculate that inhibition of SNAP29 could lead to excess of vesicle secretion in the extracellular space also in HPIV3 infected cells. In terms of virus benefits, this would represent a mechanism used by the virus to spread outside the cell. The nature of Snap29 function in inhibiting fusion events, and its involvement in unconventional secretion routes will be the focus of future investigation. In conclusion, our data and previous evidence suggest that SNAP29 might act as an inhibitor/antagonist of membrane fusion in certain membrane compartments.

6.2 Function of SNAP29 during mitosis

6.2.1 SNAP29 is required for ZWINT-1 and ZWILCH recruitment to KTs

Our analysis of *Drosophila* and Human SNAP29 during cell division indicates that SNAP29 has a novel function in controlling spindle organization and chromosome segregation during mitosis. In particular, we found that in SNAP29 depleted cells, ZWINT-1 and ZWILCH, a component of the RZZ complex are not located at KT. A possible explanation for this phenomenon is that SNAP29 interacts directly with ZWINT-

1. Interestingly, the SNAP29 paralog SNAP25 binds the N-terminal of ZWINT-1 (also called Snap25 Interacting Protein 30 KDa or SIP30) in neurons (Vlijmen et al. 2008). This, together with the fact that SNAP29 has been previously found as part of the ZWINT-1 immunoprecipitated complex (Hutchingson mitocheck), suggests that SNAP29 could bind directly ZWINT-1 at the KT.

ZWINT-1 recruits ZW10, ROD and consequently ZWILCH (Wang et al. 2004; Lin et al. 2006; Kasuboski et al. 2011). Thus, the absence of ZWILCH at KTs of SNAP29 depleted cells might be a direct consequence of the lack of ZWINT-1. This agrees also with the fact that ZWINT-1 reaches forming KTs before RZZ components (Wang et al. 2004). One point to clarify with this model is which protein could be the functional homolog of ZWINT-1 in *Drosophila*, in which a ZWINT-1 homolog has not yet been identified. Interestingly, a distantly related ZWINT-1 homolog has been found in *S. cerevisie* (Pagliuca et al. 2009), suggesting that such protein might exist also in *Drosophila*. Nevertheless, it is tempting to speculate that Snap29 might act as ZWINT-1 in *Drosophila*. Indeed, *Drosophila* Snap29 and ZWINT-1 are both coiled coil proteins which localize at KT from prophase to late anaphase and both interact with Spc105/KNL-1 and with HEC1 (Ndc80 in *Drosophila*) KT components. In addition, *Drosophil*a and mammalian cells lacking respectively Snap29 or ZWINT-1 display MT-KT attachment defects and partly loose RZZ components at KT. Prompted by this evidence in future we will test whether ZWINT-1 could substitute for Snap29 in *Drosophila*.

An alternative scenario is that SNAP29 might interact directly with components of the RZZ complex, in particular with ZW10 and ZWILCH. It is known from literature that ZW10 binds directly the Qa-SNARE proteins Syx18 and the R-SNARE p31, as part of the NRZ complex (Kops et al. 2005; Civril et al. 2010; Arasaki et al. 2006; Hirose et al. 2004; Sun et al. 2007). Thus, we postulate that the

conserved ZW10 region for SNAREs binding might also be used to bind SNAP29. Nevertheless, in contrast to Syx18 and p31, SNAP29 is a Qb-Qc SNARE. However, this would not represent a limit if we consider that the interaction might not involved membrane fusion. In this context, SNAP29 might contribute to stabilize the RZZ complex by anchoring ZW10 to ZWINT-1 or ZW10 to HEC1. It has been reported that ZWINT-1 binds ZW10 and HEC1 through its N terminal domain. However, ZW10 and HEC1 do not interact with each other. In this scenario, SNAP29 might represent the protein that stabilizes ZW10 between HEC1 and ZWINT-1. Interestingly, we found that *Drosophila* Snap29 immunoprecipitates with Ndc80 and *viceversa*, and that SNAP29 depletion in HeLa cells does not alter HEC1 localization at KT, suggesting that SNAP29 acts downstream HEC1. Consistent with this hypothesis is the fact that in mammalian cells, when SNAP29 leaves KTs at metaphase, also the RZZ complex disassembles and ZW10 and ROD move towards the midbody, while ZWINT-1 and HEC1 persist at KTs untill anaphase (Williams et al. 1996; Scaërou et al. 2001; Wang et al. 2004). In the future it would be crucial to understand the possible direct interactions between SNAP29, ZWINT-1 and RZZ components.

An aspect that still needs to be clarified is whether ZW10 is present at the KT of SNAP29 depleted cells. It is reported that in absence of ZWINT-1, ZW10 is not recruited at KTs (Wang et al. 2004) and that lack of ZW10 impairs the recruitments of SPINDLY/dynein/dynactin and of MAD1-MAD2, which are specifically recruited by ZW10 (Wojcik et al. 2001; Williams et al. 2003; Chan et al. 2009; Karess 2005; Buffin et al. 2005). In addition, SNAP29 depleted cell resembles cells treated with AURORA B inhibitors, which impair phosphorilation of ZWINT-1, an event required for RZZ recruitment to KTs (Kasuboski et al. 2011). However, SPINDLY and MAD1 persist at KTs of attached and unattached chromosomes in SNAP29 depleted cells, albeit at reduced levels compare to control. Thus, either ZW10 is still

present at KT of SNAP29 depleted cells or SPINDLY and MAD1 are also recruited to KTs by a ZW10-indipendent mechanism. Alternatively, the accumulation of SAC proteins at the KT of SNAP29 depleted cells could be due to the lack of dynein/dynactin, which is reported to mediate SAC protein removal from KT.

If Zw10 is present at KT of SNAP29 depleted cells, one possibility is that SNAP29 does not bind directly to it. In this scenario, ZWILCH could binds SNAP29 to stabilize ZWINT-1 and the RZZ complex. Interestingly, ZWILCH is the only component of the RZZ complex that is not found at the ER or Golgi Apparatus and does not act in membrane trafficking during interphase. In support of this hypothesis there is also the fact that in SNAP29 depleted cells we find ZWILCH in the cytoplasm of cells at metaphase, suggesting that ZWILCH might need SNAP29 for its recruitment to KTs. Consistent with this and similar to SNAP29, ZWILCH is not located at the midbody during cytokinesis, as is the case of ZW10 and ROD (Williams et al. 1996; Scaërou et al. 2001). Also in *in vitro* binding assays ZWILCH binds stably to ROD but weakly to ZW10 (Civril et al. 2010). In summary, we are currently testing whether SNAP29 might be the adaptor protein which tethers ZWILCH to ZW10 from prophase to metaphase and stabilizes the RZZ complex.

6.2.2 Unconventional role of SNAP29 as tethering protein at the KT

Despite intense investigation, bilayered membranes or SNARE proteins have not be reported at the KT, suggesting that SNAP29 is unlikely to work in cell division as a canonical membrane fusion Qb, Qc-SNARE protein. Consistent with a membrane independent function at KT, SNAP29 is one of the few SNARE which does not possess a transmembrane domain or residues for myristilation

or palmitoylation (Holt et al. 2006). During our analysis, we have found that Snap29 function at KTs is independent to *Syx17*, *Vamp7* and *Syb*. To conclusively address whether membrane fusion machinery is involved in Snap29 function at KT, we are currently analyzing both SNAP29 localization at KT and mitotic cell behavior in *Drosophila* cells depleted or mutated for the obligate components of the fusion machinery such as NSF, α-Snap and γ-Snap. Based on this evidence we speculate that Snap29 might have evolved to exploit SNARE-like coiled-coil interaction surfaces for tethering purposes, rather than membrane fusion. Such a non canonical role for a SNARE might have emerged early in the eukaryotic lineage. Indeed, the yeast *S. Cerevisie* possesses two Snap29/25/24 homologs called Sec9 and Spo20, involved in Golgi vesicle trafficking toward the PM and formation of the sporulation membrane, respectively. The two yeast paralogs are functionally non-redundant and emerged from a single form by duplication, that did not occur in *S.pombe*, that uses Sec9p in both processes (Yang et al. 2008). Genetic analysis has shown that Spo20 display lower ability to promote fusion than Sec9 due to amino acid change in the C-terminal half of its SNARE domains (Yang et al. 2008). We propose that Spo20 might represent an ancestral version of Snap29 that gradually evolved tethering along with fusion properties. Although it is unclear how the formation of a sporulation membrane after meiosis is related to aspects of mitosis, it is tantalizing to note that the difference between Sec9 and Spo20 arose with the diversification of interphase and cell division functions. A non-canonical role for SNAP29 during fusion have been discussed in the previous section. Further study is required to assess whether the non-canonical tethering function of SNAP29 might be related to the inhibitory function displayed during certain trafficking events in interphase.

6.2.3 SNAP29 is important to regulate MT binding at KT

The most dramatic phenotype observed in SNAP29 depleted cells is the long pro-metaphase delay which lead to generation of multinucleated cells. Similarly, depletion of ZWINT-1, ZW10 and ROD correlate with inability of chromosome to congress at the metaphase plate and with the generation of aneuployd cells. These defects are mainly due to the failure to recruit the motor protein dynein at the KT of ZW10 depleted cells. Interestingly, it has been shown that dynein contributes to efficient bipolar attachment facilitating MTs capture of monooriented KTs (Li et al. 2007). This suggests that possibly the pro-metaphase delay in SNAP29 depleted cells is due to lack of dynein. However, this hypothesis contrasts with the evidence that SPINDLY is still partially present at KT of SNAP29 depleted cells, indicating that dynein might be normally recruited at KT. Nevertheless, if MTs are not-well anchored to KTs, dynein would not be able to remove SAC components and SPINDLY. Indeed, cold shock treatment of SNAP29 depleted cells results in lack of KT-MT attachment, suggesting that in SNAP29 depleted cells, KTs are weakly bound to MTs compare to control. Thus, we hypothesized that SNAP29 might directly control the interface between KTs and MTs. Considering that HEC1 correctly localizes at KTs in SNAP29 depleted mammalian cells, it is likely that MTs binding is still in part provided by HEC1. However, lack of ZWINT-1 in SNAP29 depleted HeLa cells might results in destabilization of MT attachment to KNL-1. In addition, SNAP29 has been found co-precipitated with SKA1, a component of the SKA complex (Welburn et al. 2009) and our preliminary analysis of SNAP29 interactors in human cells confirms the presence of SKA1 among the proteins immunoprecipitated with SNAP29. On the basis of these findings, we will experimentally test whether in absence of SNAP29, KNL-1 and SKA1 are recruited at KTs.

6.2.4 Potential other roles of SNAP29 at the mitotic spindle

Interestingly, our analysis finds that both *Drosophila* and Human SNAP29 co-localize with the centrosomal protein γ-Tubulin during early prophase and during the final steps of mitosis. In addition, we found, as part of the complexes precipitated with the *Drosophila* Snap29, pericentriolar proteins, among which the anchoring/scaffolding proteins cg5726 and Gp210 and the regulatory proteins flfl, pp4R2r, pp4-19C, which are part of the mitotic PP4 complex (Haberman et al. 2012; Soukup et al. 2013) (Table 1). In agreement with the *Drosophila* data, SNAP29 precipitate with the Centrosomal Protein 110, CEP110, which controls centriols biogenesis and cell cycle progression (Kumar et al. 2013), and the Sperm Associated Antigen5 (SPAG5), another centrosome protein (Hutchins et al. 2010). It is interesting to note that SNAP29 is not associated to the centrosome in interphase, but it localizes with γ-Tubulin only at the onset of mitosis. This corresponds to the moment in which the duplicated cetrosomes induce NE invagination that starts the NEBD (Burke & Ellenberg 2002). It is important to underlie the fact that depletion of SNAP29 in HeLa cells causes an increase of 25% of monopolar spindle compared to control suggesting that it might partecipate in centrosome duplication, maturation or positioning processes by unknown mechanisms. Interestingly, SKA3, another component of the SKA complex, localizes to spindle poles during early prophase and interacts with the protein phosphatase 2 (PP2A) to regulate centrosome integrity (Chan et al. 2012; Theis et al. 2014). It would be interesting to investigate whether SNAP29 and SKA3 interact at the spindle pole and if their functions are related.

How SNAP29 might act at the spindle poles is unknown. Surprisingly, Synaptotagmin1 (Syt1), a calcium sensor which participates in exocytosis in

SNARE complex formation together with SNAP25, certain syntaxins and synaprobrevins (Rickman et al. 2004), localizes to centrosomes during prophase in mouse oocytes and acts as a MTOC-associated protein. Depletion of Syt1 results in defective localization of γ-Tubulin, formation of altered spindles and chromosomes mis-segregation (Zhu et al. 2012). It is tempting to speculate that SNAP29 might help tethering centrosomal structures to MTs in analogy with the novel function we described at KTs. In both human and *Drosophila*, such role would be supported by our findings of the MT proteins Map205, which is known to stabilize PLK1 on MTs (Archambault et al. 2008), of cg13185 and of the dynein subunit dynactin N3 (DCTN3) among SNAP29 interactors (Hutchins et al. 2010).

SNAP29 at centrosomes and KTs could act as part of a spindle matrix which surround MTs and has been proposed to tether mitotic regulators at the spindle fibers or to hols together the mitotic spindle fibers (for review Zheng 2010). In support of this hypothesis, we found the spindle matrix protein Megator (TPR in Humans) in Snap29 immunoprecipitations (Table 1). Megator localization in interphase appears quite distinct with respect to that of *Drosophila* Snap29, since the former occupies the nuclear rim and surrounds chromosomes in the intranuclear space. During mitosis, Megator distributes along the mitotic spindle, while the *Drosophila* Snap29 clearly localizes to KT. However, both are located at centrosomes after anaphase (Zick et al. 2014; Aris & Paddy 1997 Qi et al. 2004). Interestingly, the localization of human SNAP29 during interphase and mitosis in HeLa cells is instead similar to the one of Megator. Also, Megator as SNAP29, assembles in structures which are MT independent. In fact, its pattern of localization does not change upon colchicine treatment in *Drosophila* embryos (Yao et al. 2012). In addition, similarly to SNAP29, TPR, the human homolog of Megator has been

shown to have a regulatory function on the SAC at the KTs of chromosomes in metaphase. However, while Megator originates from the NE and surrounds MTs at mitosis, SNAP29 localizes at the centrosome first and then distributes along the nascent mitotic spindle. Whether the mitotic function of SNAP29 is related to the spindle matrix and whether these different sources highlight distinct step of spindle matrix function remains to be elucidated.

6.2.5 Evolutionary theory of KT formation primed by ER and Golgi

Over the last ten years, several studies showed that proteins having a function in trafficking processes during interphase surprisingly act also in cell division. Some of these proteins function during cytokinesis, such as ESCRT and Rab11, NE dynamics, such as Rab5, or spindle matrix stability, such as Epsin and Clathrin (Capalbo et al. 2011, Zeigerer et al. 2012, Liu & Zheng 2009, Royle et al. 2012, Pelissier et al. 2003, Serio et al. 2011). Other proteins exert a function at KT. This is the case of ZW10 within the RZZ complex or Beclin1. This evidence strengthens the general idea that some KT components might derive from membrane compartments which mainly function during interphase. From an evolutionary point of view, a more sensible hypothesis to explain the presence of trafficking protein at KT is that trafficking compartments are in close proximity of the KT and might assist some of its function. In this context, it is of interest to observe that ER-NE derived membranes are in proximity of KT during pro- and metaphase upon reshaping of the perinuclear ER into a tubular network after NEBD (for review Burke & Ellenberg 2002). A connection of the perinuclear ER with maturing KTs could explain the presence at KT of proteins derived from ER-NE membranes (Güttinger et al. 2009). Open mitosis evolved from ancient eukaryotes which

divide through a closed mitosis. For example, the protozoa *Thricomonas vaginalis* divides with KTs associated to the nuclear membrane that is itself attached to MT fibers (Gómez-Conde et al. 2000), suggesting that KT-MT attachment in organism with semi-open or open mitosis such as *Drosophila* and humans, respectively, might have evolved in close association with the nuclear membrane which is continuous with the ER. In agreement with this, Rab5 has been showed to have a role during ER structuring and NEBD in *C. elegans* (Audhya et al. 2007) and to regulate KT stability in mammals (Lanzetti 2012). In particular, in *C. elegans*, upon Rab5 depletion, NEBD is inhibited. As a consequence chromosomes from the oocyte and spermatocyte remain separated during their segregation on the spindle. Similarly, in mammals, Rab5 depletion causes defects during chromosome congression at the metaphase plate. In addition, in Xenopus Laevis, constituents of the Golgi Apparatus contribute to the NEBD and are found in proximity of KTs (Cotter et al. 2007). Consistent with this, SNAP29 itself and components of RZZ, ROD and ZW10, in both human and *Drosophila* cells are found enriched at the Golgi apparatus and are required for Golgi integrity (Wainman et al. 2012; Andag & Schmitt 2003). In addition, we find multiple ER/Golgi proteins, such as alphacop, calnexin99a, calreticulin, sec24, and Gp93 associated with *Drosophila* Snap29 in Mass Spectrometry analysis (Table 1). Recently, it has been shown the SAC protein MAD1, which during interphase localizes with MAD2 at the NE, is found also in Golgi vesicles where it exerts a role, independently of MAD2, in vesicle transport from Golgi to the PM (Wan et al. 2014).

One provocative parallelism to a scenario in which both ER and the Golgi Apparatus contribute to KT formation and perhaps spindle matrix organization in proximity of the NE membrane in prophase is that of maturation of the

autophagosome, another double-membrane organelle, which also requires SNAP29, ER and Golgi components (Hamasaki, Shibutani, et al. 2013; van der Vaart & Reggiori 2014). Interestingly, Beclin-1 a known autophagy regulator has been very recently found to play a role in cell division as an interactor of ZWINT-1 and of the KMN complex (Frémont et al. 2013). Thus, SNAP29 is part of group of membrane associated proteins which carry analogous evolutionary related functions during interphase and mitosis.

6.3 SNAP29 in tumor suppression and CEDNIK pathogenesis

6.3.1 SNAP29 as a Tumor Suppressor

Is the function of Snap29 during cell division tumor suppressive? One major cellular consequence in SNAP29-depleted cells is the generation of daughter cells containing mininuclei (MN). MN represent a common features in cancer cell as indicator of aneuplody and genomic instability (Fenech et al. 2009). MN originate when one or more chromosomes do not segregate properly and form a separated DNA mass, as in the case of SNAP29 depleted cells. Similar to the main nuclear mass, during telophase, mininucleai recruit NE proteins. However, it has been demonstrated that during the subsequent interphase the MN loose part of the NE barrier due to defect in LaminB organization (Hoffelder et al. 2004, Hatch et al. 2013). Although MN in SNAP29 depleted HeLa cells do not show defect in the nuclear lamina re-formation, a more detailed analysis of NE organization will need to be performed. This aspect is important because alteration of the NE causes also impairment of nuclear import of DNA damage repair (DDR) factors compromising the efficiency of DDR (Terradas et al. 2009; Terradas et al. 2012). Indeed, MNs contain DNA

breaks which render them prone to chromosome pulverization, which can cause traslocation (Xu et al. 2011). Interestingly, in *Snap29*^{B6} mutant discs we observed the presence of pH3 positive DNA fragments. Future analysis of the kariotype of *Snap29*^{B6} mutant cells will elucidate whether chromosomes pulverization and translocations are present.

In addition, MNs are subjected to DNA duplication and transcription defects (Hatch et al. 2013, Crasta et al. 2012). It has been described that MNs could be subjected to a normal re-integration in the main nucleus or reform MN in the subsequent mitosis (Crasta et al. 2012), or can be eliminated by an uncharacterized mechanism (Terradas et al. 2009). In future it would be interesting to study the contribution of MN to genetic instability in *Snap29*^{B6} mutant tissue *in vivo* and in SNAP29 depleted mammalian cells.

Together with accumulation of MN in SNAP29 depleted class, we observed that *Snap29*^{B6} mutant disc display tumor-like tissue alterations. The defects observed in Snap29 mutant organs are likely not a consequence of impairment of autophagy, as they are not observed in mutants of gene that exclusively control autophagy (Juhász et al. 2007; Takáts et al. 2013). Alternatively, they could stem from other reported function of Snap29 in non-autophagic membrane trafficking events. Indeed, discs mutant for genes controlling certain trafficking pathways such as endocytic internalization and endosomal sorting show tumor-like alterations similar to that of *Snap29*^{B6} (Lu & Bilder 2005; Vaccari & Bilder 2005). However, in *Snap29 Drosophila* mutant discs we do not detect ectopic Notch activation and the pool of Notch accumulating intracellularly has been subjected to MVB sorting and resides in the late endosomal/lysosomal lumen. Considering also that loss of genes that control post MVB sorting events generally does not perturb disc epithelium development (Akbar et al. 2009; Sevrioukov et al. 1999; Rusten et al. 2006), the defect highlighted by intracellular Notch

accumulation in *Snap29* mutant cells is *per se* unlikely to contribute to the developmental phenotypes of *Snap29* mutant organs.

Excluding routes that converge on the lysosomes, a further possibility is that the epithelial defects are due to alteration of secretory trafficking. In this scenario, excess JAK/STAT signaling could be important. In this case, excess signaling could directly originate from increased levels of active Dome on the surface of *Snap29* mutant cells. This scenario is consistent with the fact that *Drosophila* mutants preventing cargo internalization, such as those disrupting Clathrin, display increased level of cargoes at the plasma membrane and possess elevated JAK/STAT signaling and reduced Notch signaling (Vidal et al. 2010; Windler & Bilder 2010). Expression of SOCS36E, a negative regulator of JAK/STAT signaling reported to act also by enhancing endosomal degradation of Dome (Stec et al. 2013), rescues part of the epithelial defects of *Snap29* mutant discs. It has been shown that JAK/STAT signaling controls the cell cycle by acting on cdk4 and cyclin B and that upon JAK/STAT signaling up regulation cells progress faster through G1/S and G2/M (Zoranovic et al. 2013). Considering this, we hypothesize that $Snap29^{B6}$ cells could enter mitosis more often compared to control and this could cause accumulation of aberration due to defective cell division. In this scenario, defective cells might undergo mitosis more and might be more proned to death. When apoptosis is inhibited *Snap29* mutant cells might more often generate daughter cells with aberrant nuclei leading to the formation of tumor-like tissues.

Interestingly, as it occurs in $Snap29^{B6}$ discs, an increase of JNK pathway is observed in aneuploid disc cells developing in absence of the SAC regulator Bub3, or of the RZZ component Rod, or of other cell division regulators, such as *orc2*, *asp* and *dia* (Milán et al. 2014; Dekanty et al. 2012). Also, similar to depletion of other cell division components in developing discs, the tumor phenotypes of *Snap29* mutant discs are increased by a block in apoptosis,

indicating that loss of Snap29 can be tumorigenic upon evasion from cell death, a common hallmark of cancer.

6.3.2 Snap29 and CEDNIK pathogenesis.

Despite a large body of evidence on SNAP29, the pathogenesis of CEDNIK is obscure. Our genetic analysis reveals that the *Drosophila Snap29*^{B6} mutant behaves as a strong loss of function and expresses a non functional Snap29 protein, a similar situation to that reported for CEDNIK (Sprecher et al. 2005; Fuchs-Telem et al. 2011). Considering the absence of mouse mutants for *Snap29*, our findings in *Drosophila* could provide an initial framework to understand the pathogenesis of CEDNIK, which starts during fetal development and affects epithelial organs (Sprecher et al. 2005; Fuchs-Telem et al. 2011). Concerning this we find that epithelial tissue disorganization in *Snap29* mutant tissue is not related to distruption of autophagy. In fact, we find that genes specifically acting during autophagy, such as *Atg13*, *Syx17* and *Vamp7* are dispensable for eye disc development. This data agree also with the evidence that in mice and flies, Atg7 appears dispensable for skin barrier formation (Rossiter et al. 2013; Scherfer et al. 2013). This evidence predicts that impairment of autophagy does not cause the developmental alterations associated to CEDNIK at least in the skin, which have been fairly characterized (Li et al. 2011b; Sprecher et al. 2005; Fuchs-Telem et al. 2011). It is well possible that impaired autophagy plays a role in the unexplored neuronal traits of CEDNIK, considering that autophagy is a major process preventing neuro-degeneration (for review Jiang & Mizushima 2013). Which of the non-autophagy defects associated to lack of Snap29 could then be relevant to skin pathogenesis in CEDNIK? Could it be the defect highlighted by Notch accumulation in late endosomal/lysosomal compartments in our uptake experiment? Indeed, increased Notch presence at the plasma membrane, coupled with decreased Notch activation, could be relevant, since loss of Notch signaling is known to lead to epithelial alterations in skin

(Hu et al. 2012). Alternatively, SNAP29 mutations in CEDNIK patients could cause excess secretion which results in over activation of signaling pathways, as in the case of JAK/STAT in *Snap29* mutant in *Drosophila*. Finally, the other possible scenario is the impairment of cell division in CEDNIK patients. Interestingly, mutations in a number of kinetochore proteins, including Spc105 have been associated to autosomal recessive primary microcephaly (Genin et al. 2012). Moreover, depletion of ZWINT-1 and ZW10 phenocopy Roberts syndrome, a congenital disorder due to altered cell division and characterized by mental retardation and formation of multinucleated cells (Musio et al. 2004). Thus, it will be interesting to test whether the nervous system defects of CEDNIK are due to lack of the SNAP29 function in cell division.

Model for Snap29 functions

1. Snap29 is a regulatory factor for membrane fusion

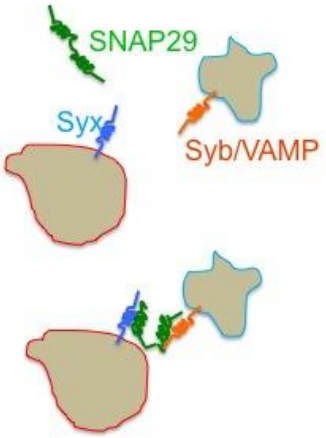

2. Snap29 acts as tethering adaptor at KT

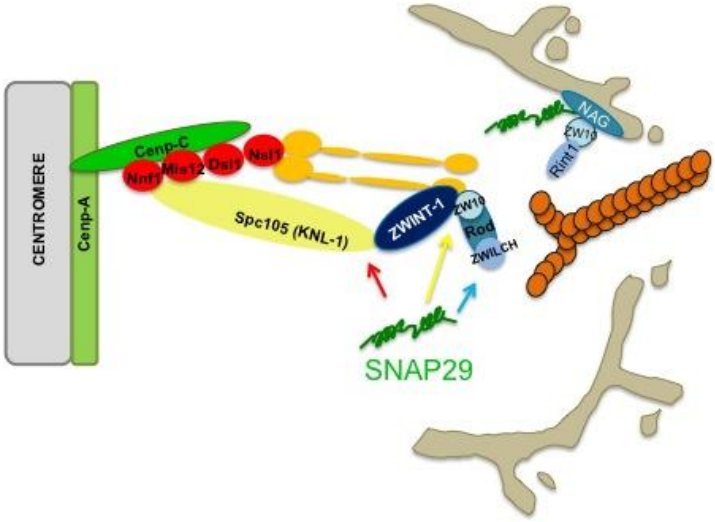

REFERENCES

Acharya, U. et al., 1998. Signaling via Mitogen-Activated Protein Kinase Kinase (MEK1) Is Required for Golgi Fragmentation during Mitosis. *Cell*, 92(2), pp.183–192.

Agromayor, M. & Martin-Serrano, J., 2013. Knowing when to cut and run: mechanisms that control cytokinetic abscission. *Trends in cell biology*, 23(9), pp.433–41.

Akbar, M.A., Ray, S. & Kramer, H., 2009. The SM protein Car/Vps33A regulates SNARE-mediated trafficking to lysosomes and lysosome-related organelles. *Mol Biol Cell*, 20(6), pp.1705–1714.

Andag, U. & Schmitt, H.D., 2003. Dsl1p, an essential component of the Golgi-endoplasmic reticulum retrieval system in yeast, uses the same sequence motif to interact with different subunits of the COPI vesicle coat. *The Journal of biological chemistry*, 278(51), pp.51722–34.

Arasaki, K. et al., 2006. RINT-1 Regulates the Localization and Entry of ZW10 to the Syntaxin 18 Complex □. , 17(June), pp.2780–2788.

Archambault, V. et al., 2008. Sequestration of Polo kinase to microtubules by phosphopriming-independent binding to Map205 is relieved by phosphorylation at a CDK site in mitosis. , pp.2707–2720.

Aris, J.P. & Paddy, M.R., 1997. A Drosophila Tpr protein homolog is localized both in the extrachromosomal channel network and to nuclear pore complexes. , 944, pp.927–944.

Audhya, A., Desai, A. & Oegema, K., 2007. A role for Rab5 in structuring the endoplasmic reticulum. , 178(1), pp.43–56.

Baixauli, F., López-Otín, C. & Mittelbrunn, M., 2014. Exosomes and autophagy: coordinated mechanisms for the maintenance of cellular fitness. *Frontiers in immunology*, 5(August), p.403.

Bannykh, S.I., Rowe, T. & Balch, W.E., 1996. The Organization of Endoplasmic Reticulum Export Complexes. , 135(l), pp.19–35.

Barlowe, C., 1998. COPII and selective export from the endoplasmic reticulum. , 1404(October 1997).

Bastiaens, P. et al., 2006. Gradients in the self-organization of the mitotic spindle. *Trends in cell biology*, 16(3), pp.125–34.

Basto, R., Gomes, R. & Karess, R.E., 2000. Rough deal and Zw10 are required for the metaphase checkpoint in Drosophila. *Nature cell biology*, 2(12), pp.939–43.

Behnia, R. et al., 2007. The yeast orthologue of GRASP65 forms a complex with a coiled-coil protein that contributes to ER to Golgi traffic. *The Journal of cell biology*, 176(3), pp.255–61.

Bethani, I. et al., 2009. Endosomal fusion upon SNARE knockdown is maintained by residual SNARE activity and enhanced docking. *Traffic (Copenhagen, Denmark)*, 10(10), pp.1543–59.

Beznoussenko, G. V et al., 2007. Analogs of the Golgi complex in microsporidia: structure and avesicular mechanisms of function. *J Cell Sci*, 120(Pt 7), pp.1288–1298.

Bharadwaj, R. & Yu, H., 2004. The spindle checkpoint, aneuploidy, and cancer. *Oncogene*, 23(11), pp.2016–27.

Blethrow, J.D. et al., 2008. Covalent capture of kinase-specific phosphopeptides reveals Cdk1-cyclin B substrates. *Proceedings of the National Academy of Sciences of the United States of America*, 105(5), pp.1442–7.

Blow, J.J. & Tanaka, T.U., 2005. The chromosome cycle: coordinating replication and segregation. Second in the cycles review series. *EMBO reports*, 6(11), pp.1028–34.

Blower, M.D. et al., 2005. A Rae1-containing ribonucleoprotein complex is required for mitotic spindle assembly. *Cell*, 121(2), pp.223–34.

Blower, M.D. & Karpen, G.H., 2001. The roleof Drosophila CID in kinetochore formation , cell-cycle progression and heterochromatin interactions. , 3(August), pp.14–16.

Bonaccorsi, S., Giansanti, M.G. & Gatti, M., 2000. Spindle assembly in Drosophila neuroblasts and ganglion mother cells. , 2(January), pp.1999–2001.

Bonifacino, J.S., 2014. Vesicular transport earns a Nobel. *Trends in cell biology*, 24(1), pp.3–5.

Bonifacino, J.S. & Glick, B.S., 2004. The Mechanisms of Vesicle Budding and Fusion. , 116(1980), pp.153–166.

Brandizzi, F. & Barlowe, C., 2013. Organization of the ER-Golgi interface for membrane traffic control. *Nature reviews. Molecular cell biology*, 14(6), pp.382–92.

Braun, S. & Jentsch, S., 2007. SM-protein-controlled ER-associated degradation discriminates between different SNAREs. *EMBO reports*, 8(12), pp.1176–82.

Bruns, C. et al., 2011. Biogenesis of a novel compartment for autophagosome-mediated unconventional protein secretion. *J Cell Biol*, 195(6), pp.979–992.

Brust-Mascher, I. et al., 2004. Model for anaphase B: role of three mitotic motors in a switch from poleward flux to spindle elongation. *Proceedings of the National Academy of Sciences of the United States of America*, 101(45), pp.15938–43.

Buffin, E. et al., 2005. Recruitment of Mad2 to the kinetochore requires the Rod/Zw10 complex. *Current biology : CB*, 15(9), pp.856–61.

Burke, B. & Ellenberg, J., 2002. Remodelling the walls of the nucleus. *Nature reviews. Molecular cell biology*, 3(7), pp.487–97.

Capalbo, L. et al., 2011. Rab5 GTPase controls chromosome alignment through Lamin disassembly and relocation of the NuMA-like protein Mud to the poles during mitosis. *Proc Natl Acad Sci USA*, 108(42), pp.17343–17348.

Carazo-salas, R.E. et al., 2001. Ran – GTP coordinates regulation of microtubule nucleation and dynamics during mitotic-spindle assembly. , 3(March).

Carpp, L.N. et al., 2006. The Sec1p/Munc18 protein Vps45p binds its cognate SNARE proteins via two distinct modes. *The Journal of cell biology*, 173(6), pp.927–36.

Chan, Y.W. et al., 2009. Mitotic control of kinetochore-associated dynein and spindle orientation by human Spindly. *The Journal of cell biology*, 185(5), pp.859–74.

Chan, Y.W. et al., 2012. network interaction. , 196(5), pp.563–571.

Chang, Y.-Y. & Neufeld, T.P., 2009. An Atg1/Atg13 complex with multiple roles in TOR-mediated autophagy regulation. *Mol Biol Cell*, 20(7), pp.2004–2014.

Cheeseman, I.M. et al., 2004. A conserved protein network controls assembly of the outer kinetochore and its ability to sustain tension. , pp.2255–2268.

Cheeseman, I.M. et al., 2006. The conserved KMN network constitutes the core microtubule-binding site of the kinetochore. *Cell*, 127(5), pp.983–97.

Cheeseman, I.M., 2014. The kinetochore. *Cold Spring Harbor perspectives in biology*, 6(7), p.a015826.

Cheeseman, I.M. & Desai, A., 2008. Molecular architecture of the kinetochore-microtubule interface. *Nature reviews. Molecular cell biology*, 9(1), pp.33–46.

Chia, P.Z.C. & Gleeson, P. a, 2014. Membrane tethering. *F1000prime reports*, 6(September), p.74.

Christoforidis, S. & Mcbride, H.M., 1999. The Rab5 effector EEA1 is a core component of endosome docking. , 397(February).

Ciferri, C. et al., 2005. Architecture of the human ndc80-hec1 complex, a critical constituent of the outer kinetochore. *The Journal of biological chemistry*, 280(32), pp.29088–95.

Ciferri, C. et al., 2008. Implications for kinetochore-microtubule attachment from the structure of an engineered Ndc80 complex. *Cell*, 133(3), pp.427–39.

Civril, F. et al., 2010. Structural analysis of the RZZ complex reveals common ancestry with multisubunit vesicle tethering machinery. *Structure (London, England : 1993)*, 18(5), pp.616–26.

Colanzi, A. et al., 2000. A Specific Activation of the Mitogen-activated Protein Kinase Kinase 1 (MEK1) Is Required for Golgi Fragmentation during Mitosis. , 149(2), pp.331–339.

Colanzi, A., Suetterlin, C. & Malhotra, V., 2003. Cell-cycle-specific Golgi fragmentation: how and why? *Current Opinion in Cell Biology*, 15(4), pp.462–467.

Collas, P., 1999. Sequential PKC- and Cdc2-mediated phosphorylation events elicit zebrafish nuclear envelope disassembly. , 987, pp.977–987.

Cotter, L. et al., 2007. Nuclear membrane disassembly and rupture. *Journal of molecular biology*, 369(3), pp.683–95.

Crasta, K. et al., 2012. DNA breaks and chromosome pulverization from errors in mitosis. *Nature*, 482(7383), pp.53–8.

D'Andrea-Merrins, M. et al., 2007. Munc18c interaction with syntaxin 4 monomers and SNARE complex intermediates in GLUT4 vesicle trafficking. *The Journal of biological chemistry*, 282(22), pp.16553–66.

Daigle, N., 2001. Nuclear pore complexes form immobile networks and have a very low turnover in live mammalian cells. *The Journal of Cell Biology*, 154(1), pp.71–84.

Dekanty, A. et al., 2012. Aneuploidy-induced delaminating cells drive tumorigenesis in Drosophila epithelia. *Proc Natl Acad Sci USA*, 109(50), pp.20549–20554.

DeLuca, J.G. et al., 2005. Hec1 and nuf2 are core components of the kinetochore outer plate essential for organizing microtubule attachment sites. *Molecular biology of the cell*, 16(2), pp.519–31.

DeLuca, J.G. et al., 2003. Nuf2 and Hec1 Are Required for Retention of the Checkpoint Proteins Mad1 and Mad2 to Kinetochores. *Current Biology*, 13(23), pp.2103–2109.

Desai, A. et al., 2003. KNL-1 directs assembly of the microtubule-binding interface of the kinetochore in C . elegans. , pp.2421–2435.

Diao, A. et al., 2003. The coiled-coil membrane protein golgin-84 is a novel rab effector required for Golgi ribbon formation. *The Journal of cell biology*, 160(2), pp.201–12.

Ding, B. et al., 2014. Phosphoprotein of human parainfluenza virus type 3 blocks autophagosome-lysosome fusion to increase virus production. *Cell host & microbe*, 15(5), pp.564–77.

Dulubova, I. et al., 1999. A conformational switch in syntaxin during exocytosis : role of munc18. , 18(16), pp.4372–4382.

Dulubova, I. et al., 2007. Munc18-1 binds directly to the neuronal SNARE complex. , 104(8).

Duran, J.M. et al., 2010. Unconventional secretion of Acb1 is mediated by autophagosomes. *The Journal of cell biology*, 188(4), pp.527–36.

Egan, D. et al., 2014. The autophagy initiating kinase ULK1 is regulated via opposing phosphorylation by AMPK and mTOR. *Autophagy*, 7(6), pp.643–644.

Ellenberg, J. et al., 1997. Nuclear Membrane Dynamics and Reassembly in Living Cells: Targeting of an Inner Nuclear Membrane Protein in Interphase and Mitosis. , 138(6), pp.1193–1206.

Emily M Hatch, 2013. NIH Public Access. , 154(1), pp.47–60.

Ems-mcclung, S.C., Zheng, Y. & Walczak, C.E., 2004. Importin ␣ / ␤ and Ran-GTP Regulate XCTK2 Microtubule Binding through a Bipartite Nuclear Localization Signal. , 15(January), pp.46–57.

Fader, C.M. & Colombo, M.I., 2009. Autophagy and multivesicular bodies: two closely related partners. *Cell death and differentiation*, 16(1), pp.70–8.

Fava, L.L. et al., 2011. Probing the in vivo function of Mad1:C-Mad2 in the spindle assembly checkpoint. *The EMBO journal*, 30(16), pp.3322–36.

Favreau, C. et al., 1996. Cell Cycle-Dependent Phosphorylation of Nucleoporins and Nuclear Pore Membrane Protein Gp210 †. , 2960(96), pp.8035–8044.

Fenech, M. et al., 2009. Report on the buccal micronucleus assay workshop organized by the International Human Micronucleus (HUMN) project--Antalya, Turkey 2007. *Mutagenesis*, 24(2), pp.199–201.

Fielding, A.B. et al., 2012. Clathrin-mediated endocytosis is inhibited during mitosis. , 2012.

Flanagan, J.J. & Barlowe, C., 2006. Cysteine-disulfide cross-linking to monitor SNARE complex assembly during endoplasmic reticulum-Golgi transport. *The Journal of biological chemistry*, 281(4), pp.2281–8.

Foley, E. a & Kapoor, T.M., 2013. Microtubule attachment and spindle assembly checkpoint signalling at the kinetochore. *Nature reviews. Molecular cell biology*, 14(1), pp.25–37.

Foltz, D.R. et al., 2006. The human CENP-A centromeric nucleosome-associated complex. *Nature cell biology*, 8(5), pp.458–69.

Fraschini, R. et al., 2001. Bub3 interaction with Mad2, Mad3 and Cdc20 is mediated by WD40 repeats and does not require intact kinetochores. *The EMBO journal*, 20(23), pp.6648–59.

Frémont, S. et al., 2013. Beclin-1 is required for chromosome congression and proper outer kinetochore assembly. *EMBO reports*, 14(4), pp.364–72.

Fuchs-Telem, D. et al., 2011. CEDNIK syndrome results from loss-of-function mutations in SNAP29. *Br J Dermatol*, 164(3), pp.610–616.

Fukuda, M., 2003. Distinct Rab binding specificity of Rim1, Rim2, rabphilin, and Noc2. Identification of a critical determinant of Rab3A/Rab27A recognition by Rim2. *The Journal of biological chemistry*, 278(17), pp.15373–80.

Funderburk, S.F., Wang, Q.J. & Yue, Z., 2010. The Beclin 1-VPS34 complex--at the crossroads of autophagy and beyond. *Trends in cell biology*, 20(6), pp.355–62.

Gadde, S. & Heald, R., 2004. Mechanisms and molecules of the mitotic spindle. *Current biology : CB*, 14(18), pp.R797–805.

Garrett, S. et al., 2001. Reciprocal activation by cyclin-dependent kinases 2 and 7 is directed by substrate specificity determinants outside the T loop. *Molecular and cellular biology*, 21(1), pp.88–99.

Gascoigne, K.E. et al., 2012. NIH Public Access. , 145(3), pp.410–422.

Gassmann, R. et al., 2008. A new mechanism controlling kinetochore-microtubule interactions revealed by comparison of two dynein-targeting components: SPDL-1 and the Rod/Zwilch/Zw10 complex. *Genes & development*, 22(17), pp.2385–99.

Gatlin, J.C. & Bloom, K., 2010. Microtubule motors in eukaryotic spindle assembly and maintenance. *Seminars in cell & developmental biology*, 21(3), pp.248–54.

Geng, J. & Klionsky, D.J., 2010. The Golgi as a potential membrane source for autophagy. *Autophagy*, 6(7), pp.950–1.

Genin, A. et al., 2012. Kinetochore KMN network gene CASC5 mutated in primary microcephaly. *Human molecular genetics*, 21(24), pp.5306–17.

Glavy, J.S. et al., 2007. Cell-cycle-dependent phosphorylation of the nuclear pore Nup107-160 subcomplex. *Proceedings of the National Academy of Sciences of the United States of America*, 104(10), pp.3811–6.

Glick, B.S., 2000. Organization of the Golgi apparatus. *Current Opinion in Cell Biology*, 12(4), pp.450–456.

Gómez-Conde, E. et al., 2000. Trichomonas vaginalis: chromatin and mitotic spindle during mitosis. *Experimental parasitology*, 96(3), pp.130–8.

Gromley, A. et al., 2005. Centriolin anchoring of exocyst and SNARE complexes at the midbody is required for secretory-vesicle-mediated abscission. *Cell*, 123(1), pp.75–87.

Grosshans, B.L., Ortiz, D. & Novick, P., 2006. Rabs and their effectors: achieving specificity in membrane traffic. *Proceedings of the National Academy of Sciences of the United States of America*, 103(32), pp.11821–7.

Guo, B. et al., 2014. O-GlcNAc-modification of SNAP-29 regulates autophagosome maturation. *Nature cell biology*, 16(12).

Guruharsha, K.G. et al., 2011. A protein complex network of Drosophila melanogaster. *Cell*, 147(3), pp.690–703.

Güttinger, S., Laurell, E. & Kutay, U., 2009. Orchestrating nuclear envelope disassembly and reassembly during mitosis. *Nature reviews. Molecular cell biology*, 10(3), pp.178–91.

Haberman, A. et al., 2012. The synaptic vesicle SNARE neuronal Synaptobrevin promotes endolysosomal degradation and prevents neurodegeneration. *J Cell Biol*, 196(2), pp.261–276.

Hailey, D.W. et al., 2011. during starvation. , 141(4), pp.656–667.

Hamasaki, M., Furuta, N., et al., 2013. Autophagosomes form at ER-mitochondria contact sites. *Nature*.

Hamasaki, M., Shibutani, S.T. & Yoshimori, T., 2013. Up-to-date membrane biogenesis in the autophagosome formation. *Current opinion in cell biology*, 25(4), pp.455–60.

Hawes, C. et al., 2010. Biogenesis of the plant Golgi apparatus. *Biochemical Society transactions*, 38(3), pp.761–7.

Hay, J.C. et al., 1997. Transport between the Endoplasmic Reticulum and Golgi Apparatus in Mammalian Cells. , 89, pp.149–158.

Hayashi-Nishino, M. et al., 2009. A subdomain of the endoplasmic reticulum forms a cradle for autophagosome formation. *Nature cell biology*, 11(12), pp.1433–7.

Hickson, G.R.X. et al., 2003. Arfophilins Are Dual Arf / Rab 11 Binding Proteins That Regulate Recycling Endosome Distribution and Are Related to Drosophila Nuclear Fallout. , 14(July), pp.2908–2920.

Hirose, H. et al., 2004. Implication of ZW10 in membrane trafficking between the endoplasmic reticulum and Golgi. *The EMBO journal*, 23(6), pp.1267–78.

Hoffelder, D.R. et al., 2004. Resolution of anaphase bridges in cancer cells. , pp.389–397.

Holt, M. et al., 2006. Identification of SNAP-47, a novel Qbc-SNARE with ubiquitous expression. *J Biol Chem*, 281(25), pp.17076–17083.

Holthuis, J.C.M., Nichols, B.J. & Dhruvakumar, S., 1998. Two syntaxin homologues in the TGN / endosomal system of yeast. , 17(1), pp.113–126.

Holubcová, Z., Howard, G. & Schuh, M., 2013. Vesicles modulate an actin network for asymmetric spindle positioning. *Nature cell biology*, 15(8), pp.937–47.

Hong, W., 2005. SNAREs and traffic. *Biochimica et biophysica acta*, 1744(2), pp.120–44.

Hood, F.E. et al., 2013. Coordination of adjacent domains mediates TACC3-ch-TOG-clathrin assembly and mitotic spindle binding. *The Journal of cell biology*, 202(3), pp.463–78.

Howell, B.J., Moree, B., Farrar, E.M., Stewart, S., Fang, G., Salmon, E.D., et al., 2004. at Kinetochores in Living Cells. , 14, pp.953–964.

Howell, B.J., Moree, B., Farrar, E.M., Stewart, S., Fang, G. & Salmon, E.D., 2004. Spindle checkpoint protein dynamics at kinetochores in living cells. *Current biology : CB*, 14(11), pp.953–64.

Hu, B. et al., 2012. Multifocal Epithelial Tumors and Field Cancerization from Loss of Mesenchymal CSL Signaling. *Cell*, 149(6), pp.1207–1220.

Hu, S. et al., 2010. Structure of the Munc18c / Syntaxin4 N-peptide complex defines universal features of the N-peptide binding mode of Sec1 / Munc18 proteins. , 104(21).

Hutagalung, A.H. & Novick, P.J., 2011. Role of Rab GTPases in membrane traffic and cell physiology. *Physiological reviews*, 91(1), pp.119–49.

Hutchins, J.R.A. et al., 2010. Systematic Analysis of Human Protein Complexes Identifies Chromosome Segregation Proteins. *Science*, 328(5978), pp.593–599.

Itakura, E., Kishi-Itakura, C. & Mizushima, N., 2012a. The Hairpin-type Tail-Anchored SNARE Syntaxin 17 Targets to Autophagosomes for Fusion with Endosomes/Lysosomes. *Cell*, 151(6), pp.1256–1269.

Itakura, E., Kishi-Itakura, C. & Mizushima, N., 2012b. The hairpin-type tail-anchored SNARE syntaxin 17 targets to autophagosomes for fusion with endosomes/lysosomes. *Cell*, 151(6), pp.1256–69.

Itakura, E. & Mizushima, N., 2013. Syntaxin 17: the autophagosomal SNARE. *Autophagy*, 9(6), pp.917–9.

Izuta, H. et al., 2006. Comprehensive analysis of the ICEN (Interphase Centromere Complex) components enriched in the CENP-A chromatin of human cells. *Genes to cells : devoted to molecular & cellular mechanisms*, 11(6), pp.673–84.

Jäger, S. et al., 2004. Role for Rab7 in maturation of late autophagic vacuoles. *Journal of cell science*, 117(Pt 20), pp.4837–4848.

Jahn, R., Lang, T. & Sudhof, T., 2003. Membrane fusion. *Cell*, 112(4), pp.519–533.

Jahn, R. & Scheller, R.H., 2006. SNAREs--engines for membrane fusion. *Nature reviews. Molecular cell biology*, 7(9), pp.631–43.

Jahreiss, L., Menzies, F.M. & Rubinsztein, D.C., 2008. The Itinerary of Autophagosomes : From Peripheral Formation to Kiss-and-Run Fusion with Lysosomes. , (5), pp.574–587.

Jesch, S.A. et al., 2001. Mitotic Golgi is in a Dynamic Equilibrium Between Clustered and Free Vesicles Independent of the ER. , 130(12), pp.873–884.

Jiang, P. & Mizushima, N., 2013. Autophagy and human diseases. *Cell Research*, 24(1), pp.69–79.

Jongsma, M.L.M., Berlin, I. & Neefjes, J., 2014. On the move: organelle dynamics during mitosis. *Trends in Cell Biology*, pp.1–13.

Juhász, G. et al., 2007. Atg7-dependent autophagy promotes neuronal health , stress tolerance , and longevity but is dispensable for metamorphosis in Drosophila. , (612), pp.3061–3066.

Kang, J. et al., 2011. Essential roles of snap-29 in C. elegans. *Dev Biol*, 355(1), pp.77–88.

Kardon, J.R. & Vale, R.D., 2009. Regulators of the cytoplasmic dynein motor. *Nature reviews. Molecular cell biology*, 10(12), pp.854–65.

Karess, R., 2005. Rod-Zw10-Zwilch: a key player in the spindle checkpoint. *Trends in cell biology*, 15(7), pp.386–92.

Karsenti, E. & Vernos, I., 2001. The Mitotic Spindle : A Self-Made Machine. , 294(October), pp.543–548.

Kasuboski, J.M. et al., 2011. Zwint-1 is a novel Aurora B substrate required for the assembly of a dynein-binding platform on kinetochores. *Molecular biology of the cell*, 22(18), pp.3318–30.

Khodjakov, A. et al., 2000. Centrosome-independent mitotic spindle formation in vertebrates. *Current Biology*, 10(2), pp.59–67.

Khvotchev, M. et al., 2007. Dual modes of Munc18-1/SNARE interactions are coupled by functionally critical binding to syntaxin-1 N terminus. *The Journal of neuroscience : the official journal of the Society for Neuroscience*, 27(45), pp.12147–55.

Kim, J.-H. et al., 2011. Involvement of mitophagy in oncogenic K-Ras-induced transformation: overcoming a cellular energy deficit from glucose deficiency. *Autophagy*, 7(10), pp.1187–98.

Kinseth, M. a et al., 2007. The Golgi-associated protein GRASP is required for unconventional protein secretion during development. *Cell*, 130(3), pp.524–34.

Kiseleva, E. et al., 2001. Steps of nuclear pore complex disassembly and reassembly during mitosis in early Drosophila embryos. , 30.

Kline, S.L. et al., 2006. The human Mis12 complex is required for kinetochore assembly and proper chromosome segregation. *The Journal of cell biology*, 173(1), pp.9–17.

Kline-smith, S.L. & Walczak, C.E., 2004. Mitotic Spindle Assembly and Chromosome Segregation : Refocusing on Microtubule Dynamics. , 15, pp.317–327.

Kops, G.J.P.L. et al., 2005. ZW10 links mitotic checkpoint signaling to the structural kinetochore. *The Journal of cell biology*, 169(1), pp.49–60.

Kowal, J., Tkach, M. & Théry, C., 2014. Biogenesis and secretion of exosomes. *Current opinion in cell biology*, 29C, pp.116–125.

Kraynack, B.A. et al., 2005. Dsl1p , Tip20p , and the Novel Dsl3 (Sec39) Protein Are Required for the Stability of the Q / t-SNARE Complex at the Endoplasmic Reticulum in Yeast □. , 16(September), pp.3963–3977.

Kumar, A. et al., 2013. CEP proteins: the knights of centrosome dynasty. *Protoplasma*, 250(5), pp.965–83.

Lanzetti, L. & Rab, K., 2012. © 2012 Landes Bioscience . , 3(3), pp.168–172.

Latham, C.F. et al., 2007. Arachidonic acid potentiates exocytosis and allows neuronal SNARE complex to interact with Munc18a. *Journal of neurochemistry*, 100(6), pp.1543–54.

Lee, I. et al., 2014. Membrane adhesion dictates Golgi stacking and cisternal morphology. *Proceedings of the National Academy of Sciences of the United States of America*, 111(5), pp.1849–54.

Levesque, a a & Compton, D. a, 2001. The chromokinesin Kid is necessary for chromosome arm orientation and oscillation, but not congression, on mitotic spindles. *The Journal of cell biology*, 154(6), pp.1135–46.

Li, Q. et al., 2011a. Abca12-mediated lipid transport and Snap29-dependent trafficking of lamellar granules are crucial for epidermal morphogenesis in a zebrafish model of ichthyosis. *Dis Model Mech*, 4(6), pp.777–785.

Li, Q. et al., 2011b. Abca12-mediated lipid transport and Snap29-dependent trafficking of lamellar granules are crucial for epidermal morphogenesis in a zebrafish model of ichthyosis. *Disease models & mechanisms*, 4(6), pp.777–85.

Li, Y. et al., 2007. Kinetochore dynein generates a poleward pulling force to facilitate congression and full chromosome alignment. *Cell research*, 17(8), pp.701–12.

Lin, C. et al., 2001. Polo-like kinase is required for the fragmentation of pericentriolar Golgi stacks during mitosis.

Lin, Y.-T. et al., 2006. Hec1 sequentially recruits Zwint-1 and ZW10 to kinetochores for faithful chromosome segregation and spindle checkpoint control. *Oncogene*, 25(52), pp.6901–14.

Littleton, J.T. et al., 2001. SNARE-complex disassembly by NSF follows synaptic-vesicle fusion. *Proceedings of the National Academy of Sciences of the United States of America*, 98(21), pp.12233–8.

Liu, L. et al., 2014. Robust autophagy/mitophagy persists during mitosis. *Cell Cycle*, 8(10), pp.1616–1620.

Liu, S.-T. et al., 2006. Mapping the assembly pathways that specify formation of the trilaminar kinetochore plates in human cells. *The Journal of cell biology*, 175(1), pp.41–53.

Liu, Z. & Zheng, Y., 2009. A requirement for epsin in mitotic membrane and spindle organization. *The Journal of cell biology*, 186(4), pp.473–80.

Lu, H. & Bilder, D., 2005. Endocytic control of epithelial polarity and proliferation in Drosophila. *Nat Cell Biol*, 7(12), pp.1132–1139.

Lüders, J., Patel, U.K. & Stearns, T., 2006. GCP-WD is a gamma-tubulin targeting factor required for centrosomal and chromatin-mediated microtubule nucleation. *Nature cell biology*, 8(2), pp.137–47.

Maiato, H., Rieder, C.L. & Khodjakov, A., 2004. Kinetochore-driven formation of kinetochore fibers contributes to spindle assembly during animal mitosis. *The Journal of cell biology*, 167(5), pp.831–40.

Malsam, J., Kreye, S. & Söllner, T.H., 2008. Membrane fusion: SNAREs and regulation. *Cellular and molecular life sciences : CMLS*, 65(18), pp.2814–32.

Manjithaya, R. et al., 2010. Unconventional secretion of Pichia pastoris Acb1 is dependent on GRASP protein, peroxisomal functions, and autophagosome formation. *J Cell Biol*, 188(4), pp.537–546.

Maresca, T.J. & Salmon, E.D., 2009. assembly checkpoint activity. , 184(3), pp.373–381.

Mari, M. & Reggiori, F., 2010. Atg9 reservoirs, a new organelle of the yeast endomembrane system? *Autophagy*, 6(8), pp.1221–3.

Matsunaga, K. et al., 2010. Autophagy requires endoplasmic reticulum targeting of the PI3-kinase complex via Atg14L. *The Journal of cell biology*, 190(4), pp.511–21.

Mayr, M.I. et al., 2007. The human kinesin Kif18A is a motile microtubule depolymerase essential for chromosome congression. *Current biology : CB*, 17(6), pp.488–98.

McIntosh, J.R. & O'Toole, E.T., 1999. Life cycles of yeast spindle pole bodies: Getting microtubules into a closed nucleus. *Biology of the Cell*, 91(4-5), pp.305–312.

Milán, M. et al., 2014. Seminars in Cell & Developmental Biology Aneuploidy and tumorigenesis in Drosophila. *Seminars in Cell and Developmental Biology*, 28, pp.110–115.

Miller, E. a & Schekman, R., 2013. COPII - a flexible vesicle formation system. *Current opinion in cell biology*, 25(4), pp.420–7.

Misura, K.M., Scheller, R.H. & Weis, W.I., 2000. Three-dimensional structure of the neuronal-Sec1-syntaxin 1a complex. *Nature*, 404(6776), pp.355–62.

Mittelbrunn, M. & Sánchez-Madrid, F., 2012. Intercellular communication: diverse structures for exchange of genetic information. *Nature reviews. Molecular cell biology*, 13(5), pp.328–35.

Mizuno-Yamasaki, E., Rivera-Molina, F. & Novick, P., 2012. GTPase networks in membrane traffic. *Annual review of biochemistry*, 81, pp.637–59.

Mizushima, N., 2014. Sugar modification inhibits autophagosome–lysosome fusion. *Nature Cell Biology*, 16(12), pp.1132–1133.

Mizushima, N. & Komatsu, M., 2011. Autophagy: renovation of cells and tissues. *Cell*, 147(4), pp.728–741.

Mora-Bermúdez, F., Gerlich, D. & Ellenberg, J., 2007. Maximal chromosome compaction occurs by axial shortening in anaphase and depends on Aurora kinase. *Nature cell biology*, 9(7), pp.822–31.

Moreau, K. et al., 2011. Autophagosome precursor maturation requires homotypic fusion. *Cell*, 146(2), pp.303–317.

Moreau, K., Renna, M. & Rubinsztein, D.C., 2013. Connections between SNAREs and autophagy. *Trends in Biochemical Sciences*, 38(2), pp.57–63.

Mori, Y., Moriishi, K. & Matsuura, Y., 2008. Hepatitis C virus core protein: its coordinate roles with PA28gamma in metabolic abnormality and carcinogenicity in the liver. *The international journal of biochemistry & cell biology*, 40(8), pp.1437–42.

Moritz, M. et al., 2000. Structure of the γ -tubulin ring complex : a template for microtubule nucleation. , 2(June), pp.365–370.

Morvan, J. et al., 2014. In vitro reconstitution of fusion between immature autophagosomes and endosomes. *Autophagy*, 5(5), pp.676–689.

Motility, M.D. et al., 2009. Article The Human Kinetochore Ska1 Complex Facilitates. *Developmental Cell*, 16(3), pp.374–385.

Mountain, V. et al., 1999. Cross-links Microtubules in the Mammalian Mitotic Spindle. , 147(2), pp.351–365.

Mühlhäusser, P. & Kutay, U., 2007. An in vitro nuclear disassembly system reveals a role for the RanGTPase system and microtubule-dependent steps in nuclear envelope breakdown. *The Journal of cell biology*, 178(4), pp.595–610.

Musacchio, A. & Hardwick, K.G., 2002. The spindle checkpoint: structural insights into dynamic signalling. *Nature reviews. Molecular cell biology*, 3(10), pp.731–41.

Musacchio, A. & Salmon, E.D., 2007. The spindle-assembly checkpoint in space and time. *Nature reviews. Molecular cell biology*, 8(5), pp.379–93.

Musio, A. et al., 2004. Recapitulation of the Roberts syndrome cellular phenotype by inhibition of INCENP, ZWINT-1 and ZW10 genes. *Gene*, 331, pp.33–40.

Nair, U. et al., 2011. SNARE proteins are required for macroautophagy. *Cell*, 146(2), pp.290–302.

Nair, U. & Klionsky, D.J., 2014. Autophagosome biogenesis requires SNAREs. *Autophagy*, 7(12), pp.1570–1572.

Nelson, W.J., 2000. W(h)ither the Golgi during Mitosis? *The Journal of Cell Biology*, 149(2), pp.243–248.

Newsome, T., Asling, B. & Dickson, B.J., 2000. Analysis of Drosophila photoreceptor axon guidance in eye-specific mosaics. *Development*, 127(4), pp.851–860.

Nezis, I.P. et al., 2008. Ref(2)P, the Drosophila melanogaster homologue of mammalian p62, is required for the formation of protein aggregates in adult brain. *J Cell Biol*, 180(6), pp.1065–1071.

Nickel, W. & Rabouille, C., 2009. Mechanisms of regulated unconventional protein secretion. *Nat Rev Mol Cell Biol*, 10(2), pp.148–155.

Nicklas, R.B. & Ward, S.C., 1994. Elements of error correction in mitosis: microtubule capture, release, and tension. *The Journal of cell biology*, 126(5), pp.1241–53.

Niemeyer, B.A. & Schwarz, T.L., 2000. SNAP-24, a Drosophila SNAP-25 homologue on granule membranes, is a putative mediator of secretion and granule-granule fusion in salivary glands. *J Cell Sci*, 113 (Pt 2, pp.4055–4064.

Nogueira, C. et al., 2014. SLY1 and Syntaxin 18 specify a distinct pathway for procollagen VII export from the endoplasmic reticulum. *eLife*, 3, p.e02784.

Oka, T. & Krieger, M., 2005. Multi-component protein complexes and Golgi membrane trafficking. *Journal of biochemistry*, 137(2), pp.109–14.

Okada, M. et al., 2006. The CENP-H-I complex is required for the efficient incorporation of newly synthesized CENP-A into centromeres. *Nature cell biology*, 8(5), pp.446–57.

Pagliuca, C. et al., 2009. Roles for the Conserved Spc105p / Kre28p Complex in Kinetochore-Microtubule Binding and the Spindle Assembly Checkpoint. , 4(10).

Pan, P.-Y. et al., 2005. SNAP-29-mediated modulation of synaptic transmission in cultured hippocampal neurons. *The Journal of biological chemistry*, 280(27), pp.25769–79.

Paumet, F. et al., 2009. Intracellular Bacteria Encode Inhibitory SNARE-Like Proteins R. H. Valdivia, ed. *PLoS ONE*, 4(10), p.e7375.

Pelissier, A. et al., 2003. Trafficking through Rab11 Endosomes Is Required for Cellularization during Drosophila Embryogenesis. , 13, pp.1848–1857.

Peplowska, K. et al., 2007. The CORVET tethering complex interacts with the yeast Rab5 homolog Vps21 and is involved in endo-lysosomal biogenesis. *Developmental cell*, 12(5), pp.739–50.

Petrovic, A. et al., 2010. The MIS12 complex is a protein interaction hub for outer kinetochore assembly. *The Journal of cell biology*, 190(5), pp.835–52.

Pinsky, B.A. & Biggins, S., 2005. The spindle checkpoint: tension versus attachment. *Trends in cell biology*, 15(9), pp.486–93.

Pircs, K. et al., 2012. Advantages and limitations of different p62-based assays for estimating autophagic activity in Drosophila. *PloS one*, 7(8), p.e44214.

Plaza, E.S., 1990. Kinetochores Are Transported Poleward along a Single Astral Microtubule during Chromosome Attachment to the Spindle in Newt Lung Cells. , I(January), pp.81–95.

Poirier, M. a. et al., 1998. Protease Resistance of Syntaxin{middle dot}SNAP-25{middle dot}VAMP Complexes: IMPLICATIONS FOR ASSEMBLY AND STRUCTURE. *Journal of Biological Chemistry*, 273(18), pp.11370–11377.

Polgár, J. et al., 2003. Phosphorylation of SNAP-23 in activated human platelets. *J Biol Chem*, 278(45), pp.44369–44376.

Powers, M.A. et al., 1997. The Vertebrate GLFG Nucleoporin, Nup98, Is an Essential Component of Multiple RNA Export Pathways. , 136(2), pp.241–250.

Prescott, A.R. et al., 2001. Evidence for Prebudding Arrest of ER Export in Animal Cell Mitosis and its Role in Generating Golgi Partitioning Intermediates. , (17), pp.321–335.

Pritchard, C.E.J. et al., 1999. RAE1 Is a Shuttling mRNA Export Factor That Binds to a GLEBS-like NUP98 Motif at the Nuclear Pore Complex through Multiple Domains. , 145(2), pp.237–253.

Przewloka, M.R. et al., 2007. Molecular Analysis of Core Kinetochore Composition and Assembly in Drosophila melanogaster. *PLoS ONE*, 2(5), p.e478.

Puthenveedu, M. a et al., 2006. GM130 and GRASP65-dependent lateral cisternal fusion allows uniform Golgi-enzyme distribution. *Nature cell biology*, 8(3), pp.238–48.

Pyrpasopoulou, A. et al., 1996. The lamin B receptor (LBR) provides essential chromatin docking sites at the nuclear envelope. , 15(24), pp.7108–7119.

Qi, H. et al., 2004. Megator , an Essential Coiled-Coil Protein that Localizes to the Putative Spindle Matrix during Mitosis in Drosophila. , 15(November), pp.4854–4865.

Rapaport, D. et al., 2010. Loss of SNAP29 impairs endocytic recycling and cell motility. *PLoS ONE*, 5(3), p.e9759.

Rappsilber, J., Ishihama, Y. & Mann, M., 2003. Stop and go extraction tips for matrix-assisted laser desorption/ionization, nanoelectrospray, and LC/MS sample pretreatment in proteomics. *Anal Chem*, 75(3), pp.663–670.

Ravichandran, V., Chawla, A. & Roche, P.A., 1996. Identification of a Novel Syntaxin- and Syntaxin- and Synaptobrevin / Expressed in Non-neuronal Tissues *. , pp.23–27.

Ravikumar, B., Moreau, K., Jahreiss, L., et al., 2010. Plasma membrane contributes to the formation of pre-autophagosomal structures. *Nature Cell Biology*, 12(8), pp.747–757.

Ravikumar, B., Moreau, K. & Rubinsztein, D.C., 2010. Plasma membrane helps autophagosomes grow. *Autophagy*, 6(8), pp.1184–6.

Reggiori, F. et al., 2004. Early stages of the secretory pathway, but not endosomes, are required for Cvt vesicle and autophagosome assembly in Saccharomyces cerevisiae. *Mol Biol Cell*, 15(5), pp.2189–2204.

Ren, Y. et al., 2010. NIH Public Access. , 139(6), pp.1119–1129.

Rickman, C. et al., 2004. Synaptotagmin interaction with the syntaxin/SNAP-25 dimer is mediated by an evolutionarily conserved motif and is sensitive to inositol hexakisphosphate. *The Journal of biological chemistry*, 279(13), pp.12574–9.

Rizo, J. & Südhof, T.C., 2002. Snares and Munc18 in synaptic vesicle fusion. *Nature reviews. Neuroscience*, 3(8), pp.641–53.

Rossiter, H. et al., 2013. Epidermal keratinocytes form a functional skin barrier in the absence of Atg7 dependent autophagy. *J Dermatol Sci*.

Rotem-Yehudar, R., Galperin, E. & Horowitz, M., 2001. Association of insulin-like growth factor 1 receptor with EHD1 and SNAP29. *The Journal of biological chemistry*, 276(35), pp.33054–60.

Rothman, J.E., 2009. Membrane Fusion : Grappling with SNARE and SM Proteins. , 323(January), pp.474–477.

Rowe, T. et al., 1996. COPII Vesicles Derived from Mammalian Endoplasmic Reticulum Microsomes Recruit COPI. , 135(4), pp.895–911.

Royle, S.J., Bright, N.A. & Lagnado, L., 2012. Europe PMC Funders Group Clathrin is required for the function of the mitotic spindle. , 434(7037), pp.1152–1157.

Rubinsztein, D.C. & Nixon, R. a, 2010. Rapamycin induces autophagic flux in neurons. *Proceedings of the National Academy of Sciences of the United States of America*, 107(49), p.E181; author reply E182.

Rusten, T.E. et al., 2006. Fab1 phosphatidylinositol 3-phosphate 5-kinase controls trafficking but not silencing of endocytosed receptors. *Mol Biol Cell*, 17(9), pp.3989–4001.

Salina, D. et al., 2002. Cytoplasmic Dynein as a Facilitator of Nuclear Envelope Breakdown. , 108, pp.97–107.

Santaguida, S. & Musacchio, A., 2009. The life and miracles of kinetochores. *The EMBO journal*, 28(17), pp.2511–31.

Santos, J.M. et al., 2013. Report Clathrin-Mediated Endocytosis Persists during Unperturbed Mitosis. , pp.659–668.

Sato, M. et al., 2011a. Caenorhabditis elegans SNAP-29 is required for organellar integrity of the endomembrane system and general exocytosis in intestinal epithelial cells. *Mol Biol Cell*, 22(14), pp.2579–2587.

Sato, M. et al., 2011b. Caenorhabditis elegans SNAP-29 is required for organellar integrity of the endomembrane system and general exocytosis in intestinal epithelial cells. *Molecular biology of the cell*, 22(14), pp.2579–87.

Satoh, A. et al., 2012. NIH Public Access. , 4(3), pp.153–161.

Scaërou, F. et al., 2001. The ZW10 and Rough Deal checkpoint proteins function together in a large , evolutionarily conserved complex targeted to the kinetochore.

Schardt, A. et al., 2009. The SNARE protein SNAP-29 interacts with the GTPase Rab3A: Implications for membrane trafficking in myelinating glia. *J. Neurosci. Res.*, 87(15), pp.3465–3479.

Scherfer, C. et al., 2013. Autophagy drives epidermal deterioration in a Drosophila model of tissue aging. *Aging (Albany NY)*, 5(4), pp.276–287.

Screpanti, E. et al., 2011. Direct binding of Cenp-C to the Mis12 complex joins the inner and outer kinetochore. *Current biology : CB*, 21(5), pp.391–8.

Seals, D.F. et al., 2000. A Ypt—Rab effector complex containing the Sec1 homolog Vps33p is required for homotypic vacuole fusion.

Serio, G. et al., 2011. Small GTPase Rab5 participates in chromosome congression and regulates localization of the centromere-associated protein CENP-F to kinetochores. *Proc Natl Acad Sci USA*, 108(42), pp.17337–17342.

Sevrioukov, E. et al., 1999. A role for the deep orange and carnation eye color genes in lysosomal delivery in Drosophila. *Mol Cell*, 4(4), pp.479–486.

Sharp, D.J., Rogers, G.C. & Scholey, J.M., 2000. Microtubule motors in mitosis. , pp.41–47.

Shima, D.T. et al., 1997. Partitioning of the Golgi Apparatus during Mitosis in Living HeLa Cells. , 137(6), pp.1211–1228.

Short, B. et al., 2001. A GRASP55-rab2 effector complex linking Golgi structure to membrane traffic. *The Journal of cell biology*, 155(6), pp.877–83.

Shorter, J. et al., 1999. GRASP55 , a second mammalian GRASP protein involved in the stacking of Golgi cisternae in a cell-free system. , 18(18), pp.4949–4960.

Shorter, J. & Warren, G., 2002. Golgi architecture and inheritance. *Annual review of cell and developmental biology*, 18, pp.379–420.

Simonsen, A. & Stenmark, H., 2008. Self-eating from an ER-associated cup. *J Cell Biol*, 182(4), pp.621–622.

Skoufias, D.A. et al., 2001. Mammalian mad2 and bub1/bubR1 recognize distinct spindle-attachment and kinetochore-tension checkpoints. *Proceedings of the National Academy of Sciences of the United States of America*, 98(8), pp.4492–7.

Sönnichsen, B. et al., 1998. A Role for Giantin in Docking COPI Vesicles to Golgi Membranes. , 140(5), pp.1013–1022.

Soukup, S.-F. et al., 2013. DLin-7 is required in postsynaptic lamina neurons to prevent light-induced photoreceptor degeneration in Drosophila. *Curr Biol*, 23(14), pp.1349–1354.

Sprecher, E. et al., 2005. A mutation in SNAP29, coding for a SNARE protein involved in intracellular trafficking, causes a novel neurocutaneous syndrome characterized by cerebral dysgenesis, neuropathy, ichthyosis, and palmoplantar keratoderma. *Am J Hum Genet*, 77(2), pp.242–251.

Stec, W., Vidal, O. & Zeidler, M.P., 2013. Drosophila SOCS36E negatively regulates JAK/STAT pathway signaling via two separable mechanisms. *Molecular biology of the cell*, 24(18), pp.3000–3009.

Steegmaier, M. et al., 2000. Syntaxin 17 Is Abundant in Steroidogenic Cells and Implicated in Smooth Endoplasmic Reticulum Membrane Dynamics. , 11(August), pp.2719–2731.

Steegmaier, M., 1998. Three Novel Proteins of the Syntaxin/SNAP-25 Family. *Journal of Biological Chemistry*, 273(51), pp.34171–34179.

Stumpff, J. et al., 2009. NIH Public Access. , 14(2), pp.252–262.

Su, C. et al., 2002. Fragmentation and Dispersal of the Pericentriolar Golgi Complex Is Required for Entry into Mitosis in Mammalian Cells. , 109, pp.359–369.

Su, Q. et al., 2001a. SNAP-29: a general SNARE protein that inhibits SNARE disassembly and is implicated in synaptic transmission. *Proc Natl Acad Sci USA*, 98(24), pp.14038–14043.

Su, Q. et al., 2001b. SNAP-29: a general SNARE protein that inhibits SNARE disassembly and is implicated in synaptic transmission. *Proceedings of the National Academy of Sciences of the United States of America*, 98(24), pp.14038–43.

Sudakin, V., Chan, G.K. & Yen, T.J., 2001. Checkpoint inhibition of the APC/C in HeLa cells is mediated by a complex of BUBR1, BUB3, CDC20, and MAD2. *The Journal of cell biology*, 154(5), pp.925–36.

Sullivan, M. & Morgan, D.O., 2007. Finishing mitosis, one step at a time. *Nature reviews. Molecular cell biology*, 8(11), pp.894–903.

Sun, Y. et al., 2007. Rab6 Regulates Both ZW10 / RINT-1 – and Conserved Oligomeric Golgi Complex-dependent Golgi Trafficking and Homeostasis. , 18(October), pp.4129–4142.

Sutton, R.B. et al., 1998. Crystal structure of a SNARE complex involved in synaptic ˚ resolution exocytosis at 2 . 4 A. , 395(September), pp.347–353.

Sztul, E. & Lupashin, V., 2006. Role of tethering factors in secretory membrane traffic. *American journal of physiology. Cell physiology*, 290(1), pp.C11–26.

Takáts, S. et al., 2013. Autophagosomal Syntaxin17-dependent lysosomal degradation maintains neuronal function in Drosophila. *The Journal of cell biology*, 201(4), pp.531–9.

Tamai, K. et al., 2012. Regulation of hepatitis C virus secretion by the Hrs-dependent exosomal pathway. *Virology*, 422(2), pp.377–85.

Tanaka, T.U. & Desai, A., 2008. Kinetochore-microtubule interactions: the means to the end. *Current opinion in cell biology*, 20(1), pp.53–63.

Tapon, N. et al., 2001. The Drosophila tuberous sclerosis complex gene homologs restrict cell growth and cell proliferation. *Cell*, 105(3), pp.345–355.

Terradas, M. et al., 2009. DNA lesions sequestered in micronuclei induce a local defective-damage response. , 8, pp.1225–1234.

Terradas, M. et al., 2012. Is DNA damage response ready for action anywhere? *International journal of molecular sciences*, 13(9), pp.11569–83.

Theis, M., Paszkowski-Rogacz, M. & Buchholz, F., 2014. SKAnking with Ska3: Essential role of Ska3 in cell division revealed by combined phenotypic profiling. *Cell Cycle*, 8(21), pp.3435–3437.

Tighe, A., Staples, O. & Taylor, S., 2008. Mps1 kinase activity restrains anaphase during an unperturbed mitosis and targets Mad2 to kinetochores. *The Journal of cell biology*, 181(6), pp.893–901.

TM, K., 2006. References and Notes 1. , 311(January), pp.388–392.

Togneri, J. et al., 2006. Specific SNARE complex binding mode of the Sec1/Munc-18 protein , Sec1p.

Toonen, R.F.G. & Verhage, M., 2007. Munc18-1 in secretion: lonely Munc joins SNARE team and takes control. *Trends in neurosciences*, 30(11), pp.564–72.

Tripathi, A. et al., 2009. Structural characterization of Tip20p and Dsl1p, subunits of the Dsl1p vesicle tethering complex. *Nature structural & molecular biology*, 16(2), pp.114–23.

Ungar, D. et al., 2006. Retrograde transport on the COG railway. *Trends in cell biology*, 16(2), pp.113–20.

Ungermann, C. et al., 1999. Complex on Isolated Vacuoles , Are Essential for Homotypic Fusion. , 145(7), pp.1435–1442.

Van der Vaart, A. & Reggiori, F., 2014. The Golgi complex as a source for yeast autophagosomal membranes. *Autophagy*, 6(6), pp.800–801.

Vaccari, T. et al., 2009. Comparative analysis of ESCRT-I, ESCRT-II and ESCRT-III function in Drosophila by efficient isolation of ESCRT mutants. *J Cell Sci*, 122(14), pp.2413–2423.

Vaccari, T. & Bilder, D., 2005. The Drosophila tumor suppressor vps25 prevents nonautonomous overproliferation by regulating notch trafficking. *Developmental cell*, 9(5), pp.687–98.

Varlamov, O., 2004. i-SNAREs: inhibitory SNAREs that fine-tune the specificity of membrane fusion. *J Cell Biol*, 164(1), pp.79–88.

Vidal, O.M. et al., 2010. Negative regulation of Drosophila JAK-STAT signalling by endocytic trafficking. *J Cell Sci*, 123(20), pp.3457–3466.

Vigers, G.P., 1991. A distinct vesicle population targets membranes and pore complexes to the nuclear envelope in Xenopus eggs. *The Journal of Cell Biology*, 112(4), pp.545–556.

Vilinsky, I. et al., 2002. A Drosophila SNAP-25 Null Mutant Reveals Context-Dependent Redundancy With SNAP-24 in Neurotransmission. , 271(September), pp.259–271.

Vlijmen, T. Van et al., 2008. A unique residue in rab3c determines the interaction with novel binding protein Zwint-1. , 582, pp.2838–2842.

Voets, T. et al., 2001. Munc18-1 Promotes Large Dense-Core Vesicle Docking. , 31, pp.581–591.

Vorozhko, V. V et al., 2008. Multiple mechanisms of chromosome movement in vertebrate cells mediated through the Ndc80 complex and dynein/dynactin. *Chromosoma*, 117(2), pp.169–79.

Wainman, A. et al., 2012. The Drosophila RZZ complex - roles in membrane trafficking and cytokinesis. *Journal of cell science*, 125(Pt 17), pp.4014–25.

Wan, J. et al., 2014. Report A Golgi-Localized Pool of the Mitotic Checkpoint Component Mad1 Controls Integrin Secretion and Cell Migration. *Current Biology*, 231, pp.1–6.

Wang, H. et al., 2004. Human Zwint-1 specifies localization of Zeste White 10 to kinetochores and is essential for mitotic checkpoint signaling. *The Journal of biological chemistry*, 279(52), pp.54590–8.

Wang, H.-W. et al., 2008. Architecture and flexibility of the yeast Ndc80 kinetochore complex. *Journal of molecular biology*, 383(4), pp.894–903.

Waters, J.C. et al., 1998. Localization of Mad2 to Kinetochores Depends on Microtubule Attachment, Not Tension. , 141(5), pp.1181–1191.

Welz, T., Wellbourne-Wood, J. & Kerkhoff, E., 2014. Orchestration of cell surface proteins by Rab11. *Trends in cell biology*, 24(7), pp.407–415.

Whyte, J. et al., 2008. Phosphorylation regulates targeting of cytoplasmic dynein to kinetochores during mitosis. *The Journal of cell biology*, 183(5), pp.819–34.

Whyte, J.R.C. & Munro, S., 2002. Vesicle tethering complexes in membrane traffic.

Willett, R., Ungar, D. & Lupashin, V., 2013. The Golgi puppet master: COG complex at center stage of membrane trafficking interactions. *Histochemistry and cell biology*, 140(3), pp.271–83.

Williams, B.C. et al., 2003. Zwilch , a New Component of the ZW10 / ROD Complex Required for Kinetochore Functions. , 14(April), pp.1379–1391.

Williams, B.C., Gatti, M. & Goldberg, M.L., 1996. Bipolar spindle attachments affect redistributions of ZW10, a Drosophila centromere/kinetochore component required for accurate chromosome segregation. *The Journal of cell biology*, 134(5), pp.1127–40.

Wilson, G.M. et al., 2005. The FIP3-Rab11 Protein Complex Regulates Recycling Endosome Targeting to the Cleavage Furrow during Late. , 16(February), pp.849–860.

Windler, S.L. & Bilder, D., 2010. Endocytic Internalization Routes Required for Delta/Notch Signaling. *Current Biology*, 20(6), pp.538–543.

Wojcik, E. et al., 2001. Kinetochore dynein : its dynamics and role in the transport of the Rough deal checkpoint protein. , pp.1001–1008.

Wu, H., Wang, M.C. & Bohmann, D., 2009. JNK protects Drosophila from oxidative stress by trancriptionally activating autophagy. *Mechanisms of development*, 126(8-9), pp.624–637.

Wu, M., Pastor-Pareja, J.C. & Xu, T., 2011. Interaction between RasV12 and scribbled clones induces tumour growth and invasion. *Nature*, pp.1–5.

Xie, Z. & Klionsky, D.J., 2007. Autophagosome formation: core machinery and adaptations. *Nature cell biology*, 9(10), pp.1102–9.

Xu, B. et al., 2011. Replication Stress Induces Micronuclei Comprising of Aggregated DNA Double-Strand Breaks. , 6(4).

Yang, H.-J. et al., 2008. Binding interactions control SNARE specificity in vivo. *The Journal of cell biology*, 183(6), pp.1089–100.

Yang, L., Guan, T. & Gerace, L., 1997. Integral Membrane Proteins of the Nuclear Envelope Are Dispersed throughout the Endoplasmic Reticulum during Mitosis. , 137(6), pp.1199–1210.

Yao, C. et al., 2012. A nuclear-derived proteinaceous matrix embeds the microtubule spindle apparatus during mitosis.

Zaal, K.J.M. et al., 1999. Golgi Membranes Are Absorbed into and Reemerge from the ER during Mitosis. , 99, pp.589–601.

Zeigerer, A. et al., 2012. Rab5 is necessary for the biogenesis of the endolysosomal system in vivo. *Nature*, 485(7399), pp.465–70.

Zhai, R.G. et al., 2003. Mapping Drosophila mutations with molecularly defined P element insertions. *Proceedings of the National Academy of Sciences of the United States of America*, 100(19), pp.10860–10865.

Zheng, Y., 2010. A membranous spindle matrix orchestrates cell division. *Nat Rev Mol Cell Biol*, 11(7), pp.529–535.

Zhong, Y. et al., 2009. Distinct regulation of autophagic activity by Atg14L and Rubicon associated with Beclin 1-phosphatidylinositol-3-kinase complex. *Nature cell biology*, 11(4), pp.468–76.

Zhou, J., Yao, J. & Joshi, H.C., 2002. Attachment and tension in the spindle assembly checkpoint. *Journal of cell science*, 115(Pt 18), pp.3547–55.

Zhu, X.-L. et al., 2012. Synaptotagmin1 is required for spindle stability and metaphase-to-anaphase transition in mouse oocytes. *Cell cycle (Georgetown, Tex.)*, 11(4), pp.818–26.

Zick, M. et al., 2014. Membranes linked by trans -SNARE complexes require lipids prone to non-bilayer structure for progression to fusion. , pp.1–13.

Zoranovic, T., Grmai, L. & Bach, E.A., 2013. Regulation of proliferation , cell competition , and cellular growth by the Drosophila JAK-STAT pathway. , (September), pp.1–7.

Zuccolo, M. et al., 2007. The human Nup107-160 nuclear pore subcomplex contributes to proper kinetochore functions. *The EMBO journal*, 26(7), pp.1853–64.